Reaction Dynamics under Weak UV Illumination on TiO_2 Film Photocatalyst

（酸化チタン薄膜光触媒の微弱な紫外光下での反応ダイナミクス）

大古 善久

Reaction Dynamics under Weak UV Illumination on TiO_2 Film Photocatalyst

(酸化チタン薄膜光触媒の微弱な紫外光下での反応ダイナミクス)

Yoshihisa OHKO

(1998)

The University of Tokyo

論文の内容の要旨

論文題目　Reaction dynamics under weak UV illumination on TiO_2 film photocatalyst
（和訳　酸化チタン薄膜光触媒の微弱な紫外光下での反応ダイナミクス）

氏名　　大古　善久

1．緒言

よく知られているように、ZnO、CdS、TiO_2などの半導体にバンドギャップ以上のエネルギーをもつ光が吸収されると、電子−正孔対が生成し、電子と正孔がそれぞれ表面吸着物と室温，大気圧で化学的に反応する。中でもTiO_2は気相中や液相中で化学的に安定であるため扱いやすく、正孔のもつ強い酸化力のためにほとんど全ての有機物の分解に有効である。

これまでTiO_2に関する数多くの研究は、有害物の速い除去速度を目的として水銀灯などの強い紫外光源が使用された。これに対して当研究室では、光強度を弱くすると量子効率が上昇することに着目し、通常の生活空間で問題になるような微量な物質の分解には特に光源を用意する必要がなく、通常の空間に存在する程度の微弱な光強度でよいと主張して来た。この時、問題となる反応物濃度はppbv-ppmv程度である。さらに，高い光触媒能を持つTiO_2担持材料を大面積で利用することにより、新しい気相静置系の環境浄化システムを提案してきた。しかし、このような微弱な紫外光下での光触媒反応ダイナミクスの理論的考察やモデル化はほとんど成されてこなかった。

そこで本研究では薄膜TiO_2光触媒を用いた気相分子分解反応のダイナミクスを取り扱った。本研究の特徴は入射光子数と反応物質の数を対応させながら反応速度を考察した点にある。極微弱光下では光触媒反応は完全な光量律速となる。一方、強い光強度でTiO_2表面が非常に活性化された状態では、触媒表面への物質供給過程が律速になる。これらの完全な光量律速条件，完全な物質供給律速条件を気相の2-プロパノールの分解反応に関して、光量および気相物質濃度の関数として実験的に明らかにした。また、これらの解析を通して、光触媒表面での·OHの拡散距離や、拡散律速時に光触媒気相界面に生ずる境界層の厚さなどを見積もることが出来た。本研究は、環境触媒として汎用性が期待されるTiO_2光触媒反応の速度論的解析の基礎を成すものである。

2．量子効率の光強度依存性（光量律速領域）

ガラス基板上に焼結したアナターゼ型のTiO_2膜を用いた。光触媒反応により、微弱な

紫外光の下で2-プロパノールは選択的にアセトンに酸化される（図１）。その素過程はまず次式のように、·OHにより α 水素が引き抜かれ、

$CH_3CH(OH)CH_3 + \cdot OH \rightarrow CH_3C\cdot(OH)CH_3 + H_2O$ （１）

不安定ラジカル $CH_3C\cdot(OH)CH_3$ が生成する。このラジカルは以下の様に酸素と反応しアセトンに自動酸化される。

$CH_3CH(OH)CH_3 + O_2 \rightarrow CH_3COO\cdot(OH)CH_3$ （２）

$CH_3COO\cdot(OH)CH_3 \rightarrow CH_3COCH_3 + H^+ + O_2^-$ （３）

また、いわゆる電流2倍効果によってもこのラジカルはアセトンに分解される。いずれにしても、アセトン１分子の生成は１光子反応として扱うことが出来る。反応の量子効率を酸化チタンが吸収した光子数の関数として表したのが図２である。吸収光子数が減少すると量子効率は上昇する。しかし、光量が非常に小さくなると量子効率は光量に依存せず一定になる。例えば、1000 ppmvでは4×10^{11} quanta·cm^{-2}·s^{-1}光子数以下の領域で量子効率は28 %であった。これは完全な光量律速に入ったことを意味している。また，量子効率の吸収光子数に対するカーブの形が異なる初期濃度で同じであり、初期濃度が高くなると同じ量子効率を与える時に必要な吸収光子数が増加した。

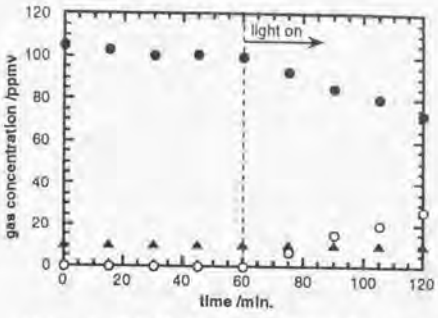

図１　2-プロパノール分解反応の各ガス成分の変化（●2-プロパノール,○アセトン ▲CO_2, 2-プロパノール初期濃度 100 ppmv, 照射光量 45 μW·cm^{-2}）

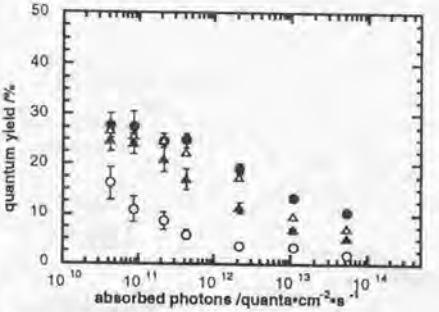

図２　2-プロパノール分解反応の量子効率の吸収光子数依存性（2-プロパノール初期濃度●1000 ppmv △100 ppmv, ▲10 ppmv, ○1 ppmv）

そこで、量子効率を吸収光子数と反応物の表面吸着分子数の比（I_{norm}）に対してプロットし直すと、1-1000 ppmvの異なる初期濃度にも拘わらず、同一の曲線に乗った（図３）。また、10^{-4} /s^{-1}以下のI_{norm}で完全な光量律速になることがわかった。この時、·OHあるいは2-プロパノールが、2-プロパノール分子間距離以上の広い距離を表面拡散して常に2-プロパノールと反応していると考えられる。この距離は今回の実験の最小濃度1 ppmvの吸着量から計算して11 nm以上であると推定できた。ここで、一連の光触媒反応過程の速度と光子の吸収頻度を比べると、本実験条件での単位時間当たりの吸収光子数が非常に少ないことがわかる（図４）。すなわち、一連の光触媒反応はms以内に終了するのに対し、光触媒に吸収される光子は1cm^2あたり10^3秒に一回程度である。このことは光触媒中に存在する電子-正孔の定常濃度は限りなく小さいことを示している。

これらの考察から、量子効率の最大値（28％）はこのサンプルの電荷分離効率を意味し、また量子効率の低下は、表面活性種同志の反応（式４）の増加によるものであると考えられる。

$$\cdot OH + HO_2\cdot \rightarrow H_2O + O_2 \quad (4)$$

もし、反応物の分子間距離が·OH拡散距離に比べて非常に離れた極微量な表面濃度の場合は量子効率が低下すると予想できるが，実験の可能な濃度領域ではこのような現象は観測されていない。

３．反応速度の光強度依存性（物質輸送律速域）

比較的強い光強度域での2-プロパノールの分解反応速度を吸収光子数に対して両対数プロットしたのが図５である。0.1-100 ppmvまでの各初期濃度で吸収光子数の増加に対して反応速度は増加し、さらに吸収光子数が多くなると一定速度となることが示された。この時、触媒表面への反応物の拡散律速になっていることは気相を強制撹拌した実験からも確認できた。また、表１に示すように拡散律速条件での反応速度は気相濃度に比例して上昇した。これは、反応物の触媒表面への流束が気相濃度に比例するからである。一方、気相濃度が高くなると一定速度になり始める時の吸収光子数の値は増加したが、完全な物質輸送領域以外では、それらは比例関係になかった（表１）。これは、光触媒反応の速度が表面吸着量とも相関があることに起因していると予想される。すなわち気相濃度が高くなる程、表面反応速度が流束の増加に上回って拡散律速に入るためには、より多く光子数が必要となるためと考えられる。

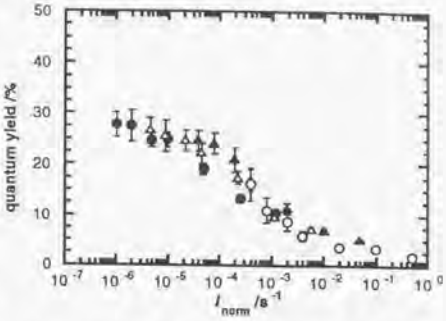

図３　吸収光子数と2-プロパノール吸着分子数の比（I_{norm} /s^{-1}）に対する量子効率（2-プロパノール初期濃度●1000 ppmv △100 ppmv, ▲10 ppmv, ○1 ppmv）

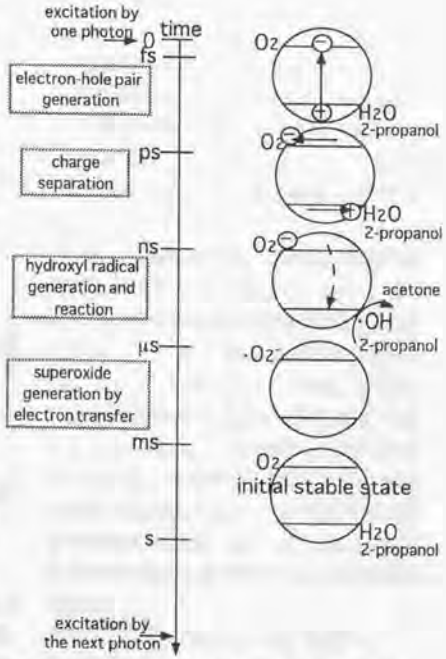

図４　一連のTiO_2光触媒反応過程のダイヤグラム

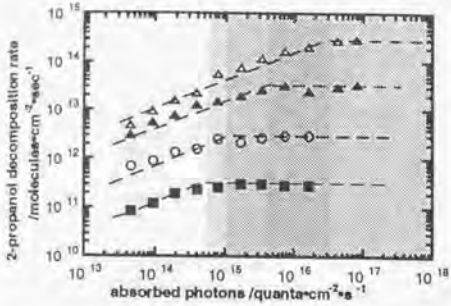

図5　静置系での2-プロパノール分解速度の吸収光量依存性（2-プロパノール初期濃度●1000 ppmv △100 ppmv, ▲10 ppmv, ○1 ppmv）

気相濃度の比	拡散律速の時の反応速度の比	光量律速の反応速度の比	拡散律速に入る光量の比
10 (100 ppmv /10 ppmv)	10	3	8
10 (10 ppmv /1 ppmv)	10	6	4
10 (1 ppmv /0.1 ppmv)	10	9	2

表1　初期濃度の増加に伴う拡散律速時の反応速度の比、光量律速時の反応速度の比および拡散律速に入る時の吸収光子数の比

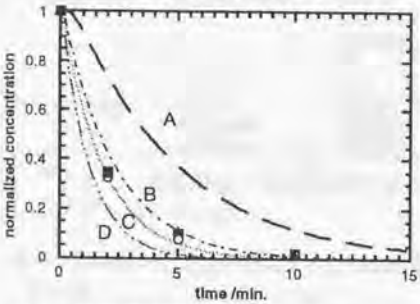

図6　拡散律速時の濃度変化のシミュレーション（拡散係数D=0.099 $cm^2 \cdot s^{-1}$、境界層の厚さ line A: 8.0 cm, line B: 2.0 cm, line C: 1.5 cm, line D: 1.0 cm、実験データのマークは図5と同じ）

次に、拡散律速条件でのガラス容器内の濃度変化について、拡散方程式（式4）を用いたシミュレーションを行なった。

$$\partial C/\partial t = -D(\partial^2 C/\partial x^2) + V \cdot \partial C/\partial x \quad (5)$$

まず、静置系の実験ではガラス容器内の中の正味の風速は0と仮定して、1次元の差分法により計算した。計算方法は、ある時間のx'の位置における気相濃度をC(x',t')、時間dt経過後の同位置における気相濃度C(x',t'+1)として次のよう行なった。

$$C(x',t'+1) = C(x',t') + D'[\{C(x'+1,t') - C(x',t')\} + \{C(x'-1,t') - C(x',t')\}] \quad (6)$$

$$C(z',t'+1) = C(z',t') + D'\{C(z'-1,t') - C(z',t')\} \quad (7)$$

境界条件1：x' = 1でC = 0、

境界条件2：x' = z'（z' = z/dx, z=ガラス容器の高さ 8 cm）で$\partial C/\partial x = 0$、拡散係数D=0.099$cm^2 \cdot s^{-1}$、D'はD=$(dx)^2(dt)^{-1}$D'となる無次元数である。

しかしこの条件では、実際の濃度の減少の方が速かった（図6A）。一方、ガラス容器内の自然対流の可視化を実験的に見積もったところ、その流速は平均V=1 $cm \cdot s^{-1}$であった。この時、理論的には境界層の厚さは2.4 cm付近と見積もることが出来、この対流を入れて計算を行なった。すなわち、境界層の厚さをk番目の位置までとし、ガラス容器上部までの残りの空間（k' < x' < z'）は境界層内の濃度変化を希釈すると仮定する（式8）。

$$C(k',t'+1) = C(k',t') + D'\{C(k'-1,t') - C(z',t')\}/(z' - k') \quad (8)$$

その結果、境界層δc=1.5cmとすると実験を良く再現出来た。（図6C）

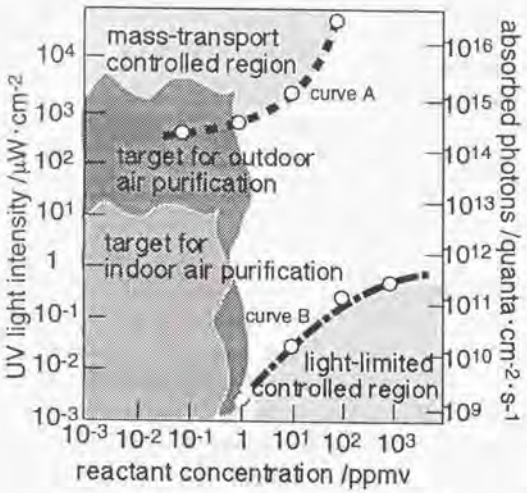

図7　光量律速反応と拡散律速反応の条件を反応物濃度と光強度の関係から表した図（カーブA：拡散律速の境界条件、カーブB：光量律速の境界条件）

	最大反応速度に影響を与える要因	各律速条件の境界となる光量に影響を与える要因
拡散律速領域	拡散係数（境界層厚一定の時）	膜厚
		表面積
		吸着水量
		表面水酸基量
		吸着酸素量
光量律速領域	金属担持	膜厚
	格子欠陥	表面積
	吸着水量	吸着水量
	表面水酸基量	表面水酸基量
	吸着酸素量	吸着酸素量

表2　拡散律速・光量律速条件に影響を与える様々な要因

また、アセトアルデヒドの分解反応においても同様に異なる光量で分解実験を行なったところ、その拡散律速時の反応速度は、同じ初期濃度の2-プロパノールの速度とほとんど同じであった。気相分子の拡散係数D=0.1 $cm^2 \cdot s^{-1}$が分子種にほとんど依存しないことを考えると、図5から得られる拡散律速条件は全ての気相分子に通用できると予想される。

4．まとめ

以上の結果を基に、反応物濃度と光強度をx、y軸にとって完全な光量律速条件と完全な拡散律速条件を図示したものが図7である。拡散律速条件を分けるカーブ（カーブA）は濃度の増加に伴って急激に増加した。一方、完全な光量律速条件を分けるカーブ（カーブB）は、濃度が増加すると光量の増加率は減少することがわかった。量子効率は反応物の吸着分子数と吸収光子数の比によって決まるので、この光量律速に入る光強度は、吸着分子数によって決まっている。この図で横軸は気相濃度であるので、このカーブの形は、Langmufr型の吸着等温線の形を反映している。

さらに、カーブAの増加率が減少すると、カーブBの増加率が急激に上昇するという相互関係があることが読み取れる。これは、気相からの反応物の流束の増加に対して表面反応速度が上回って拡散律速に入るためには、より多く光子数が必要となるためである。

なお、反応速度は、膜厚や表面積に依存する。また、酸素や湿度の影響を受ける。すなわち、各律速条件の境界光量はそれらに応じて変化するだろう。しかし、光量律速や拡散律速の反応速度の最大値は、電荷分離効率、そして気相拡散係数のみにそれぞれ依存すると考えられる（表2）。

5．結論

本研究より、気相中の極低濃度の反応物がTiO_2光触媒の表面にまばらに吸着していても、非常に少ない光子から生成した·OHが広く表面拡散して効率良く反応するモデルを立てることに成功した。また、静置系での触媒表面への物質供給モデルも、移動速度論を基に立てることができた。これらの結果より、我々が目指すTiO_2を用いた環境浄化システムの速度論的解析が可能となった。

6．発表状況

(1)"Kinetics of photocatalytic reactions under extremely low-intensity UV illumination on titanium dioxide thin films"
Y. Ohko, K. Hashimoto, and A. Fujishima
J. Phys. Chem. A 101, 43, 8057, 1997.

(2)"Kinetic analysis of photocatalytic degradation of gaseous 2-propanol under mass-transfer-limited conditions with TiO_2 film photocatalyst"
Y. Ohko, K. Hashimoto, and A. Fujishima
J. Phys. Chem. in press.

(3)"Autoxidation of acetaldehyde initiated by TiO_2 photocatalysis under weak UV illumination"
Y. Ohko, D. A. Tryk, K. Hashimoto, and A. Fujishima
J. Phys. Chem. accepted.

(4)"Photokilling effect of titanium dioxide containing papers"　投稿準備中

参考

(5)"Thermal variation of free-volumess size distribution in polypropylenes probed by positron annihilation technique"
Y. Ohko, A. Uedono, and Y. Ujihira
J. Polym. Sci. B: Polym. Phys., 33, 1183 , 1995.

(6)"陽電子消滅によるアイオノマーの自由体積の評価"
古崎典子, 大古善久, 氏平祐輔
高分子論文集, 969, 50 (1993).

Preface

Photocatalytic reactions using TiO_2 semiconductor have been studied intensively as one of the light-energy conversion technologies to solve the environmental problems. In the present study, reaction dynamics under weak UV illumination on TiO_2 film photocatalyst was treated. This is because a unique type of passive-type purification system for indoor working and living environments using essentially transparent titanium dioxide (TiO_2) with large area and under daily weak UV light has been received much attention recently. Many different types of TiO_2-coating building materials incorporate deodorizing, antibacterial and self-cleaning functions and are also "maintenance free" semipermanently. The combination of TiO_2 and weak UV light is safe for the human body and for our environment, a feature which is distinct from other purification techniques, for example, the use of sterilizing lamps and chemical oxidants such as ozone, chlorine, and so forth.

Here, I present the kinetics of the degradation of gaseous organic molecules mainly, which were investigated using TiO_2 film photocatalysts in a batch-type reaction system, and then new types of reaction dynamics on the TiO_2 surface were examined. The consideration of the degradation rate from the standpoint of the relative magnitudes of the numbers of absorbed photons and the numbers of adsorbed or impinging reactant molecules on the TiO_2 surface is an important characteristic of this study. This is different to the other research concerning to TiO_2 photocatalyst. Needless to say, other researchers have not paid much attention to such a slow reaction under weak UV light, either experimentally or theoretically. However, in the nearly 30 years since the discovery of photocatalytic water cleavage on TiO_2 electrodes, the reaction dynamics and reaction mechanisms on the TiO_2 surface were believed so complicated and so difficult to solve that, in fact, the most important factor

dominating photocatalysis has not been proven yet.

Chapter 1 is prepared as a general introduction to the present study. I describe, here, the principle of TiO_2 photocatalysis and the basic viewpoints of the quantum yield and the motivation of this study. In order to provide background for the necessity to solve the photocatalytic dynamics under low-intensity UV light, the previous studies reported for the purpose of water and air purification are overviewed in terms of the reactant concentration of target molecules and the UV light intensity, and the transition for use of TiO_2.

In Chapter 2, the new reaction dynamics on the TiO_2 surface under extremely low-intensity UV light illumination are described, which was solved out for the first time. Specifically, the quantum yield of gaseous 2-propanol decomposition is found to be determined by the ratio of the number of absorbed photons to the number of adsorbed reactant molecules. From these results, the charge-separation efficiency and the diffusion length of ·OH radicals on the TiO_2 surface are able to be discussed for the TiO_2 thin film. To help readers in understanding these findings easily, the preparing procedure of the TiO_2 sample film and its characteristics, and the estimation of absorbed photon numbers are explained in this experimental section.

In contrast to Chapter 2, the completely mass transport-limited conditions are investigated experimentally when relatively-higher intensity UV illumination was employed in Chapter 3. Mass-tranfer of gaseous reactants is influenced by velocity of air-flow. As described in detail in Section 3.4.1., I compare the mass transport-limited conditions under natural- and forced-convection flow and the time course of 2-propanol concentration changes in a 1-liter reactor under mass-transport-limited conditions is modeled well using the one-dimensional diffusion equation, considering the thickness of the boundary layer. Moreover, as a short summary at this stage, I depict these two regions of mass-transport-limited conditions and of purely light-limited conditions for the photocatalytic degradation of gaseous organic molecules as functions of the reactant concentration (x-axis) and the UV light intensity (y-axis) in Section 3.4.2. From the graphical representation, one can estimate the maximum value of light intensity necessary to obtain the maximum reaction rate for a given target concentration of reactant.

I tried applying this new model for the reaction dynamics on the

TiO_2 surface under weak UV light to the degradation of another gaseous reactant, acetaldehyde. This is because acetaldehyde is decomposed with a radical-chain mechanism (autoxidation mechanism) in air in contrast to 2-propanol. I discuss the degradation mechanism dependent on the light intensity and the reactant concentration, and the chain length of the radical reaction for production of acetic acid. These results are described in Chapter 4.

In Chapter 5, anti-bacterial effects are examined in order to determine whether they are also dependent on the concentration of *E. coli* cells and light intensity, using TiO_2 containing papers.

I summarized the results of the present dissertation in Chapter 6. Finally, the possibility of this unique purification system in the practical environments and how to develop a more effective purification system are described.

I have described this dissertation for the degree of Doctor of Philosophy not like enumeration of my innumerable results and efforts but to try explaining the procedure of experiments as followers will be able to review them, displaying the meaningful results simply and accurately, and discussing them logically as far as possible. Actually, the reaction rate is so slow that I spent longer time than nobody can expect. However, by showing the reliability of my experimental results and the rationality of discussion here , I hope that followers will derive another new finding of photocatalysis spending their shorter time than I did, and my work will go a long way toward developing the field of photocatalysis.

Contents

List of Figures

List of Tables

Chapter 1

Principle

1.1 Photocatalytic reaction

It is well known that when UV light irradiates a n-type TiO_2 electrode using a mercury lamp under a small electrochemical bias, hydrogen (H_2) gas and oxygen (O_2) gas are generated from the Pt electrode and from the TiO_2 electrode, respectively . The redox reaction starts from an electron-hole pair generation when photons with energies greater than the bandgap are absorbed in TiO_2 semiconductor:

$$h\nu \longrightarrow h^+ + e^- \tag{1.1}$$

which electron and hole react with the substrates, H^+ and H_2O at the interface, respectively:

$$2h^+ + 2H_2O \longrightarrow \frac{1}{2} O_2 + 2H^+ \tag{1.2}$$

$$2e^- + 2H^+ \longrightarrow H_2 \tag{1.3}$$

Especially, water decomposition reaction using TiO_2 electrodes like this is called the Honda-Fujishima effect. [2] This important thing is that a reaction ($H_2O \rightarrow H_2 + \frac{1}{2}O_2$ with the Gibbs energy of 56.7 kcal mol^{-1}) can be driven by the assistant energy of photons without heat. As proven from above, this "photocatalytic" reaction is to convert the energy of light into electrochemical energy. This circuit is called "a photoelectrochemical cell" (Figure1.1).

The possibility and selectivity of redox reaction depends on the energy position of their respective energy band edges, the conduction band ($C.B.$) for electrons and the valence band ($V.B.$) for holes. Then Band edge positions of several semiconductors and oxidation potentials of organics are shown in Figure 1.2

Another important term is a space charge layer to influence the charge separation efficiency in photocatalysis. The electron-hole pairs are efficiently separated by the energy band bending at the space charge layer whose width (d) is given by the following equation,

$$d = \left(\frac{2\varepsilon\varepsilon_0 \Delta V}{qN_0} \right)^{\frac{1}{2}} \tag{1.4}$$

where ΔV is the potential drop in the space charge layer, q is the elementary charge, N_0 is the concentration of the majority charge carriers, and e and e_0 are the static dielectric constants of the semiconductor and the permittivity of vacuum, respectively. As proven by the eq. 1.4, the width of space charge layer depends on the donor concentration and the height of the band bending. The electrons separated by the band bending at the space charge layer move to the counter Pt-electrode by the applied bias and are consumed for the hydrogen evolution. Therefore only the photogenerated holes can move to the surface to cause oxidative oxygen evolution from water as shown in Figure1.1-(1). This redox reactions also occur using small particles and thin films of semiconductor as shown in Figure1.1-(2). However, for a small particle and a thin film with a size (thickness) less than 1 mm, however, the situation is quite different. If the radius (thickness) is smaller than the thickness of the space charge layer formed in the TiO_2 electrode (given by the equation 1.4), the potential drop in the semiconductor becomes small. Under these conditions all the donors are ionized and there are no electrons left in the conduction band. The total absence of electrons in the conduction band and the small value of potential difference inside the semiconductor has the important feature of the small size photocatalyst. In the case of colloidal semiconductors the band bending is small and charge separation occurs via diffusion only. Applying a random walk model to describe the motion of the charge carriers, one obtains for the average transit time from the interior of the

particle to the surface the expression

$$\tau_d = \frac{{r_0}^2}{\pi^2 D} \tag{1.5}$$

, where r_0 is the distance from the center of the particle and D is the diffusion coefficient of electrons in TiO_2 (0.02 $cm^2\ s^{-1}$). For colloidal semiconductors td is at most a few picoseconds. [3] Thus for colloidal TiO_2 with a radius of 10 nm, the average transit time of electron is ca.100 ps. On the other hand the time of electron-hole recombination process is reported 10 ns inside a semiconductor. [4,5] Then it is reasonable to see that recombination reaction can't occur inside the particle of photocatalyst. However when the space charge layer given by the equation1.4 is thick enough, its electric field pushes the electrons back to the bulk of the semiconductor. Under these conditions only the holes are consumed to oxidize chemical species, but the electrons are not, resulting in the accumulation of the electrons in the semiconductor in principle.

Furthermore, the surface of the TiO_2 photocatalysts usually contain a lot of coordinatively unsaturated bonds whose energy levels locate in the forbidden zone of the ideal semiconductor. These surface states mediate the electron transfer from the semiconductor to the solution upward the bending of the band.

Photogenerated electrons and holes, migrated to the surface by the mechanism mentioned above, soon recombine as follows,

$$h^+ + e^- \longrightarrow \text{heat} \tag{1.6}$$

unless the adequate surface traps of the electrons or the holes exist on the surface before electrons transfer between the adsorbed subjects and TiO_2. Reactions on the TiO_2 surface trapping process of the electrons and the holes is competitive to electron-hole recombination. Therefore, retardation of the recombination process by supplying electron captures sufficiently [6–8] and by creating surface traps, for example deposited metals, [9–18] is essential for the enhancement of the photocatalytic efficiency to use for air and water purification. The process of photocatalytic reactions can be summarized in Table 1.1.

Table 1.1: The process of photocatalytic reactions

1) production of electron-hole pairs, generated by absorption of light energy
2) migration of the electrons and the holes to the surface
3) charge separation of electrons and holes by traps available on the TiO_2 surface
4) a redox process by the separated electrons and holes with species on the surface
5) desorption of the products and reconstruction of the surface

1.2 Quantum yield

The primary term of photocatalytic efficiency is the quantum yield (QY). Gerischer has discussed the quantum yield in dependence of the light intensity, the radius of the semiconductor particles assumed as spherical and the rate constants of the various reactions as follows. [19–21]

The driving force of photocatalysis by semiconductor particles is the excess free energy of electron-hole pairs generated in the particles by light absorption. This energy $n_s p_s / N_c N_v$, where n_s and p_s are the surface concentrations of electrons and holes on the irradiated particles, N_c and N_v are the respective densities of states in the conduction and valence band. The quantum yield is determined by the competition between the individual reactions of electrons and holes at the surface of the particles and their recombination in the bulk or at the surface. The individual reaction of electrons are the reduction of the electron acceptors, in practical systems of oxygen, those of holes the oxidation of electron donors, in practice organic or inorganic molecules or ions.

The quantum yield under high intensity UV light can be described in dependence of the marameter, m, as follows. The slowest reaction of the electronic charge carriers is assumed, then if the competition between charge transfer reactions and recombination is characterized like below:

$$k_{const} c_s + k_{sr} c_s^2 + \frac{k_r}{R} c_s^2 = \frac{gR}{3} \tag{1.7}$$

$$k_{const} = k_{ox} c_D = k_{red} c_A \tag{1.8}$$

where c_D is the concentration of donor, c_D is the concentration of acceptor, R is the radius of the semiconductor.

$$\textit{an electron hole generation rate} = \frac{4}{3}\pi R^3 g \tag{1.9}$$

where g is an approximately homogenerous rate electron hole pair generation. Then the decisive equation for quantum yield is:

$$\phi = \frac{1}{2m}(\sqrt{1+4m} - 1) \tag{1.10}$$

$$m = \frac{k_s r + \frac{k_r R}{3}}{k_c t} \frac{gR}{3k_c t} \tag{1.11}$$

Increasing k_{ct} reduces m and is very favorable for the yield. Increasing light intensity and light absorption has the opposite influence as also increasing R. The influence of R, however, does not exist for the volume recombination but only for the surface recombination. Besides, the smaller particle is better because some primary products such as $HO_2\cdot$ is difficult to accumulate that induce the reverse reaction ($h^+ + A^- \rightarrow A$).

The photogenerated electron-hole pair disappears through (1) the reaction with substrates, (2) the bulk recombination, and (3) surface recombination. The other considerable factors to influence quantum yield are listed in table 1.2.

The apparent QY values[1] are calculated using the following equation:

$$\begin{aligned} \mathrm{QY} = \; & \Sigma_{(\text{all products})} \; (\text{participating } h^+ \text{ number per product}) \\ & \times \quad \frac{\text{number of product molecules}}{\text{number of absorbed photons}} \end{aligned} \tag{1.12}$$

, which means how much effectively the reaction products generate by one photone being absorbed. Needless to say, this calculation should be based on the reliable reaction mechanism. There is one example to calculate of CO_2 generation from CH_3COOH degradation as follows:

[1]They usually use the term, "the apparent QY." This is because they usually detect the concentration changes in the bulk, not on the surface and because they cannot estimate the reverse reactions. It is ideal that the mass of decomposition and generation is balancing. However the reaction products often distribute and they doesn't desorb to the bulk in heterogeneous reaction.

Table 1.2: The influencing factors to quantum yield

1) the energy band for holes and the conduction band for electrons
2) the concentration of the reaction partners at the interface
3) reverse reactions for electrons with the oxidation products of holes
4) reverse reactions for holes with the reduction products of electrons
5) volume recombination
6) surface recombination
7) defects in particles
8) particle size or surface area
9) depositing metal clusters
10) reaction rates of substrates
11) excess charges of particles
12) desorption of byproducts on particles
13) slow mass transfer of reactants to particles

$$CH_3COOH + 8\ h^+ + H_2O \longrightarrow 2CO_2 + 8\ H^+ \tag{1.13}$$

$$QY = 4 \times \frac{\text{number of } CO_2 \text{ molecules}}{\text{number of absorbed photons}} \tag{1.14}$$

which is based on the hypothesis of only hole oxidation. However as I demonstrate in Chapter 4, like this estimation includes misunderstanding as if photocatalysis is much effective system than other energy conversion system. This is why recently it used to be proved that organic molecules are decomposed via. some radical chain reactions on TiO_2 surface.

1.3 Reaction mechanism

As seen from Figure 1.2, TiO_2 (~3.0 V vs. SCE) has beneficial characteristics of the strong oxidizing power of the photogenerated holes, with which almost organic compounds can be oxidized to carbon dioxide at ambient temperature and pressure.

Heterogeneous photocatalytic oxidation of single compound feeds has been previously demonstrated for alcohols, [?, 1, 22–48] inorganics, [49–

51] and bacteria [52–58] There are two oxidation pathways of organic molecules via direct oxidation by photogenerated holes thermodynamically and via reaction with ·OH radical produced subsequently. In the liquid phase, the order of anordic oxidation rate for organics depends on the turn of the electrolytic dissociation, R(CO)OH ¿ H_2O ¿ ROH, RR'O. For example, so-called photo-kolbe reaction of acetic acid is well know as follows,

$$CH_3(CO)O^- + h^+ \longrightarrow CH_3(CO)O\cdot \longrightarrow CO_2 + CH_3\cdot \qquad (1.15)$$

In contrast, the main pathways in degradation of alcohols are discussed via ·OH radical reaction, while their direct oxidation appears only in the case of high concentration of reactant on the surface.

So far, the degradation mechanism of organic molecules on the TiO_2 photocatalyst had seemed to be also complicated. However, recently it has been proved and acknowledged widely that not only holes but also electrons participate in the oxidation reaction and that molecular oxygen has two rules: it accepts the electron generated in a TiO_2 crystallite and is reduced to a superoxide radical (O_2^-, HO_2); and it combines with the organic radical, generated upon the hole or ·OH radical reaction with the reactant, to produce an organoperoxyradical (ROO·).

Under the ambient conditions, photocatalytic degradation of organic molecules follows the typical reaction mechanism of small hydrocarbons. Here I introduce the degradation mechanism of ethanol using TiO_2 photocatalyst as a typical example to explain my experimental data in Chapter 2-5.

Reaction mechanism of ethanol photocatalytic decomposition

At first, the photogenerated holes oxidize surface hydroxyl groups or adsorbed water as follows,

$$h^+ + OH^-(s) \longrightarrow \cdot OH, \text{ or } h^+ + H_2O \longrightarrow \cdot OH + H^+ \qquad (1.16)$$

α hydrogen atom is split off from ethanol by an ·OH radical,

$$CH_3CH_2OH + \cdot OH \longrightarrow CH_3C\cdot HOH + H_2O \qquad (1.17)$$

Then the ethanol radical can combine with molecular oxygen to produce an organoperoxy radical,

$$CH_3C{\cdot}HOH + O_2 \longrightarrow CH_3CH(OH)OO{\cdot} \tag{1.18}$$

This organoperoxy radical react with other ethanol molecule, producing an acetaldehyde and H_2O_2. Thoroughly the chain reaction, in other words, auto-oxidation of ethanol will proceed,

$$CH_3CH(OH)OO\cdot + CH_3CH_2OH \longrightarrow CH_3C{\cdot}HOH + CH_3CH(OH)OOH \tag{1.19}$$

$$CH_3CH(OH)OOH \longrightarrow CH_3CHO + H_2O_2 \tag{1.20}$$

Ikeda et al. observed concentration changes in the photocatalytic reaction of ethanol of dissolved O_2 near the surface of a partially Pd-covered TiO_2 film using microelectrode techniques. It was found that dissolved O_2 consumed not only over Pd-covered surface (reduction cite) but also over the bare TiO_2 (oxidation site). [59] In the similar fashion, photogenerated $HO_2{\cdot}$radical generated via equations and may also react with the $CH_3CH(OH)OO{\cdot}$ radical,

$$e^- + O_2(s) \longrightarrow {O_2}^- \tag{1.21}$$

$${O_2}^- + H^+ \longrightarrow HO_2{\cdot} \tag{1.22}$$

$$CH_3CH(OH)OO\cdot + HO_2{\cdot} \longrightarrow CH_3CH(OH)OOOOH \tag{1.23}$$

The unstable tetraoxide is decomposed quickly to acetaldehyde and H_2O_2,

$$CH_3CH(OH)OOOOH \longrightarrow CH_3CHO + O_2 + H_2O_2 \tag{1.24}$$

These reaction pathways are well-known as the Russel reaction[2] that is the autoxidation reaction of hydrocarbons in the presence of oxygen as shown like below. [60–62] This mechanism is also able to be applied to

[2]Tetraoxides have been widely studied and are accepted intermediates in the radiolysis of aerated aqueous solutions containing organic compounds.

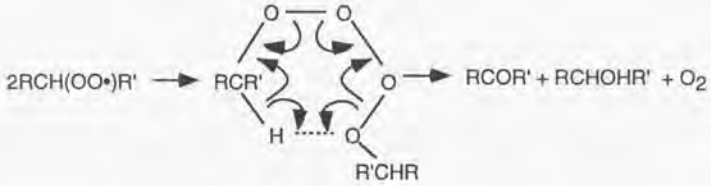

Russel reation

photocatalytic oxidation of another organic molecules such as aldehydes, ketones and so on. Another important reaction pathway exist, which is the so-called current-doubling reaction, expressed by

$$CH_3C{\cdot}HOH \longrightarrow CH_3CHO + H^+ + e^- \text{ (C.B.)} \qquad (1.25)$$

The current-doubling reaction tend to occur in photocatalytic degradation of first- and second-class alcohols, aldehydes, and holmic acid. Because the energy level of unstable organic radicals is higher than that of the semiconductor conduction band as shown in Figure1.2, unstable intermediate radicals release one electron into TiO_2 via only one-photogenerated hole oxidation. The apparent QY of this reaction is approached up to 200%. These degradation pathways of ethanol are summarized to show in Figure 1.3. [63] In this dissertation, 2-propanol was chosen as a unique model reactant because a single photon is considered to participate in the generation of each acetone molecule, and its auto-oxidation is negligible in Chapter 2. In contrast, acetaldehyde was also chosen as another unique model reactant because of its autoxidation mechanism in Chapter 4. I summarized these reaction pathways of organic compounds in Table 1.3.

1.4 Kinetics of heterogeneous photocatalysis

Generally speaking, kinetic study provide a reaction rate constant that is useful for both the scientists and the chemical plant designer to

Table 1.3: The reaction mechanism of organics in photocatalytic reactions[a]

current-doubling reaction
$CH_3C{\cdot}HOH \longrightarrow CH_3CHO + H^+ + e^-$ (C.B.)
alkane
$RCH(OOOOH)R' \longrightarrow RCOR' + O_2 + H_2O$
alcohol
$RCOH(OOOOH)R' \longrightarrow RCOR' + O_2 + H_2O_2$
ketone
$RCH_2COCH(OOOOH)R' \longrightarrow RCHO + R'CHO + CO_2 + H_2O$
carbonic acid
$RCH_3COOH + h^+(\cdot OH) \longrightarrow RCH_2\cdot + CO_2 + H^+$
$RCH_2\cdot + O_2 + \longrightarrow RCH_2OO\cdot$
$RCH_2OO\cdot + \cdot OOH \longrightarrow RCH_2COOOOH$
$RCH_2COOOOH + RCH_2COOOOH \longrightarrow RCHO + RCH_2OH + H_2O + O_2$
hydrocarbon chloride
$Cl\cdot + CH_3Cl \longrightarrow HCl + \cdot CH_2Cl$

[a] from the state of tetraoxides

control and conjugate the reaction safety and repeatedly. In heterogeneous TiO_2 photocatalysis, the popular isotherm and reaction equation are Langmuir-type adsorption isotherm and Langmuir Hinshelwood equation, respectively. Reaction rate on the photocatalyst surface depends on not only the band edge position but also the concentration of the reactants at the interface. It is easy to think about the faster surface reaction proceeds under the more adsorbed molecules of reactants. However, the important thing is that there is the region of experimental condition that the reaction rate is purely proportional to only absorbed photons, not concerning the reactant concentration at all.

1.4.1 Langmuir-type adsorption isotherm

In a number of the earlier literature, the adsorption isotherm of organic molecules on the TiO_2 surface is well described the Langmuir-type isotherm as follows,

$$M = \frac{\mu TC}{1 + TC} \tag{1.26}$$

, where M is the weight of adsorbed 2-propanol on the TiO_2 thin film (mg^{-1}), C is the reactant concentration (mg m^{-3}) in the bulk, μ is the maximum weight of molecules in an adsorbed monolayer, for a given TiO_2 sample, and T is the adsorption binding constant. This equation assumes an adsorption state of equilibrium. A standard means of using this equation is to demonstrate linearity of the data when plotted as the inverse initial rate versus inverse initial concentration,

$$\frac{1}{M} = \frac{1}{\mu} + \frac{1}{\mu TC} \tag{1.27}$$

which requires both a positive slope $(= (\mu T)^{-1}]$ and intercept (μ^{-1}) as shown in Figure 2.4 in Chapter 2.

1.4.2 Langmuir Hinshelwood equation

As proved from above, in the analysis of heterogeneous kinetics of photocatalyzed reactions, a number of the earlier literature results were fitted by a simple rate equation of the form:

$$rate = r = \frac{kI_{abs}{}^{\alpha}KC}{1+KC} \tag{1.28}$$

, where k is reaction constant, K is adsorption binding constant. r is proportional to the amount of adsorbed reactants, [1,39,40,40–43,45, 64] , while the value of the exponent power of light intensity ($I_{abs}{}^{\alpha}$) in this equation is well known in heterogeneous photocatalysis, that, under light-rich conditions, the reaction rate is often characterized by an a value of 1/2 due to domination by the second-order-dependent carrier-recombination process. Since there is negligible recombination at sufficiently lower light intensities, QY value should be close to unity, in other words, $\alpha = 1$.

I suppose it is difficult fo obtain a single product under sufficiently high intensity of light conditions , misleading the evaluation of QY values because the photocatalytic decomposition of organic materials is so complicated. For example, ethanol is photooxidized though a multispecies network including acetaldehyde, formaldehyde, and carbon dioxide as shown previously. Several of the intermediates and products adsorb simultaneously on the adsorption site of a given reactant, then the reaction equation can be transformed as follows,

$$r = \frac{kI_{abs}{}^{\alpha}KC}{1+\sum_{(all\ reactants)} K_iC_i + \sum_{(all\ intermediates)} K_jC_j + \sum K_sC_s} \tag{1.29}$$

, where K_i and C_i are binding constant and concentration of i-th reactant,K_j and C_j are those of j-th intermediates, K_s and C_s are those of solvents including O_2, water, and other inhibitors, respectively. [65–72]

From analysis using this equation, three kinds of information are obtained as follows; (1) the rate constant and binding constant for a given reactant from its initial degradation rate, (2) variety of adsorption site, (3) the concentration changes modeling oxidation kinetic networks. Ohtani et al. reported the analysis results assuming 2 kinds of adsorption site for 2-propanol, one is competitive with water in solution. [69] Ollis et al. modeled the ethanol and acetaldehyde photocatalyzed oxidation kinetic networks using this Langmuir-Hinshelwood rate forms combined with adsorption isotherms for reactant, intermediates, and product CO_2, as shown for an example in Figure 1.4. [1]

$$r = kI_{abs}{}^{a}\left(\frac{KC}{1 + \sum_{(all\ reactants)} K_i C_i + \sum_{(all\ intermediates)} K_j C_j + \sum K_s C_s}\right)^{n} \tag{1.30}$$

It is not too much say that the number of absorbed photons are rate-determining in photocatalytic reaction. In conventional, almost researchers employed the strong UV light sources for sufficient reaction rates to TiO_2. However, available information of reaction dynamics on the TiO_2 surface dependent on light intensity has not been discussed quite well so far. [73–87]

It should be noted that Nosaka et al. reported that the Langmuir-type relationship between the reaction yield and the reactant concentration is not applicable at higher photon fluences. [88–92] Transient absorption after laser pulse was measured for various methylviologen (MV^{2+}) concentrations at various photon fluences. The fast electron transfer can occur only for adsorbed molecules and diffusion of viologen was also reported to control the reaction in the μs-ms range at very high photon fluences. [93–97] For the surface electron transfer at illuminated colloidal semiconductor particles in the case of colloidal CdS to MV^{2+} within 100 ps in aqueous solution was observed by a picosecond transient absorption measurement. [98] The study on the fluorescence quenching with MV^{2+} revealed that the electron transfer is as fast as the rate-determining step of the fluorescence or the rate of releasing electrons from the shallowest traps which is formed within 10^{-13} s. [99] It means when the diffusion rate is low, the mass-transfer process of reactants, O_2 and organic molecules, could tend to be rate limiting step and one should not be apply the analytical equation of Langmuir-Hinshelwood type.

The extremely high values of QY of gaseous phase photocatalytic reaction exceeding 100% have become reported these days. However, those estimations include the several factors due to errors of estimation of absorbed photons, and those of calculation caused by the current doubling effect and radical chain reactions. Besides, the number of absorbed photons is difficult to estimate because of the high refraction factor (2.7) of TiO_2 in general.

1.5 Motivation

1.5.1 Background

The phenomenon of photooxidation was observed and recognized in 1921 by Renz [100], who oxidized many organic molecules in the presence of TiO_2 and ultra-violet light. Later, the photocatalyzed reactions on the irradiated TiO_2 surface have been paid significant attentions since the discovery by Honda and Fujishima in 1972. [2] They reported that water could be split upon the illuminated TiO_2 single-crystal electrode under a small electrochemical bias. This observation prompted extensive work focusing on efficiently production of hydrogen from the point of solar energy conversion. [30, 101–105]

Few years after that, it was also shown that the heterogeneously dispersed TiO_2 semiconductor particles could also activate other molecules, whose redox reactions would be beneficial not only for energy storage, but also for organic synthesis, detoxification of hazard compounds, water purification. Furthermore, TiO_2 films, prepared by coating microcrystalline TiO_2 on the various substrates, have gathered much attention as the photocatalysts especially for the degradation of the organic impurities and the hazardous compounds using its strong oxidation power in recent years.

Unlike dispersed powders, the film catalysts have the advantages such that they can be used repeatedly without problem in terms of separation from the solution after treatments. I illustrated the study history of TiO_2 from the point of the transition of employment in Figure 1.5.

However, the disadvantage of photocatalysis using semiconductor is its low photocatalytic efficiency. Recently Bolton el al. reported the QY value of 0.04 for ·OH radical generation using TiO_2 colloids. [106, 107] Traditionally, high pressure mercury and xenon lamps have been used in most photocatalytic research for the purpose of high-rate photodecomposition and also to compensate for the low photocatalytic efficiency of TiO_2 itself. In recent years, since Heller et al. reported the oxidative stripping of oil sheens from the surface of sea water with buoyant photocatalyst-coated ceramic microbubbles, [8] the field of environmental purification has been devoting increasing attention to photocatalysis using sunlight and black-light-type fluorescent lamps as UV light sources, i.e., at the sev-

eral mW cm^{-2} level, which is safe for human exposure. The phenomenon that the QY values increase with decreasing UV light intensity has been recognized since before, however, its reason is explained irresponsiblely that the frequency of recombination reaction of electrton-hole pair inside TiO_2 decrease with decreasing number of absorbed photons. However any scientists have not switched their idea to the new system under weak UV light that our group has been proposed as mentioned below. Overviewing the region of research as a function of light intensity and reactant concentration in Figure 1.7, the area which consists of high intensity of light and high concentration of reactant is characteristic of their research. Even for low concentration of reactant, they used to employ strong UV light sources. Then, the dynamics and mechanism of TiO_2 photocatalytic reaction under strong UV light reported previously are so complicated that the most important factor determining the photocatalytic reaction efficiency has not been solved by a number of extensive research during almost 30 years since the discovery by Honda and Fujishima.

In contrast, I have been aware of that photocatalytic reaction proceeds at a sufficient rate even under weak UV light since 1992 as shown for examples in Figure 1.6. [108] I directed to construct a new system using TiO_2-containing building materials with a large area. It is a unique type of passive-type purification system for indoor working and living environments which incorporates deodorizing, antibacterial and self-cleaning functions under lower level illumination from room light. In connection with this concept, many different types of TiO_2 materials which exhibit higher photocatalytic activities than P-25 powder, which is known for its highly photocatalytic activity, have been prepared. [33–35, 108–110] For example, the QY value of close to 100% have been achieved under 0.5 mW cm^{-2} irradiance for 1000 ppmv gaseous acetaldehyde decomposition using TiO_2-containing paper and semi-transparent TiO_2 thin films formed on glass. In addition, I have found that *E. coli* cells can be completely killed on TiO_2 coated glass tiles even under room light. I illustrate the imaging space of the new purification system using these materials in Figure 1.8.

As seen in Figure 1.7, the region of our research which consists of low intensity of light and low concentration of reactant is completely distinct from those in many other reports. There is few fundamental research of reactions under weak UV light theoretically and experimentally so far. However new aspects of photocatalysis can be expected to be dis-

covered using these materials under weak UV illumination down to nW cm^{-2} levels. Therefore I started kinetic study of degradation of gaseous 2-propanol molecules using TiO_2 film photocatalyst in a batch system under weak UV light illumination to discover new reaction dynamics of photocatalytic reaction in Chapter 2 and Chapter 3. 2-propanol was well known to be decomposed to acetone via simple mechanism as described in details in Chapter 2. My unique approach to the region of our research is to consider the degradation rate from the relation between numbers of absorbed photons and numbers of adsorbed or collided reactants on the TiO_2 surface.

1.5.2 Characteristics of TiO_2 photocatalyst

Among several semiconductors, TiO_2 photocatalyst is only gathered much attention to the practical application for water and air purification these days. Many characteristic aspects of TiO_2 photocatalyst are pointed out in Table .

ZnO and CdS photocatalysts have been investigated also extensively for fundamental research in comparison with TiO_2.photocatalyst. [101, 103,111–114] Especially for the solar energy conversion H_2 production using CdS was expected because its bandgap energy is equivalent to visible light with 496 nm-wavelength. However, any excellent material beyond TiO_2 has not found yet. As I know, the values of quantum yield was approximately similar to those semiconductors each other. For example using as electrode of photoelectochemical cell, the photocurrent efficiencies were reported almost same values of $\tilde{1}.0$ for TiO_2, ZnO, and CdS, respectively. [102] On the other hand, using photocatalyst, the values of quantum yield of H_2 production were reported about 0.05. [115, 116] The most negligible problem of the other semiconductors than TiO_2 is unstability via photocorrosion reaction as follows,

$$CdS + 2h^+ \longrightarrow Cd^{2+} + S \tag{1.31}$$

$$h^+ + S^{2-}(s) \longrightarrow S^- \cdot \tag{1.32}$$

$$S^- \cdot + O_2 \longrightarrow S\downarrow + O_2^- \tag{1.33}$$

Table 1.4: Characteristics of TiO_2 photocatalysis

	advantages		disadvantages
(1)	strong oxidation power (~ 3.0 V vs. SCE)	(1)	charking
(2)	no photocorrosion (stable in gas and liquid phase)	(2)	inhibition by some anions (SO_4^-, Cl^-)
(3)	operation at ambient temperature and pressure	(3)	agrigation at medium pH
(4)	heterogeneous reaction (at liquid-solid and air-solid interfaces)	(4)	forbidden three dimensional utility
(5)	safe for human body (food additives)	(5)	a low quantum efficiency
(6)	absorption of UV light	(6)	useless of visible solar light
(7)	low price (ex. 400 yen kg^{-1})	(7)	high reflectivity due to high refractive index (2.7)
(8)	use of oxygen as the oxidant		
(9)	final oxidation products are innocuous (CO_2 and H_2O etc.)		
(10)	transparency (in principle)		
(11)	semipermanent (in principle)		

Especially, CdS and ZnO produce the harmful ions of Zn^{2+} and Cd^{2+}. Therefore the photocatalytic reactions using CdS and ZnO were avoided to use practically because of their characteristics of photocorrosion generating harmful Zn^{2+} and Cd^{2+} irons.

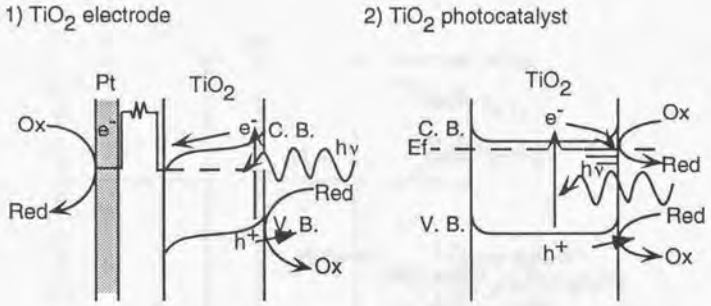

Figure 1.1: Schematic illustration of the energy diagram for a TiO_2 semiconductor electrode and a TiO_2 photocatalyst

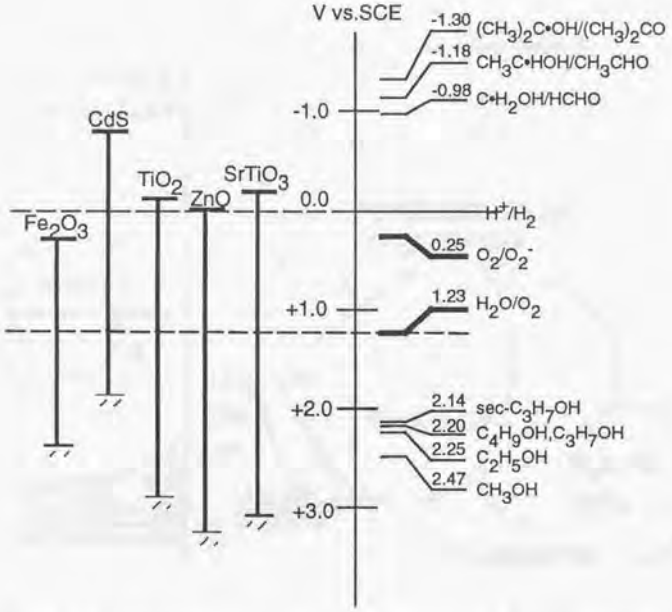

Figure 1.2: Band edge positions of several semiconductors and oxidation potentials of organics

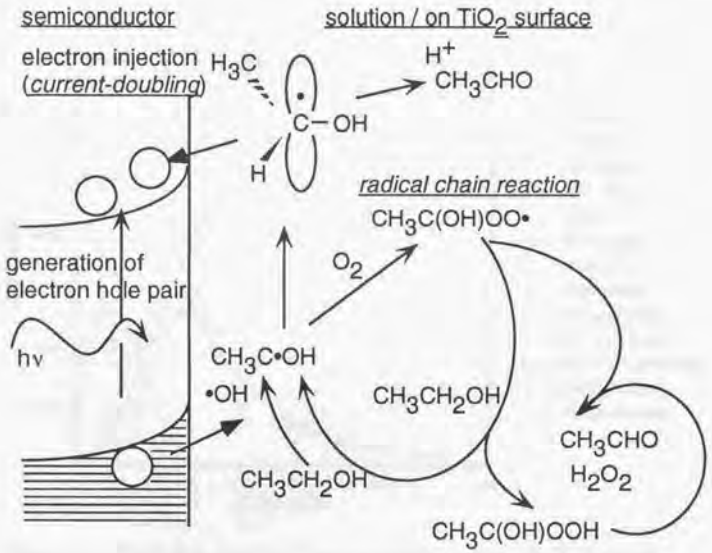

Figure 1.3: Schematic representation of mechanism of photocatalytic degradation of ethanol

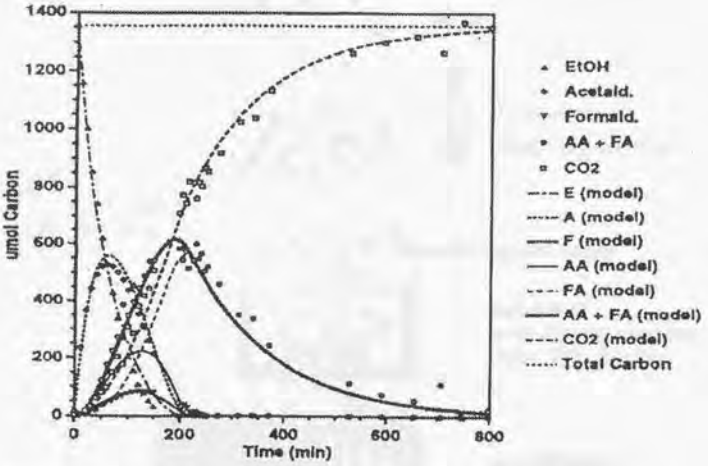

Figure 1.4: Predictive model of the concentration changes of photocatalytic degradation of ethanol. [1]

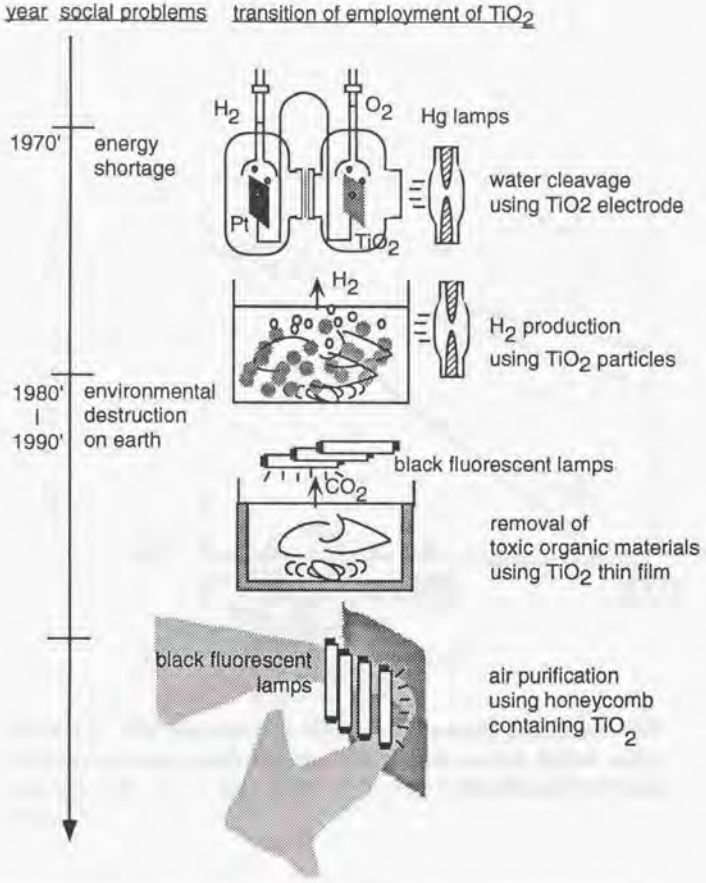

Figure 1.5: Transition of employment of TiO_2 for air and water purification under strong UV light.

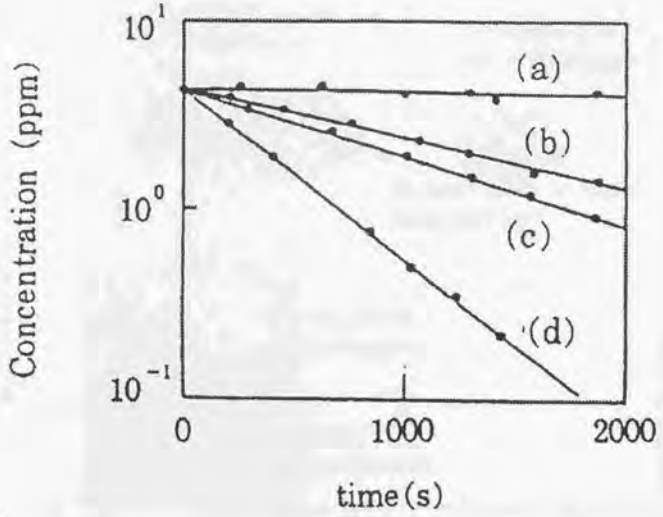

Figure 1.6: The concentration changes of photocatalytic degradation of methylmelcaptan using different type of light sources; a)dark condition, b)pink fluorescent light, c)white fluorescent light, d)black fluorescent light. [108]

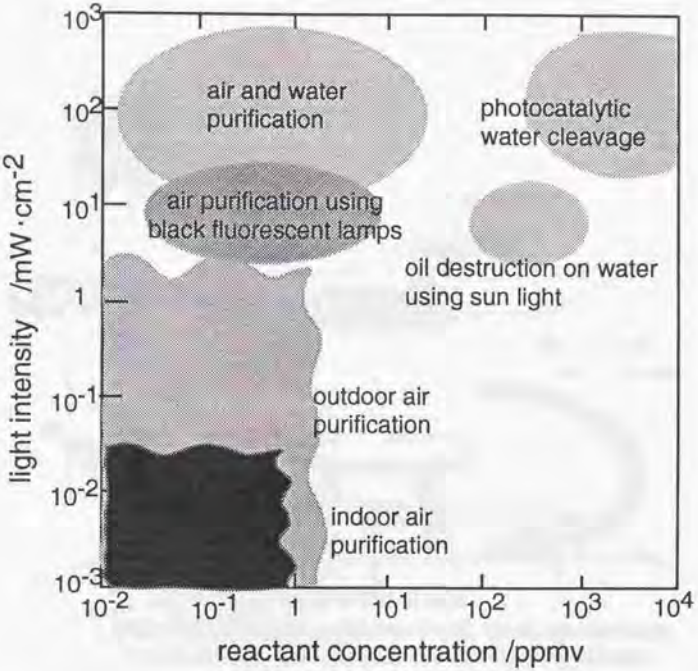

Figure 1.7: Illustration of regions of the previous studies reported for the purpose of water and air purification as functions of the reactant concentration of target molecules and the UV light intensity. (The regions of indoor and outdoor air purification are our target.)

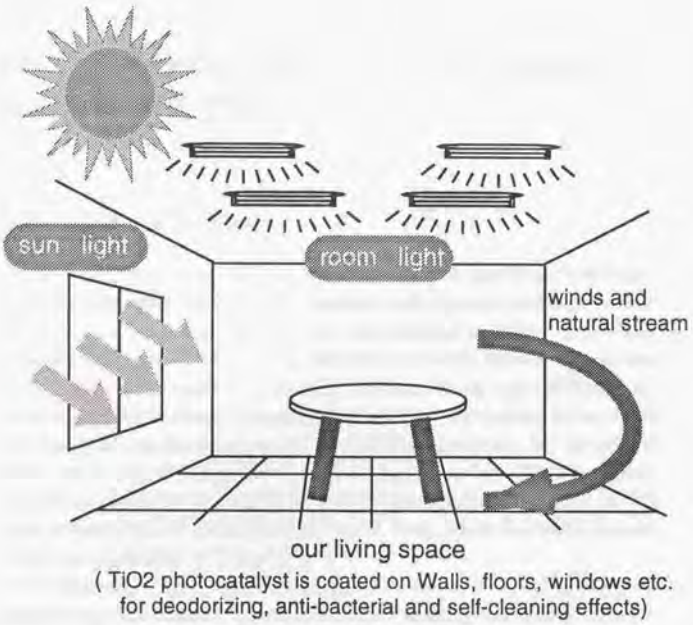

Figure 1.8: Illustration of our proposing system under weak UV light for air purification in our living space.

Chapter 2

Photocatalytic reactions under extremely low-intensity UV illumination

2.1 Introduction

As described in the previous chapter, TiO_2 in particular has beneficial characteristics, such as its chemical and physical stability, as well as the strong oxidizing power of the photogenerated holes, with which most organic compounds can be oxidized to carbon dioxide at ambient temperature and pressure. [2, 23, 117] In recent years, since Heller et al. reported the oxidative stripping of oil sheens from the surface of sea water with buoyant photocatalyst-coated ceramic microbubbles, [8] the field of environmental purification has been devoting increasing attention to photocatalysis using sunlight and black-light-type fluorescent lamps as UV light sources, i.e., at the several μW cm^{-2} level, which is safe for human exposure. [118–120]

In contrast, I have been devoting our attention to a unique type of passive-type purification system for indoor working and living environments. These systems incorporate deodorizing, antibacterial and self-cleaning functions under lower level illumination from room light. In connection with this concept, many different types of TiO_2 materials which exhibit higher photocatalytic activities than P-25 powder, which is known for its highly photocatalytic activity, have been prepared. [32, 35, 53, 109] For example, quantum yields (QY) of close to 100% have been achieved under 0.5 mW cm^{-2} irradiance for 1000 ppmv gaseous acetaldehyde decomposition using TiO_2-containing paper [109] and semi-

transparent TiO_2 thin films formed on glass. [32,35] In addition, I have found that *E. coli* cells can be completely killed on TiO_2 coated glass tiles even under room light. [53] Using these materials, I can also investigate the kinetics of photocatalytic reactions under even lower-intensity UV illumination, e.g., at nW cm^{-2} levels. Using this approach, new aspects of photocatalysis, distinct from those associated with the higher-intensity UV illumination employed in many other reports, can be expected to be discovered.

In this chapter, I have examined the stationary photocatalytic decomposition of dilute gas-phase 2-propanol on a TiO_2 thin film under extremely low-intensity UV illumination, from as little as 10 nW cm^{-2} and ranging up to 10 mW cm^{-2}, for the first time. I have paid particular attention to the dependence of the QY values on the number of absorbed photons ($[Photon]_{ab}$) and on the number of 2-propanol molecules ($[M]_{ad}$) adsorbed on the surface of the film. Consequently, I found that the ratio of $[Photon]_{ab}/[M]_{ad}$ uniquely determines QY, even with a wide range of different initial concentrations, i.e., 1 - 1000 ppmv. I have discussed the diffusion length of ·OH radicals on the TiO_2 surface and the charge-separation efficiency of the TiO_2 film based on these results.

The reasons that 2-propanol was chosen as a reactant for these experiments were (i) that it is efficiently photodecomposed to acetone, which undergoes further reactions at a much slower rate, (ii) acetone can be detected sensitively using gas chromatography (GC), (iii) a single photon is considered to participate in the generation of each acetone molecule, and (iv) its self-oxidation is negligible. The latter aspect is distinct from the aldehydes, which are decomposed via free radical chain reactions involving reduced oxygen species [48,59], and therefore, the reaction dynamics cannot be accounted for in a simple fashion. It should also be noted that, under very low-intensity illumination conditions, the adsorption of the reactant on the TiO_2 surface is essentially at equilibrium. I am currently examining mass transport effects at higher UV light intensities.

2.2 Experimental section

2.2.1 Preparation of TiO_2 thin films

TiO_2 thin films were prepared on soda lime glass by a conventional spin coating process, using a commercial TiO_2 anatase aqueous sol (Ishihara Sangyo Kaisha, Ltd., STS-21, 20 nm particle diameter, 50 m^2 g^{-1} surface area as shown in Figure 2.1). A 7 cm × 7 cm piece of glass was spun at 1500 rpm for 10 s. After air drying, a second coating was applied in the same manner over the coated gel. The resulting sample was calcined at 450°C for 1.5 h in air. The thickness of the semitransparent film was about 1.7 mm, according to cross-sectional observation by atomic force microscopy. The weight of the film was 0.40 mg cm^{-2}. The roughness factor of the film was estimated to be about 150 cm^2 cm^{-2}, by measuring the amount of adsorbed cyanine dye on the sample surface. Scanning electron micrographic observation showed that the film consisted of particles with diameters of about 50 - 100 nm due to particle growth during the sintering step as shown in Figure 2.2.

2.2.2 Measurement of photocatalytic reaction

An O_2 (20%) - N_2 gas mixture, which was passed through a 16°C water humidifier in order to adjust the relative humidity to 50%, was used to fill the 1-L Pyrex glass photocatalytic reaction vessel. For purposes of preparing the gas mixtures containing various concentrations of 2-propanol, the non-humidified O_2-N_2 mixture gas was first saturated with 2-propanol (Kosou Kagaku Yakuhin) by passage through a 2-propanol liquid reservoir at room temperature, resulting in a concentration of 5 vol.%, as measured using GC (see below) after dilution. Measured quantities of the 2-propanol-saturated gas were then injected into the 1-L vessel using a syringe.

For the photocatalytic decomposition of gaseous 2-propanol, the TiO_2 thin film was illuminated with a Hg-Xe lamp (Hayashi Tokei, Luminar Ace 210). To obtain monochromatic UV light, a 365 nm band-pass filter (FWHM = 2 nm, Kenko, BP-W1-365) was used. In order to control the intensity, polyethylene terephthalate sheets were used as neutral density filters. The UV intensity was measured using a UV power meter

(TOPCON UVR-1) that had previously been corrected against a thermopile meter (No. 30198E6, The Eppley Laboratory, Inc.). Because the detection limit of the power meter was 1 mW cm^{-2}, I used extrapolated values below 10 mW cm^{-2} incident UV light. Illumination was conducted at room temperature after equilibrium between gaseous and adsorbed 2-propanol on the TiO_2 thin film was achieved, as evidenced by a constant 2-propanol concentration. The 2-propanol concentration was measured using a GC (Shimadzu Model GC-8A) equipped with a 5 m PEG1000 column and a flame ionization detector, using N_2 as the carrier gas. The CO_2 concentration was measured using the same GC, equipped with a 2 m Porapak-Q column, with a methanizer and a flame ionization detector, also using N_2 as the carrier gas. The detection limits for both acetone and CO_2 were approximately 0.1 ppmv.

2.2.3 Estimation of absorbed photons

All of the data were collected using the same TiO_2 thin film in order to avoid variations in activity caused by the difference of the surface area and thickness. The photocatalytic activity of the film was able to be fully regenerated by illumination with 5 mW cm^{-2} UV light in fresh humid air for 120 min. The absorbed photon flux was estimated as shown in Figure 2.4. The incident photon flux (I_0) can be expressed as follows; [121]

$$I_0 = I_a + I_t + I_f + I_b \tag{2.1}$$

where I_a is the intensity of light absorbed in the film, I_t is the transmitted intensity, I_f is the forward-scattered intensity, and I_b is the back-scattered intensity. I_0 was measured directly using the UV power meter. However there was some degree of non-uniformity of intensity over the illuminated area because of passage of the UV light though a 1 m glass fiber light pipe. Therefore I_0 was estimated in a manner analogous to that described by Hill et al. [74] for the measurement of I_b. This involves the establishment of a contour map of light intensity and subsequent calculation of the average intensity over the illuminated area. The full-strength intensity of I_0, after passing through the light pipe, was 45 μW cm^2. The sum of I_t and I_f was determined using a conventional integrating sphere (Shimadzu ISR-260). The modified method of Bolton et al. [107] was

not used, because I_b was measured separately (see below). The sample was placed at the sample position of the integrating sphere with a piece of glass plate similar to that used as a support for the TiO_2 film as the reference. The apparent transmission factor, $(I_t + I_f)/I_0$, reading of the instrument was 0.30 at 365 nm as shown in ?? I_b from the sample was estimated using a method similar to that of Hill et al. [74] I_b at normal incidence was extrapolated by measuring I_b as a function of the incident light angle. The factor I_b/I_0 evaluated following this methodology was 0.05. The factor I_a/I_0 for the sample TiO_2 film was calculated to be 0.65. The above procedures are shown in Figure 2.4. The UV absorption by 2-propanol on the film (365 nm) was considered to be negligible.

The amount of physically adsorbed water on the TiO_2 surface was estimated using a differential thermobalance (Shikuu Riko TGD 7000RH) for the TiO_2 powder (Ishihara Sangyo Kaisha, Ltd., ST-21 the commercial powder corresponding to that dispersed in STS-21 sol, which was used after it was subjected to the same heat treatment that was used to prepare the film (see above).

The amount of 2-propanol adsorbed on the TiO_2 sample was estimated by measuring the decrease in the balance of 2-propanol gas concentration in the glass vessel containing the TiO_2 film sample versus that in a separate empty glass vessel. The concentrations were measured one hour. after a given concentration gas mixture was introduced into each glass vessel.

2.3 Results

Figure 2.6 shows the experimental data for the adsorption isotherm in the form of an inverse plot, the weight of adsorbed 2-propanol on the TiO_2 thin film (M mg^{-1}) vs. the gaseous 2-propanol concentration (C /mg m^{-3}). These data were analyzed in terms of a Langmuir-type isotherm, which is described as follows,

$$\frac{1}{M} = \frac{1}{\mu} + \frac{1}{\mu TC} \tag{2.2}$$

where μ is the maximum weight of molecules in an adsorbed monolayer, for a given TiO_2 sample, and T is the adsorption binding constant.

The values of m and T were ca. 0.33 mg and 0.00063 m^3 mg^{-1}, respectively. These results will be used in the discussion of the QY values for 2-propanol decomposition in the next section.

Figure 2.7 shows a typical experimental data set for the concentration changes of gaseous 2-propanol, acetone, and CO_2 as a function of time in the decomposition of gaseous 2-propanol (incident UV intensity, 45 μW cm^{-2}; initial 2-propanol concentration, 100 ppmv). After 60 minutes, when equilibrium between gaseous and adsorbed 2-propanol on the TiO_2 thin film had been achieved, UV light illumination was initiated. The amount of generated acetone was equivalent to that of the decomposed 2-propanol and the generation of CO_2 and other stable intermediates were not detected, within experimental error. Under the present experimental conditions, i.e., 1 - 1000 ppmv initial 2-propanol concentration and 36 nW - 45 μW cm^{-2} incident UV light intensity, only acetone was generated stoichiometrically.

Figure 2.8 shows log-log plots of the acetone generation rates (R) versus the number of absorbed photons (I). R decreased with decreasing I, in essentially a linear fashion, with slopes which were almost constant regardless of the initial 2-propanol concentration. The higher the initial 2-propanol concentration, the higher the value for the same UV intensity. The value of the slope, i.e., the exponent α in the $R = KI^{\alpha}$ relation, is ca. 0.7 0.8. It is well known in heterogeneous photocatalysis, that, under light-rich conditions, the reaction rate is often characterized by an a value of 0.5 due to domination by the second-order-dependent carrier-recombination process. [122, 123] Conversely, the light-limited reaction rate is represented as $\alpha = 1$. [31,87] Thus the present experimental regime is in a transition region between the two asymptotic values. a values of ca. 0.7 were also reported in the photodecomposition of formic acid by Hill et al. [74] and of acetone by Ollis et al. [39] under several μW cm^{-2} UV irradiation. For 365 nm light, an incident UV light intensity of 1 μW cm^{-2} corresponds to a photon flux of 1.8×10^{12} quanta cm^{-2} s^{-1}, of which the TiO_2 film absorbs 1.2×10^{12} quanta cm^{-2} s^{-1}. I calculated the initial rates using the conventional least squares method over the first one hour and used the least squares statistics to calculate the error ranges, based on a 50% confidence level. Only for the plots in which 2-propanol was exponentially decomposed, i.e., at the highest light intensity, the initial amount of acetone generated in 15 minutes was used as the initial rate.

Figure 2.9 shows semi-log plots of I versus the apparent QY values for acetone generation. The apparent QY values were calculated using the following equation:

$$\mathrm{QY} = \frac{\text{number of generated acetone molecules}}{\text{number of absorbed photons}} \tag{2.3}$$

Error bars associated with the QY values were evaluated based on the total error of measuring the acetone concentration and extrapolating the value of the UV light intensity. However, good repeatability, within 7% , was obtained even for the lowest I values. The QY values increased gradually with decreasing I and finally saturated for the highest initial 2-propanol concentration (1000 ppmv) for I less than 4×10^{11} quanta cm^{-2} s^{-1}, and thus a purely light-limited condition ($\alpha = 1$) was reached, where the maximum QY value was $27.8 \pm 2.5\%$. This maximum QY value also appeared to be approached for lower initial concentrations. Moreover, the curve shapes for the different initial 2-propanol concentrations are similar regardless of the initial concentration. For a given QY value, increasing the initial 2-propanol concentrations by a factor of ten leads to an increased value of I. However, the increases became smaller with increasing concentration: 10 times, 6 times, and only 2 times for 1 to 10 ppmv, 10 to 100 ppmv, and 100 to 1000 ppmv, respectively.

2.4 Discussion

The mechanisms for the photocatalytic decomposition of 2-propanol to acetone has been described. [59,124] The photocatalytic processes prior to the initiation of 2-propanol decomposition are well-known;

$$h\nu \longrightarrow \mathrm{h}^+ + \mathrm{e}^- \tag{2.4}$$

$$\mathrm{h}^+ + \mathrm{OH}^-(\mathrm{s}) \longrightarrow \cdot\mathrm{OH}, \text{or } \mathrm{h}^+ + \mathrm{H_2O} \longrightarrow \cdot\mathrm{OH} + \mathrm{H}^+ \tag{2.5}$$

$$\mathrm{e}^- + \mathrm{O_2(s)} \longrightarrow \cdot\mathrm{O_2^-} \tag{2.6}$$

$$\cdot\mathrm{O_2^-} + \mathrm{H}^+ \longrightarrow \mathrm{HO_2}\cdot \tag{2.7}$$

The generated ·OH radical reacts with 2-propanol, abstracting its hydrogen atom to form a radical:

$$CH_3CH(OH)CH_3 + \cdot OH \longrightarrow CH_3C\cdot(OH)CH_3 + H_2O \qquad (2.8)$$

This $CH_3C\cdot(OH)CH_3$ radical is decomposed to acetone through several reaction pathways. One of these is the so-called current-doubling reaction, expressed by

$$CH_3C\cdot(OH)CH_3 \longrightarrow CH_3COCH_3 + H^+ + e^-(C.B.) \qquad (2.9)$$

where e^- (C.B.) represents an electron in the TiO_2 conduction band. [63] Under ambient conditions, however, O_2 can attack the radical, producing an unstable peroxo radical, which decomposes to acetone:

$$CH_3C\cdot(OH)CH_3 + O_2 \longrightarrow CH_3COO\cdot(OH)CH_3 \qquad (2.10)$$

$$CH_3COO\cdot(OH)CH_3 - - > CH_3COCH_3 + H^+ + O_2^- \qquad (2.11)$$

In the same manner, $HO_2\cdot$ radicals generated via equations [6] and [7] may also react with the $CH_3C\cdot(OH)CH_3$ radical,

$$CH_3C\cdot(OH)CH_3 + HO_2\cdot \longrightarrow CH_3COOH(OH)CH_3 \qquad (2.12)$$

$$CH_3COOH(OH)CH_3 \longrightarrow CH_3COCH_3 + H_2O_2 \qquad (2.13)$$

Note that there is no chain reaction involved in the above processes. Overall, only one photon participates in generating one molecule of acetone, and therefore QY values were calculated using equation 2-3. Considering that no radical chain reactions are involved, the maximum QY value obtained (28%) is very high. I have previously reported that QY values for the decomposition of gaseous acetaldehyde ranged up to nearly 100%, [32,35,109] but this reaction involves chain reactions. [34]

In the present experiments, in which very low-intensity UV light was used, the frequency of the reaction of each adsorbed molecule with photoproduced reactive species such as ·OH is very low. Let us estimate the frequency, for example, for the case of a light intensity of 1 mW cm^{-2} and

a gaseous 2-propanol concentration of 1000 ppmv. From the Langmuir adsorption isotherm in Figure 2.6, the area occupied by each molecule is estimated to be 0.3 nm^2. 1 mW cm^{-2} of 365 nm UV light corresponds to 2×10^{12} quanta cm^{-2} s^{-1}. Therefore on the average, each 2-propanol molecule can encounter a photogenerated ·OH radical only once every 10^3 seconds if a single photon always generates a ·OH radical. Conversely, the time scale of one series of photocatalytic processes including charge-separation and charge-transfer processes is very short. The time scale of electron-hole pair generation is on the order of 100 fs. [4,5] Thus, hole-trapping and electron-trapping at the TiO_2 surface, in other words, the charge-transfer processes to the surface, are completed in the ps-ns region. [80,125] For example, electron migration to the TiO_2 surface is estimated to be 0.83 ns using $D = 0.02$ cm^2 s^{-1} in a 100 nm-TiO_2 particle. ·OH radicals are formed in on the order of 10 n, and 2-propanol oxidation occurs in on the order of 100 ns. Electron-hole recombination proceeds in the 10 - 100 ns range. [126,127] Electron transfer to O_2 molecules is usually assumed to proceed more slowly [107,127] but still much faster than the time interval of the overall reaction frequency. These processes are schematically summarized in Figure 2.10. As seen in Figure 2.10, the charge-separation efficiency must be independent of I. Therefore, the maximum QY value of 28% can be considered to represent the intrinsic charge-separation efficiency of this TiO_2 film . The remaining 72% must be converted into heat in a charge-recombination process, as shown below.

$$h^+ + e^- \longrightarrow \text{heat} \tag{2.14}$$

On a photoirradiated TiO_2 surface, various types of active oxygen species exist. These species react with each other, forming stable products, as follows:

$$\cdot OH + HO_2\cdot \longrightarrow H_2O + O_2 \tag{2.15}$$

$$\cdot OH + \cdot OH \longrightarrow H_2O_2 \tag{2.16}$$

Therefore, when the 2-propanol concentration is low, these reactions predominate. Conversely, with decreasing light intensity, these recombination reactions proceed less efficiently, and the QY values for 2-propanol

Table 2.1: Correlation of the initial 2-propanol concentration, its adsorbed amount, and absorbed photons at a QY value of 15%.

initial concentration of 2-propanol /ppmv	adsorbed amount of 2-propanol /molecules cm^{-2}	absorbed photons /quanta cm^{-2} s^{-1}
1000	4.4×10^{16}	1×10^{13}
100	9.6×10^{15}	3×10^{12}
10	1.1×10^{15}	5×10^{11}
1	1.1×10^{14}	5×10^{10}

decomposition increase. Because ·OH radicals are much more reactive than HO_2· radicals, the steady-state ·OH concentration is probably much less than that of HO_2·. Moreover, the reaction rates of ·OH with ·HO_2 and with ·OH were estimated to be 1.1×10^{-10} and 1.8×10^{-12} cm^3 mol^{-1} s^{-1}, respectively. [128] Therefore, I can assume that reaction [15] is the main recombination process on the TiO_2 surface.

Next, let us consider the variation of the QY-absorbed photon curves on the reactant concentration in Figure 2.9. By decreasing the reactant concentration in the gas phase, the curve shifted to the lower light intensity direction. If I assume that both incident photon and reactant molecule flux arriving at the TiO_2 surface react immediately, the QY values should be determined by the ratio of the light intensity to the gas concentration. In other words, when the gas concentration increases by a factor of ten, the same QY value should be obtained with a factor of ten higher light intensity. As can be seen in Figure 2.9, however the experimental results do not support this model, showing that the factor correlating the QY values with the photon flux is not the flux of 2-propanol molecules under the present experimental conditions.

It is reasonable to consider that the adsorbed amount of 2-propanol is more important in determining the QY values. For example, in Table 2.1 are shown the initial 2-propanol concentrations (ppmv), the amounts of adsorbed 2-propanol molecules on TiO_2 (molecules cm^{-2}), and the numbers of absorbed photons (quanta cm^{-2} s^{-1}) at a QY of 15% , as determined from Figure 2.9. The adsorbed amounts of 2-propanol were

estimated from the Langmuir isotherm in Figure 2.6. A good proportionality between the amount of adsorbed 2-propanol molecules and the number of absorbed photons is suggested in this table. Even over the wide range of QY values shown in Figure 2.9, this relationship is satisfied. In other words,QY values appear to be determined by the ratio between the number of adsorbed 2-propanol molecules ($[M]_{ad}$) and the number of absorbed photons ($[Photon]_{ab}$).

Here I define the normalized photon number (I_{norm}) as $[Photon]_{ab}$ divided by $[M]_{ad}$ and have re-plotted the QY values as a function of I_{norm} in Figure 2.11. In spite of the wide range of different initial concentrations of 2-propanol, the plots fall on the same curve. The value of QY increases as I_{norm} decreases, and finally becomes constant at 28% for I_{norm} values below 10^{-4} (s^{-1}). Because $[Photon]_{ab}$ is defined as the number of photons being absorbed in one second, I_{norm} has the dimension of s^{-1} in Figure 2.11.

This result indicates that either reactive species (·OH) or reactant (2-propanol) diffuses on the TiO_2 surface and the decomposition reaction efficiency is determined by the collision probability of these species. Moreover, it is suggested that the oxidation rate of 2-propanol by ·OH (equation 2-7) is much faster than the deactivation rates of ·OH (equations 2-14 and 2-15). In other words, in the region where the QY value is constant whith respect to I_{norm}, the ·OH produced by one photon always reacts with 2-propanol not with either HO_2· or ·OH. From Figure 2.6, for 1 ppmv , i.e., of the lowest initial 2-propanol concentration in this study, I might also expect that QY approaches 28%. Based on this concentration, an intermolecular distance of adsorbed 2-propanol of ca. 11 nm can be calculated from the adsorption isotherm in Figure 2.6, making use of the surface area of this film (roughness factor of 150 cm^2 cm^{-2}) Therefore the possible diffusion length of either ·OH radicals or 2-propanol may be at least 11 nm. However, when the average 2-propanol intermolecular distance becomes greater than the ·OH radical diffusion length, the QY values can decrease against totally I_{norm} in Figure 2.11. In the present study, I used a pure anatase TiO_2 sintered thin film, which has sufficient surface adsorbed water and oxygen [119] for electron-hole pairs to transfer at the TiO_2 interface. However, some lattice defects or doping transition metals exist in the bulk of TiO_2. These behave as trapping sites or recombination sites for electron-hole pairs. [126, 129, 130] Thus

the variable amounts of these in different samples could influence the QY values vs. I_{norm} in Figure 2.11. In addition, the variation of the amounts of surface hydroxyl groups, water and oxygen molecules can also influence the charge-transfer process at the surface, and thus to the ·OH radical diffusion distance (Figure 2.12).

2.5 Conclusions

From the present kinetic study of the photocatalytic decomposition efficiency of gaseous 2-propanol using purely anatase TiO_2 sintered thin film under very weak UV light, it can be concluded for the first time that QY values are determined by the ratio of the number of adsorbed 2-propanol molecules to the number of absorbed photons. This phenomenon indicates that either ·OH radicals or 2-propanol can diffuse on the TiO_2 surface at least ca. 11 nm. The decrease in QY is attributed to increases in the rates of reaction for ·OH radicals with HO_2· radicals and ·OH with itself, relative to that with 2-propanol. The maximum QY value of 28% represents the intrinsic charge-separation efficiency of this sample. It is interesting that I can apply this reaction dynamics for such a wide 2-propanol concentration range. I believe that these findings can to become significant models for photocatalysis involving more complex reactions, for example, in the case of reactants which are easily oxidized via radical chain reactions. At last in Figure 2.12 I illustrated the schematic diagram of this new model of reaction dynamics on the TiO_2 surface under extremely weak UV light illumination.

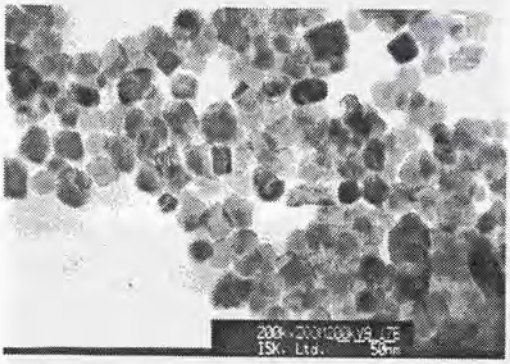

Figure 2.1: Transmission electron micrographic observation of the TiO_2 particle.

(1) Top view

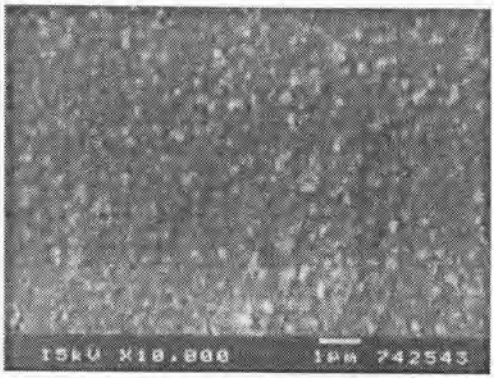

(2) Cross section

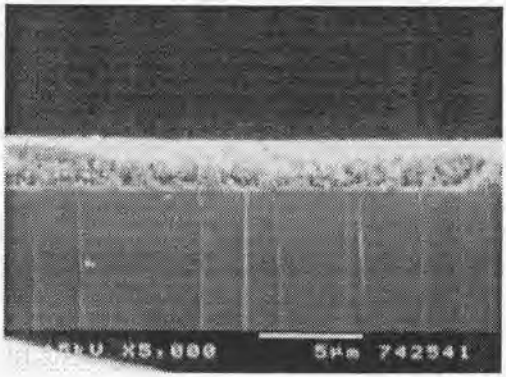

Figure 2.2: Scanning electron micrographic observation of the TiO_2 sample film. This sample was prepared on soda lime glass by a conventional spin coating process, using a commercial TiO_2 anatase aqueous sol (Ishihara Sangyo Kaisha, Ltd., STS-21, 20 nm particle diameter, 50 $m^2\ g^{-1}$ surface area). The resulting sample was calcined at 450°C for 1.5 h.

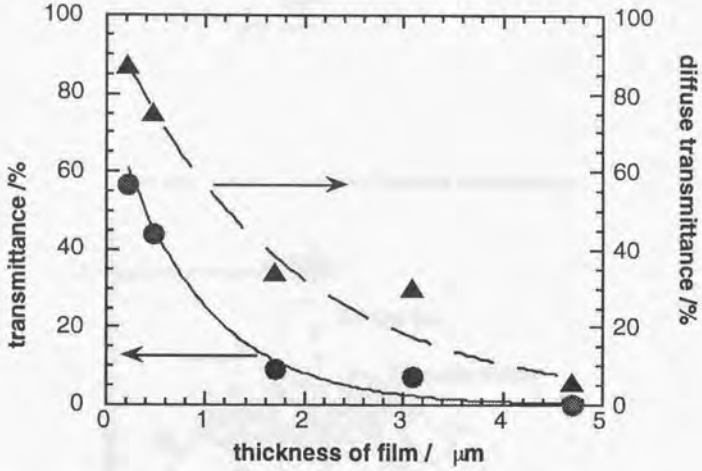

Figure 2.3: Transmittance and diffuse transmittance of the TiO_2 sample films as a function of the thickness of the films.

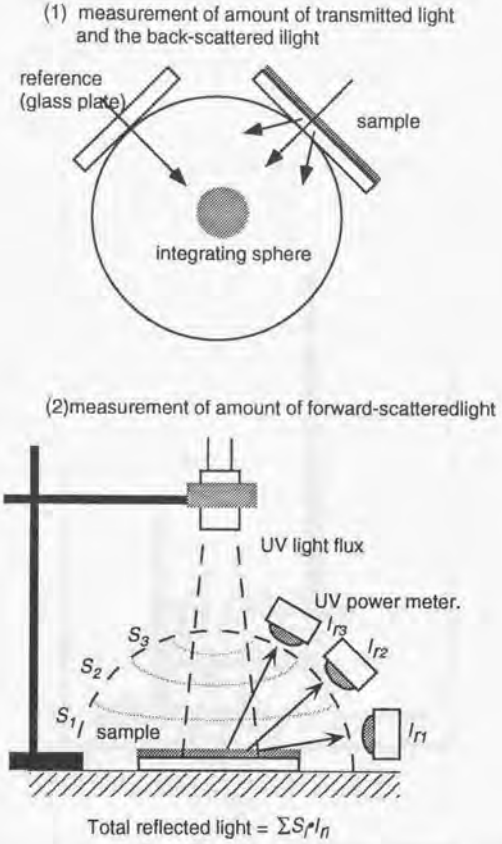

Figure 2.4: The estimation of absorbed photon flux in the sample film(I_a). The incident photon flux (I_0) can be expressed in eq.2.1, where the transmitted intensity (I_t) and the back-scattered intensity(I_b) was measured using integrating sphere as shown in (1),the forward-scattered intensity (I_f) was estimated to establish a contour map of light intensity and subsequent calculation of the average intensity over the illuminated area.as shown in (2).

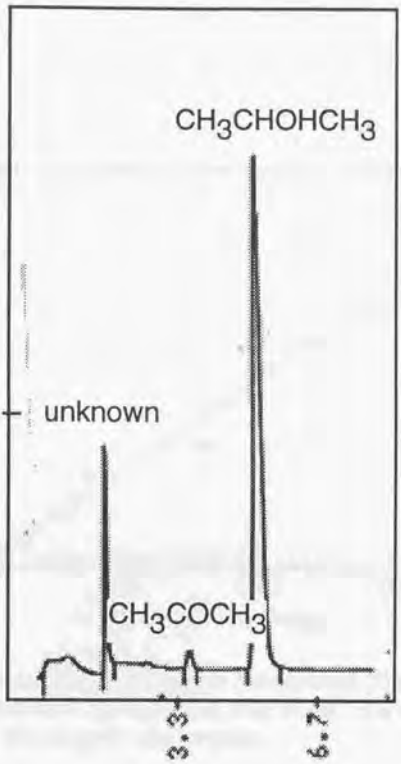

Figure 2.5: Chromatogram of gaseous products. detector: FID, carrier gas: N_2, column:PEG1000 5m, gas concentration: acetone, 300 ppbv, 2-propanol, 10 ppmv. I can detect them with sensitivity of one order higher than this experiment(see in Chapter 3).

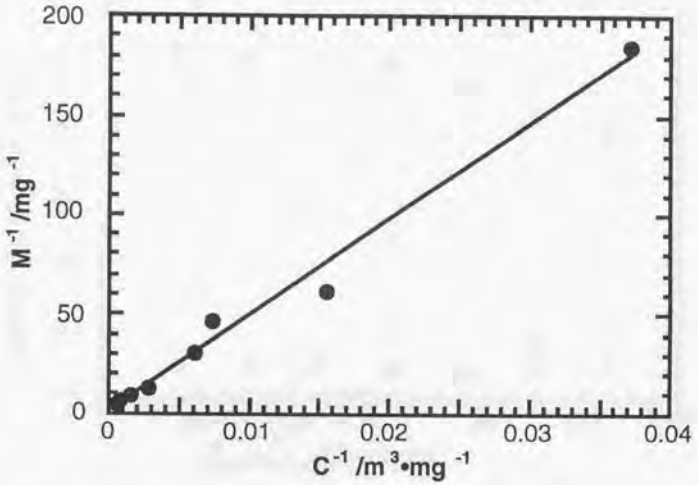

Figure 2.6: Inverse plots of the gaseous concentration (C /mg m^{-3}) and the weight of adsorbed 2-propanol (M /mg) on the TiO_2 thin film used for analysis of the Langmuir-type isotherm.

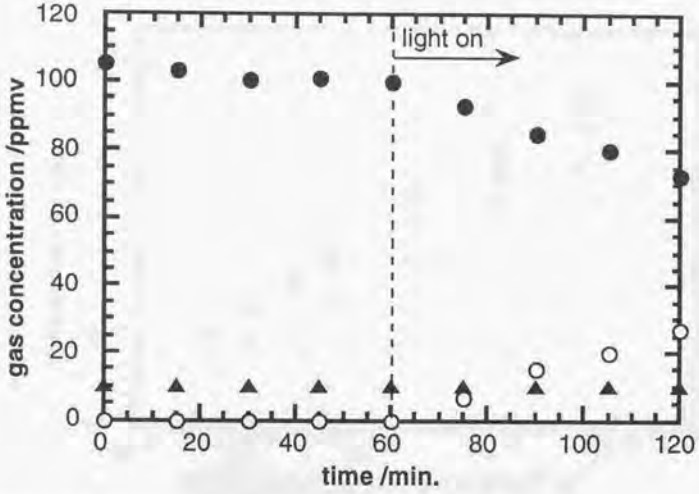

Figure 2.7: Concentration changes of gaseous 2-propanol, acetone, and CO_2 as a function of time in the decomposition of gaseous 2-propanol (incident UV intensity, 45 μW cm^{-2}; initial 2-propanol concentration, ●,2-propanol; ○,acetone; ▲,carbon dioxide).

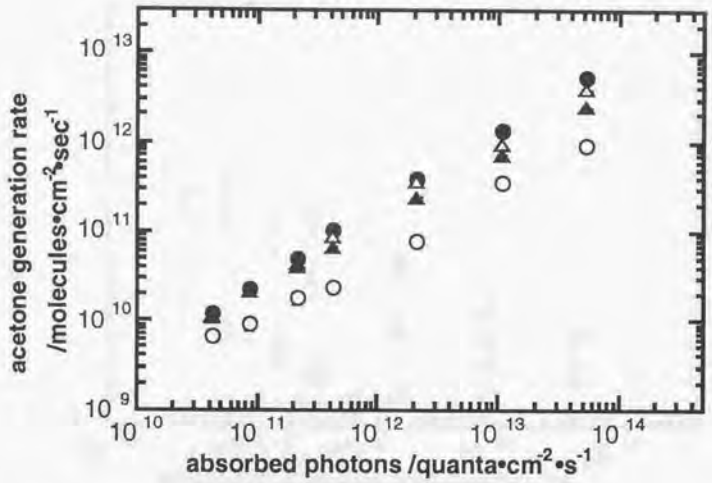

Figure 2.8: Dependence of the acetone generation rate on the absorbed photons (initial 2-propanol concentration; ● 1000 ppmv △ 100 ppmv, ▲ 10 ppmv, ○ 1 ppmv).

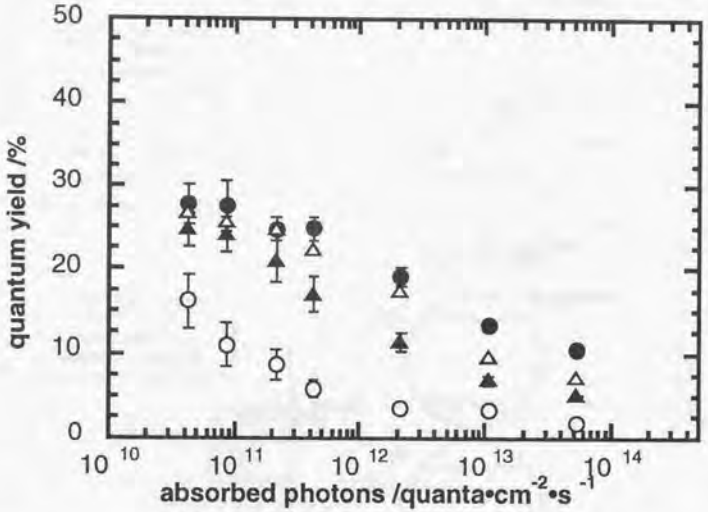

Figure 2.9: Dependence of QY on absorbed photons (initial 2-propanol concentration; ● 1000 ppmv △ 100 ppmv, ▲ 10 ppmv, ○ 1 ppmv).). Error bars for 100 ppmv are omitted for clarity.

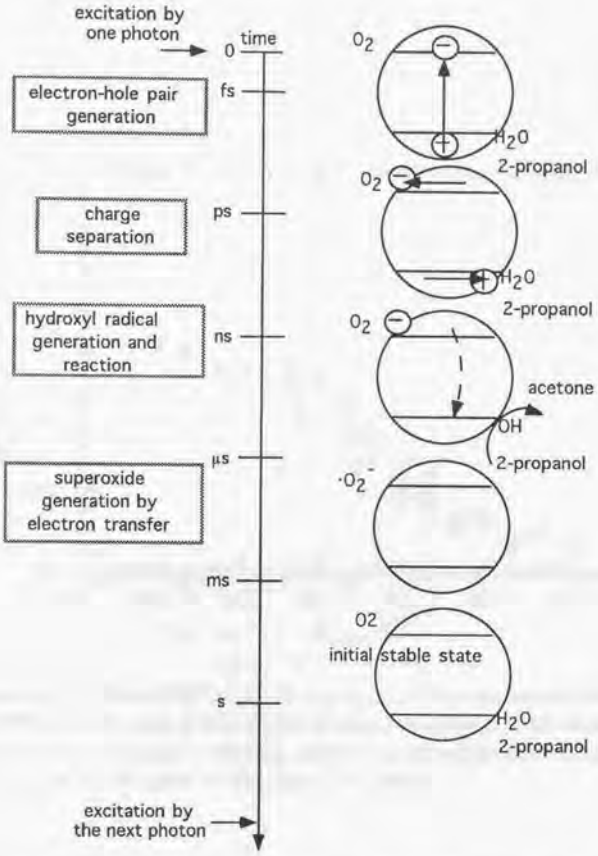

Figure 2.10: Schematic diagram of a series of photocatalytic processes along the time axis. The time interval of excitation by photons in this figure is assumed to be that for an experimental condition of 1 μW cm^{-2} incident UV intensity and 1000 ppmv initial 2-propanol concentration.

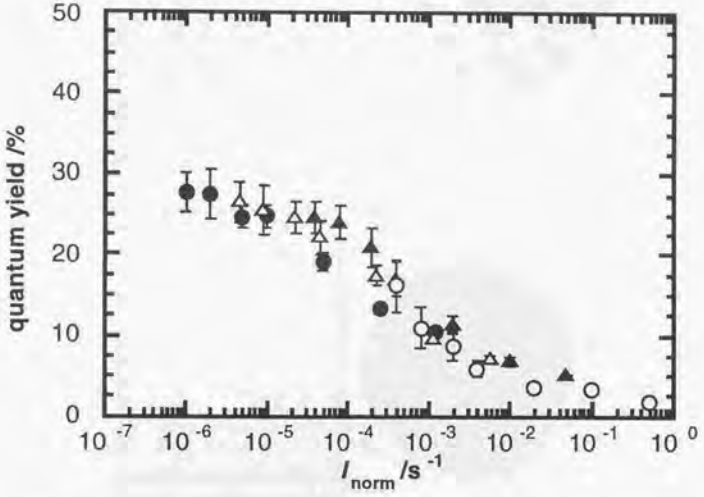

Figure 2.11: Plots of QY values vs. log I_{norm} ($/\mathrm{s}^{-1}$), a parameter which is defined as the ratio of the number of absorbed photons to the number of adsorbed 2-propanol molecules. (initial 2-propanol concentration; ● 1000 ppmv △ 100 ppmv, ▲ 10 ppmv, ○ 1 ppmv).

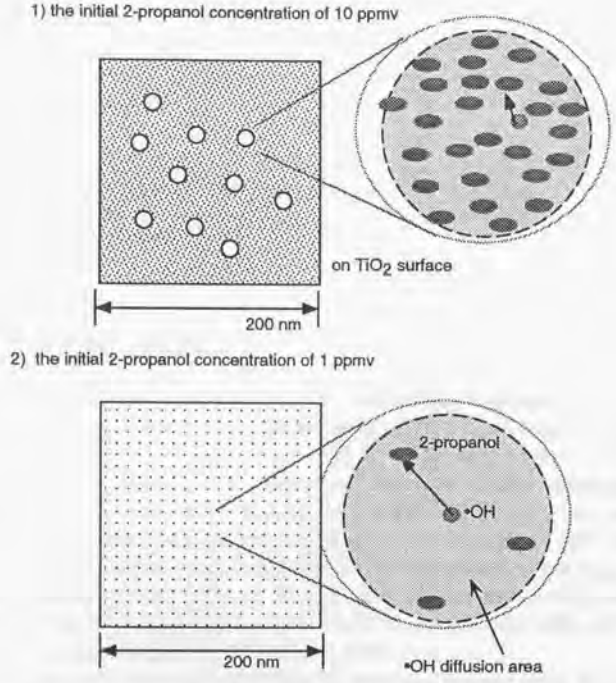

Figure 2.12: Schematic diagram of the new dynamics of TiO_2 photocatalytic reaction under extremely low-intensity UV light illumination for the initial 2-propanol concentration of 10 ppmv and 1 ppmv, respectively. The dots inside the square representes the adsorbed 2-propanol molecules. The ratio of the number of absorbed photons to the number of adsorbed 2-propanol molecules determine the value of QY, purely light limited conditions appeares for the value of Inorm less than $10^{-4}(s^{-1})$.

Chapter 3

Photocatalytic reaction under mass transport-limited conditions

3.1 Introduction

Almost researches have been directed towards the large-scale removal of toxic organics in air via the development of TiO_2-based photoreactor devices. [1, 3, 38–40, 49, 119, 123, 131–134] For example, Suzuki et al. reported the degradation of 20-ppmv acetaldehyde using TiO_2-containing honeycomb material, with illumination from a 500-W mercury lamp inside a 20 L-vessel, with an air-stream velocity of 5 L min^{-1}. [38] Anderson and co-workers reported that 99.3% photooxidation of 500 ppmv-trichloroethylene was achieved using TiO_2-containing pellets lining an 11-cm tube reactor equipped with four 4-W black light-type bulbs, with an air-stream velocity of 300 ml min^{-1}. [132]

In contrast, I have been devoting our attention to novel types of passive purification systems for indoor and outdoor spaces using large area TiO_2-containing building materials. [135] The use of very low-intensity UV light and natural convective air-flows which are normally present in living and working environments is one of the key characteristics of this approach. For example, a typical UV light intensity level of 1 mW cm^{-2} is obtained on the floors of rooms illuminated with white fluorescent-type light fixtures. Reactants are transported to the surface of the TiO_2 photocatalyst by air currents and concentration gradients. Our group has reported interesting self-cleaning, anti-bacterial [53] and deodorizing [136] effects under low-intensity UV illumination using TiO_2-containing mate-

rials such as ceramic tiles [108] and glass. [32, 34, 35, 110] I have also reported the kinetics of the degradation of gas-phase 2-propanol under purely light-limited conditions with extremely low-intensity UV light illumination (36 nW cm^{-2} - 45 μW cm^{-2}). [137]

Photocatalytic degradation of gas-phase 2-propanol is a good model system, because the initial reaction pathway involves almost exclusively the partial oxidation to acetone. In this chapter, a kinetic study of the degradation of gas-phase 2-propanol, present at initial concentrations in the 0.1-100 ppmv range, was carried out using a TiO_2 film photocatalyst in a batch-type reactor with comparatively high-intensity UV illumination, in the range of 35 μW cm^{-2} to 60 mW cm^{-2}. I estimated the purely mass transport-limited conditions for various initial 2-propanol concentrations. Moreover, I modeled the concentration changes of 2-propanol under mass transport-limited conditions using the one-dimensional diffusion equation, assuming various boundary layer thicknesses. Based on these results, I discuss, in terms of a light intensity vs. reactant concentration plot, regions of pure mass transport-limiting conditions and pure light intensity-limited conditions for the photocatalytic degradation of gas-phase organic compounds.

3.2 Experimental section

TiO_2 thin films were prepared on soda lime glass by a conventional spin coating process, using a commercial TiO_2 anatase aqueous sol (Ishihara Sangyo Kaisha, Ltd., STS-21, 20 nm particle diameter, 50 m^2 g^{-1} surface area). The resulting sample was calcined at 450°C for 1.5 hour in air. The thickness of the semitransparent film was approximately 1.7 mm. The roughness factor of the film was estimated to be 150 cm^2 cm^{-2} by measuring the amount of a cyanine dye adsorbed on the sample surface. The sample size used for the experiments was 3.5 × 3.5 cm^2. All of the data were collected using the same TiO_2 thin film in order to avoid variations in activity caused by differences in surface area or thickness. The photocatalytic activity of the film was able to be fully regenerated by illumination with 30 mW cm^{-2} UV light in fresh humid air for 60 min. This was confirmed by the fact that no further CO_2 was produced from the sample.

An O_2 (20%)-N_2 gas synthetic air mixture, adjusted to a relative humidity of 50 %, was used to fill the 1-L Pyrex glass photocatalytic reaction vessel. For purposes of preparing gas mixtures containing various initial concentrations of 2-propanol, measured quantities of 2-propanol-saturated gas (approximately 5 vol.% in the dry O_2-N_2 gas mixture), which was prepared in a 2-propanol liquid reservoir (Kosou Kagaku Yakuhin), were injected into the 1-L reactor using a syringe.

For the photocatalytic decomposition of gas-phase 2-propanol, the TiO_2 thin film was illuminated with an Hg-Xe lamp (Hayashi Tokei, Luminar Ace 210). To obtain monochromatic UV light, a 365-nm band-pass filter (FWHM = 2 nm, Kenko, BP-W1-365) was used. The UV intensity was measured using a UV intensity meter (TOPCON UVR-1) that had previously been corrected against a thermopile meter (No. 30198E6, The Eppley Laboratory, Inc.). In order to avoid turbulence caused by infrared light emitted from the Hg-Xe lamp, an IR-cut-off filter (TOSHIBA IR-25) was used.

The 2-propanol and acetone concentrations were measured using a gas-chromatograph (Shimadzu Model GC-8A) equipped with a 5 m PEG1000 column and a flame ionization detector. The CO_2 concentration was measured using the same gas-chromatograph, equipped with a 2 m Porapak-Q column, with a methanizer and a flame ionization detector. The gas samples were withdrawn from a sampling port on the side of the vessel and injected into the gas chromatograph using a syringe. The detection limits for 2-propanol, acetone and CO_2 were approximately 1 ppbv, which necessitated the use of the highest available purities for the gases used in these experiments, i.e., N_2 (Suzuki Shokan, 99.99995%) as the GC carrier gas, H_2 (Suzuki Shokan, 99.99995%), used in the flame ionization detector, and the O_2 (20%) - N_2 mixture, which was purified by passage through activated carbon and silica gel, as synthetic air mixture used in the photoreactor.

The ratio of the photon flux absorbed by the sample TiO_2 film to the incident photon flux was determined to be approximately 0.65. [137] Under static conditions, the average gas velocity caused by the UV illumination was determined by visually examining the gas flow after smoke was introduced into the reaction vessel. Forced convection was obtained using a miniature electric fan (SHICOH, IC FAN, 3 cm diameter), and the gas velocity at the sample position was determined to be approxi-

mately 50 cm s^{-1} by use of a hybrid anemometer (Hiyoshi, model dp 70). All of the measurements were carried out at room temperature.

3.3 Results

Figure 3.1 shows a typical experimental data set for the concentration changes of gas-phase 2-propanol, acetone, and CO_2 as a function of time with an incident UV light intensity of 8.2 mW cm^{-2}. The UV illumination was initiated after equilibrium had been achieved between the gas-phase and adsorbed 2-propanol on the TiO_2 thin film, as evidenced by the relatively constant concentration. The percentage conversion of 2-propanol to acetone was 93%, while that to CO_2 was 7%, after a 10-min illumination. As I reported previously, in the case of low-intensity UV illumination (36 nW - 45 mW cm^{-2}), the conversion percentage for acetone was 100%, and CO_2 was undetectable. [137] In contrast, under the present experimental conditions of relatively high-intensity UV illumination, a small amount of CO_2 was generated but no other stable intermediates were detectable in the gas phase. In the present work, because I are interested in the influence of the reactant mass-transport on the TiO_2 photocatalytic reaction, only the initial degradation rates of 2-propanol, which were determined after two minutes, were used. The photodegradation of 2-propanol has been examined by several other groups, and all have found that, if initial rates are used, it is possible to assume that acetone is the only product (see Reference 21 and references therein).

Figure 3.2 shows log-log plots of the 2-propanol degradation rates (R) at different initial concentrations versus the number of photons (I) absorbed by the TiO_2 per unit time (s). As seen from this figure, for each initial concentration in the range of 0.1 - 100 ppmv, the curves were roughly divided into two I regions, a low light intensity region (region A) in which R increased linearly with increasing I, with all of the curves exhibiting a linear dependence on $I^{0.7}$, and a higher light intensity region (region B), in which R was essentially constant. For example, for the initial concentration of 1 ppmv, R increased as a function of $I^{0.7}(8)$ but became constant at 2.6×10^{12} molecules cm^{-2} s^{-1} for I greater than approximately 1×10^{15} quanta cm^{-2} s^{-1}. The I values for the break points (I_b), at which mass transport control is reached, increased with

increasing initial 2-propanol concentration. However, the rate of increase was not proportional to the 2-propanol concentration, as illustrated by the shaded regions in the figure. Similarly, the R values in region A (R_A) for given I values increased with increasing 2-propanol concentration, but also not in a linear fashion, as seen by the fact that the curves are increasingly close together with increasing concentration. Conversely, the R values in region B (R_B) increased proportionally to the 2-propanol concentration, as seen by the equally spaced curves. These data are summarized in Table 1, which shows the rates of increase for the various parameters when the 2-propanol concentration is increased by factors of ten over the whole concentration range.

Similar experiments were carried out under forced-convection conditions for initial concentrations of 0.1 ppmv. The velocity of the gas flow at the sample position was 50 cm s^{-1}. The results are shown in Figure 3.3. The R values obtained with forced convection were greater than those obtained with natural convection in region B but were almost the same in region A. These data show that, with natural convection at higher light intensities, i.e., region B, the adsorbed reactants on the TiO_2 surface are decomposed relatively quickly, and mass transport to the TiO_2 surface becomes rate-limiting. It should be also noted that the light intensity region in which R is proportional to $I^{0.7}$ is extended to higher light intensities under forced-convection conditions. Moreover, as in the case of natural convection, the R reached a plateau under forced convection. However, not surprisingly, the plateau was observed at higher I values, greater than approximately 1×10^{16} quanta cm^{-2} s^{-1} (region C). The R values in this region were correspondingly higher (ca. 2.1×10^{12} molecules cm^{-2} s^{-1}).

3.4 Discussion

3.4.1 mass-transfer in natural air flow

In region A in Figure 3.2, the overall rate is postulated to be limited by the rate of the reaction on the TiO_2 surface, whose rate should be proportional to the number of adsorbed reactant molecules. The adsorption process on TiO_2 has been found to follow Langmuir-type behavior(21), and thus, the higher the gas-phase 2-propanol concentration, the more

gradual the increase in the number of adsorbed molecules, particularly as the saturation point is approached. Therefore, with increasing initial 2-propanol concentration, the rate of increase of R in region A decreases. In contrast, in region B, the overall rate appears to be controlled by mass transport to the TiO_2 surface. The flux of 2-propanol to the TiO_2 surface should then be, to a first approximation, proportional to the gas-phase concentration. This is consistent with the good proportionality of R to the 2-propanol concentration in region B. This is also consistent with the fact that, at the higher initial concentrations, the larger numbers of absorbed photons are necessary to overcome the increased reactant flux.

Up to now, most of the research in gas-phase photocatalytic reactions has involved flow-type systems, with the aim of destroying air contaminants at high rates. However, our orientation is towards novel types of passive air purification systems, i.e., not involving forced convection, for indoor living and working spaces. In order to facilitate the understanding of such systems, a modeling analysis based on fluid dynamics was carried out.

Because the R values in region B are proportional to the initial gas-phase concentration, it is reasonable to assume that the effect of natural convection in the reactor on the 2-propanol degradation dynamics is essentially independent of concentration in that region. Therefore, I have attempted to model the time dependence of the 2-propanol concentration inside the reactor under mass transport-limited conditions. In order to simplify the model, I have carried out experimental measurements of 2-propanol decomposition with the whole floor of the glass reactor covered with TiO_2 thin film, so that I could employ a one-dimensional mass-transport model.

At first, I use the one-dimensional form of the diffusion equation3.1 under the assumption that no convective gas flow exists inside the reactor and that the reactant transport is simply due to a concentration gradient.

$$\partial C/\partial t = -D(\partial^2 C/\partial x^2) \tag{3.1}$$

where D [$cm^2\ s^{-1}$] is the diffusion coefficient (2-propanol: $D = 0.099\ cm^2\ s^{-1}$), C[$mol\ cm^{-3}$] is the 2-propanol concentration, x [cm] is the distance from the substrate, and t is the UV irradiation time. This equation is converted to a dimensionless form using the definition of the dimensionless diffusion coefficient ($D = (dx)^2(dt)^{-1}D'$) and solved using the finite

difference method:

$$C(x',t'+1) = C(x',t')+D'[C(x'+1,t) - C(x',t')+C(x'-1,t) - C(x',t')] \quad (3.2)$$

where x' and t' are dimensionless distance (x/dx) and dimensionless time (t/dt), respectively. The initial condition is $C(x \neq 0,0) = C_0$; however, the concentration on the TiO_2 surface is assumed to be zero during UV illumination: $C(0,t') = 0$. At the top of the reactor $(x = z)$ the 2-propanol concentration is described as follows:

$$C(z',t'+1) = C(z',t') + D'C(z'-1,t) - C(z',t') \quad (3.3)$$

where z' is dimensionless distance (z/dx) between the substrate and the top of the reactor.

The calculated results are shown as curve A in Figure 3.4. However the actual degradation rates were approximately 4 5 times faster than the calculated one, indicating that natural convection cannot be neglected.

In fact, a natural gas-flow pattern was visually observed inside the reactor, as indicated by the shaded arrow in Figure 3.5. Its average velocity (V) was observed to be approximately 1 cm s^{-1}. This type of flow pattern was approximately treated as a laminar flow with a Reynolds number (Re) of 27 ($Re = LV/n$, $V = 1$ cm s^{-1}, $L = 4$ cm was the estimated cross-sectional width of the gas stream, and $n = 0.15$ cm^2 s^{-1} is the kinematic viscosity). Theoretically, the concentration distribution in this stream takes on a parabolic shape convex to the direction of the stream. The boundary layer can be approximated by the half-width of the gas stream. [138]

Then, I calculated the 2-propanol concentration as a function of time based on a model considering the thickness of the boundary layer (k [cm]) as follows. In the boundary layer, the reactant molecules are transferred by the concentration gradient. Therefore $C(x',t')$ $(0 \leq x' < k')$ follows eq. 2. Here k' is the dimensionless thickness of the boundary layer (k/dx). The concentration decrease in the boundary layer is compensated by supply of reactant from the bulk gas phase. Therefore the concentration at the boundary is expressed as

$$C(k',t'+1) = C(k',t') + D'C(k'-1,t) - C(k',t')/(z'-k') \quad (3.4)$$

The concentration in the gas phase outside the boundary layer ($k' \leq x' \leq z'$) decreases, but it can be assumed to be constant: $C(k'+1,t') = C(k'+2,t') = \ldots = C(z',t')$. Our treatment of the convection is meant to be as simple as possible. The mass transport model basically involves a coupling of diffusion within a boundary layer and a flat concentration profile outside the layer. The only aspect which might involve an oversimplification is the assumption of flat concentration profile in the case of non-forced convection. Of course, in the case of forced convection, there is no oversimplification. However, under the present experimental conditions, i.e., a relatively small cubic space, this assumption appears not to be critical. The time dependence of the concentration depends strongly on the thickness of the boundary layer. Curves B, C and D in Fig. 4 were obtained with thicknesses of 2.0 cm, 1.5 cm and 1.0 cm, respectively. Comparison of these curves with the experimental data indicates that the latter is consistent with a boundary layer thickness of approximately 1.5 cm under the present conditions. Interestingly, the fact that the experimental concentration vs. time behavior can be well simulated by such a diffusion model implies that the reactant is completely consumed at the photocatalyst surface, and thus that the active sites of the photocatalyst are occupied by reactant molecules to a negligible extent. In other words, the photocatalyst surface is highly active.

Similar experiments were done for the degradation of acetaldehyde instead of 2-propanol. Mass transport-limited conditions appeared at almost the same light intensity and the degradation rate was also essentially the same as that for 2-propanol. This is because the diffusion coefficients of gas-phase molecules in a given atmosphere are almost the same regardless of the species. [139] Under forced convection conditions, the saturation R value was ca. 7 times larger than that under natural convection. This factor agrees well with the ratio of the square roots of the gas flow velocities ($= \sqrt{50 \text{ cm s}^{-1}/1 \text{ cm s}^{-1}}$). Similarly the boundary layer thickness under forced convection conditions was estimated to be 0.21 cm, since it is inversely proportional to the square root of the velocity. This value is consistent with that determined using a quantitative flow visualization technique.(24)[1]

[1]In this paper, the thickness of an air boundary layer on a flat plate at a flow rate of 50 cm s^{-1} was estimated to be ca. 0.42 cm at a point 4.2 cm away from the edge of a plate facing the convection source. In the present work, the conversion source was

Table 3.1: Porous size and effective diffusion coefficiency[a]

porous size	effective diffusion coefficiency
nm	$m^2\ s^{-1}$
10^3	3×10^{-6}
10^2	2×10^{-6}
10^1	5×10^{-7}
10^0	5×10^{-8}

[a] effective diffusion coefficiency: $D_e = \frac{\varepsilon}{\tau}$: ε is and τ is .

Table 3.2: Diffusion coefficiency (272-299 °C)

compounds	diffusion coefficiency (air) $cm^2\ s^{-1}$	diffusion coefficiency (water) $cm^2\ s^{-1}$
2-propanol	0.099	
acetone	0.099	1.25×10^{-5}
metane	0.2190	
metanol	0.132	1.28×10^{-5}
benzene	0.0962	

Summarizing, the support for our simplified mass transport model includes the following: 1) direct visual observation of the flow pattern, 2) the fact that the ratio of the saturation R values is quite close to the square root of the ratio of the gas velocities (comparing the forced and non-forced convection cases), and 3) the fact that a good fit was obtained to the experimental data (Fig. 4). Additional support for the value of the boundary layer thickness obtained in the forced convection case has been obtained using quantitative flow visualization techniques, as discussed above [140].

3.4.2 Regions of mass-transpot limited condition and light-limited condision

I reported previously on measurements of the photocatalytic decomposition of 2-propanol under pure light intensity-limited conditions for various initial concentrations, [137] while I have examined purely mass transport-limited conditions in the present work. I have depicted these two limiting conditions as functions of the reactant concentration (x-axis) and the UV light intensity (y-axis) in Figure 3.9. Curve A, the boundary of the mass transport-limited region, and curve B, the boundary of the purely light-limited region, are characterized by different characteristic shapes. The slope of curve A increased but that of curve B decreased with increasing reactant concentration. Interestingly, the shape of curve B is similar to that of the Langmuir isotherm, because it turns out that the y-axis of Figure 3.9 represents the relative amounts of adsorbed reactants for curve B, as reported previously. This is because pure light intensity-limited conditions for different initial 2-propanol concentrations were reached at the same ratio of adsorbed reactants to absorbed photons. [137] Moreover, because the reaction rate on the surface is proportional to the numbers of adsorbed reactant molecules, the y-axis for curve B also represents the overall reaction rate R on the TiO_2 surface.

Conversely, curve A represents the boundary of the mass transport-limited region. As shown in Table 1, the light intensity I_b at the break point increases with increasing reactant concentration. This is due to the

adjacent to the TiO_2 film, so that the average distance from the edge was 1.75 cm. Thus, the boundary layer would be expected to be correspondingly smaller, i.e., on the order of one-half, in agreement with the value obtained (0.21 cm).

fact that in region A (Figure 3.2) R is not proportional to the reactant concentration in the gas phase, while in region B R is proportional. In region A, R is consistent with a Langmuir-Hinshelwood model. In other words, the gradually increasing slope of curve A with increasing reactant concentration is also reflected by the Langmuir isotherm.

As seen from Figure 3.9, for gas concentrations lower than 1 ppmv and natural convection, a mass transport-limited condition is obtained at the relatively low 1 mW cm^{-2} level. This means that, for air purification employing TiO_2-containing materials outdoors in summer in the northern hemisphere (UV intensity: 3 mW cm^{-2}), the degradation of toxic organic compounds is expected to be under mass transport control. In other words, no increase of the degradation rate is expected even if higher intensity UV illumination is employed.

From this figure, I can estimate both the maximum value of effective light intensity and the time necessary to remove the reactants. For example, let us consider the 99% degradation of a 100-ppbv reactant using a TiO_2 film covering all of the wall area in a 27-m^3 cubic space. With a natural convective flow of 1 cm s^{-1}, the maximum value of effective light intensity would be 0.5 mW cm^{-2}, as seen from curve A in Figure 3.9, and the conversion time would be approximately 1 hour,[2] if the thickness of the boundary layer is assumed to be 1.5 cm. When a forced convective flow of 100 cm s^{-1} exists on all of the walls, the thickness of the boundary layer becomes 0.15 cm. In this case, R increases by a factor of 10, and the degradation time is estimated to be only 6 minutes. The maximum value of effective light intensity, however, increases to 14 mW cm^{-2}, based on the result that R is proportional to $I^{0.7}$, as seen in Figure 3.3. Thus, for this particular gas flow velocity, curve A shifts up to curve A', as shown in Figure 3.9. As seen from these examples, this type of figure could be

[2]The estimation of the removal time for a gas-phase compound in air in a 27-m^3 cubic space of was carried out using the following assumptions. Initially, the time necessary to remove the reactant bymeans of a photocatalytic reaction on one of the walls was calculated on the basis of a one-dimensional mass-transport model, using eqs. 2 and 4 with $z = 3$ m. This time was then divided by a factor of 6 due to the presence of 6 walls. The concentration decrease in the boundary layer was assumed to be compensated by the supply of the compound from the bulk of the gas phase, and the dilution ratio in the bulk phase was assumed to be proportional to the distance from the substrate. However, the circulation time outside the boundary layer for dilution was not considered.

useful in the design of practical photocatalytic devices for air purification.

It should be emphasized that this type of figure will be most useful in a generic sense, since the precise details of the placement of the various regions will depend upon the particular experimental conditions. For example, the R values obtained for a given TiO_2 surface will depend on the thickness of the sample film and its surface area. The R values will also be influenced by the relative humidity and oxygen concentration of the gas phase. The boundary values for I for both of the limiting conditions also depend to some extent on these parameters. However, there are intrinsic limitations: 1) the maximum value of the quantum yield is determined only by the charge-separation efficiency under light-limited conditions, as discussed in a separate paper; [137] and 2) the degradation rate is ultimately limited by the diffusion coefficient under pure mass transport-limited conditions.

It has long been recognized that, under intense illumination conditions, photocatalytic reaction rates can be mass-transport limited. In the present work, I can now more precisely determine where the transitions are between pure mass transport control, mixed control, and light intensity control. This will help other workers to more clearly understand the influence of mass transport and thus to better interpret their kinetic results. Because I are providing a simple, straightforward analysis of mass-transport for a relatively simple physical system, I are purposefully using the simplest possible model as a first step. I are also using one of the simplest possible physical systems, i.e., a very flat photocatalyst thin layer, which in fact allows us to use such a simple mass transport model, because I can effectively ignore the mass transport within the photocatalyst layer itself and treat only that in the bulk gas phase, which is not possible in the case of conventional packed-bed reactors using TiO_2 powder. [39, 119, 134]

3.5 Conclusions

Based on the quantitative modeling of this system, which is simple both from kinetic and physical viewpoints, I have been able to map out a vast range of experimental conditions, covering six orders of magnitude of reactant concentration and eight orders of magnitude of light intensity,

in terms of mass-transport vs light-intensity control. This unified view of photocatalysis, here provided for this simple system, could provide a starting point for other studies of more complex systems and a conceptual framework for both fundamental and applied studies. From the graphical representation (intensity vs. concentration), I can estimate the maximum value of light intensity necessary to obtain the maximum reaction rate for a given target concentration of reactant.

I consider the possibility of a new environmental purification system employing many different types of TiO_2-containing building materials with high photocatalytic activities and large surface areas under low-intensity UV light and natural convection. Even under extremely low-intensity UV illumination, OH radicals are generated on the TiO_2 photocatalyst surface, and photocatalytic reactions can occur at measurable rates. [137] However, under some conditions, the removal rate may be too low for practical indoor air purification under low-intensity UV light. In such cases, it is suggested that this type of system can be used in conjunction with relatively intense UV light sources, particularly for small closed spaces, particularly considering the requirement that no additional noxious compounds be generated as intermediates. The present work may also be useful in the design of equipment employing TiO_2 and UV light sources for air purification.

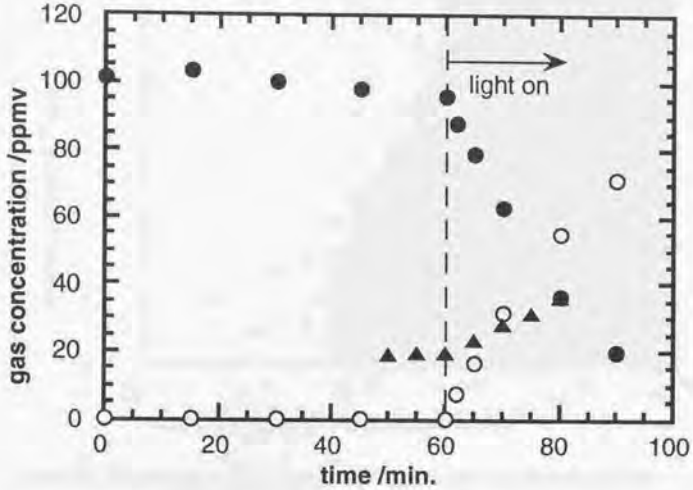

Figure 3.1: Concentration changes of gas-phase 2-propanol, acetone, and CO_2 as a function of time during the photodecomposition of 2-propanol (incident UV intensity, 8.2 mW cm^{-2}; initial 2-propanol concentration, 100 ppmv, ●,2-propanol; ○,acetone; ▲,carbon dioxide).

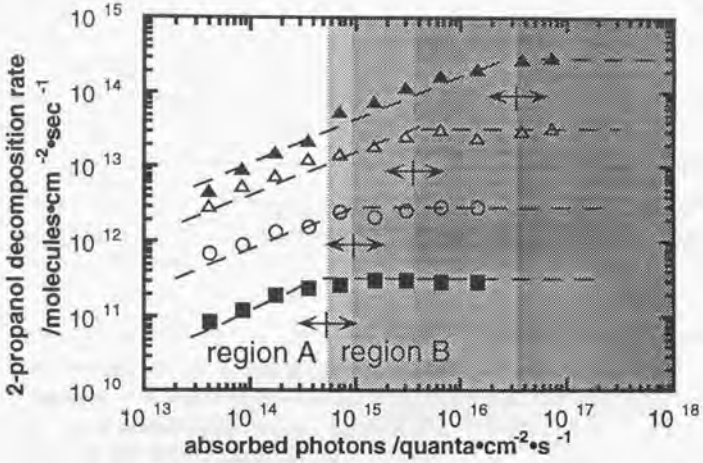

Figure 3.2: Dependence of the 2-propanol degradation rate on the number of photons absorbed per unit time (s). The initial 2-propanol concentrations were: ▲,100 ppmv; △,10 ppmv; ○,1 ppmv; ■,0.1 ppmv. In all cases, the error bars were smaller than the plot symbols. For each of the curves, the corresponding region B (pure mass transport-limited conditions) is shown as a gray shade, with darker shading corresponding to higher initial concentration.

Table 3.3: Increase factors[a] for various photocatalytic reaction rate parameters for gas-phase 2-propanol.[b]

Range of initial reactant[c] concentration	R_A^d (higher conc.) / R_A(lower conc.)	I_b^e(higher conc.) / I_b(lower conc.)	R_B^f(higher conc.) / R_B(lower conc.)
100 ppmv/10 ppmv	3	8	10
10 ppmv/1 ppmv	6	3	10
1 ppmv/0.1 ppmv	9	2	10

[a] the increase factor is defined as the ratio of the value for the parameter in question at a higher initial reactant concentration to the value at a lower initial concentration.
[b] based on the data in Figure 3.2
[c] 2-propanol.
[d] decomposition rates (R_A) in region A.
[e] number of absorbed photons per second at the onset of the mass transport-controlled region (I_b).
[f], R_B values in region B, the mass transport-control region.

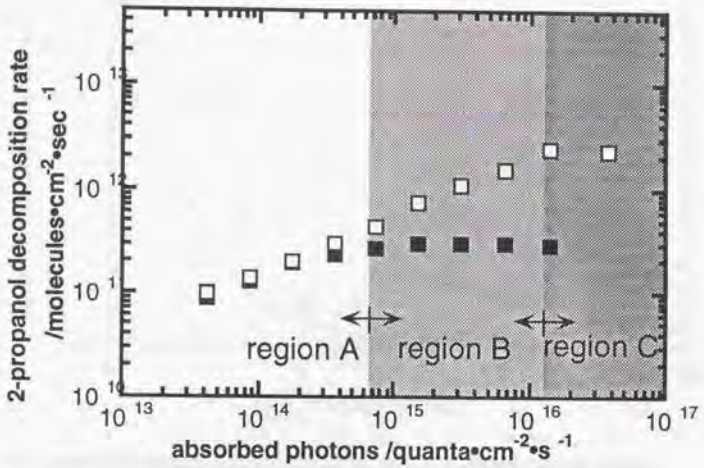

Figure 3.3: Comparison of the dependence of the 2-propanol degradation rate on the number of photons absorbed per unit time (s) under forced vs. natural convection (initial 2-propanol concentration, 0.1 ppmv; □,forced convection, with a gas-flow velocity of 50 cm s^{-1} at the sample position; ■,natural convection).

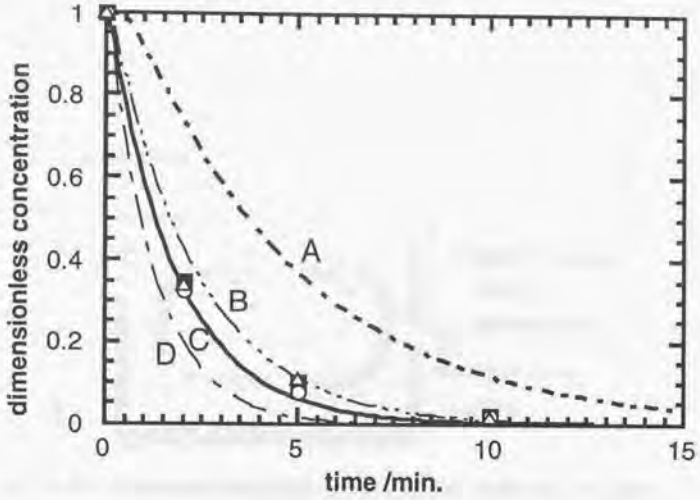

Figure 3.4: Model calculations, based on Eqs. 2-4, of 2-propanol concentrations as a function of time during degradation in the 1-L glass reactor under mass transport-limited conditions (diffusion coefficient D = 0.099 $cm^2\ s^{-1}$; boundary layer thickness: curve A, 8.0 cm; curve B, 2.0 cm; curve C, 1.5 cm; curve D, 1.0 cm). The data points shown in the plot represent the actual rates determined by the experiments (the respective initial 2-propanol concentrations and UV light intensities were: △, 10 ppmv and 12 mW cm^{-2}; ○, 1 ppmv and 3 mW cm^{-2}; and ■,0.1 ppmv and 3 mW cm^{-2}).

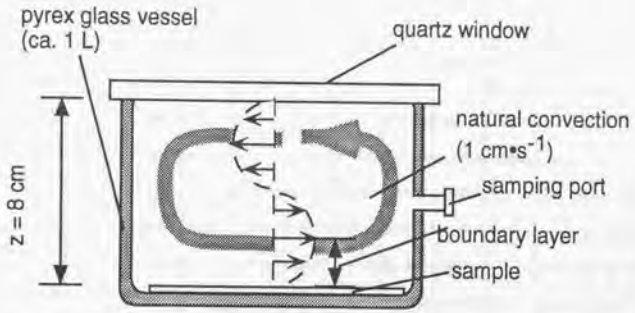

Figure 3.5: Schematic illustration of the gas flow inside the 1-L glass photoreactor. The slow circulating gas stream (velocity, 1 cm s^{-1}), which was visually observed after smoke was introduced into the reactor, is designated by the shaded arrow. No thermally-generated gas streams, i.e., due to heat generated by the sample, were observed, even under the highest intensity illumination, 60 mW cm^{-2}.

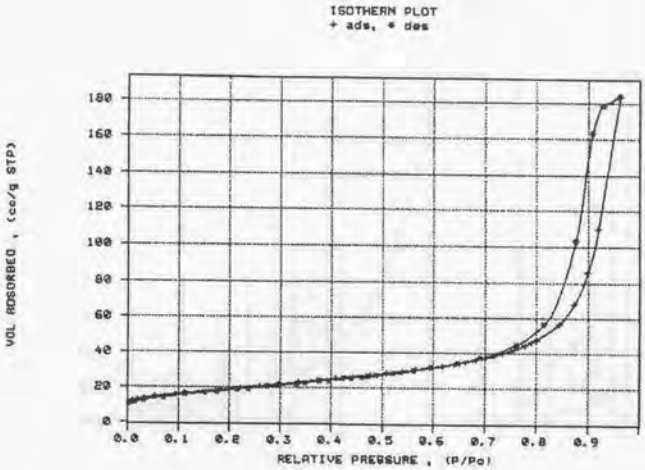

Figure 3.6: Adsorption isotherm of this TiO_2 sample film measured by Asap 2000 (Micrometrix).

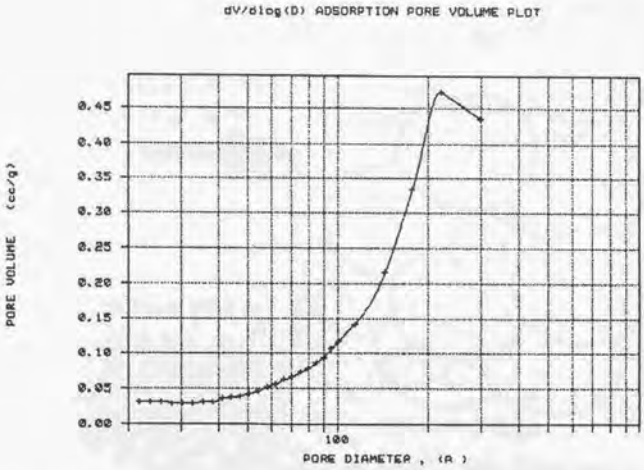

Figure 3.7: Porous size distribusion of sintered TiO_2 sample film measured by Asap 2000 (Micrometrix).

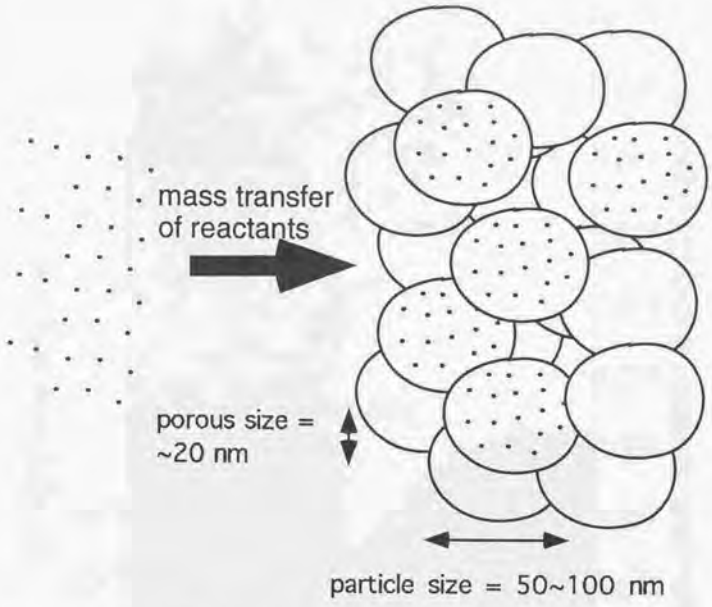

Figure 3.8: Expanding Image of photocatalytic reaction on TiO_2 thin film. Reactants can diffuse in this porous sample unless the diffusion rate changes because the porous size is more than 10 nm (meso-porous).(TiO_2 particles are covered with reactants, ·; some parts are omitted; the reactant concentration is about 1 ppmv)

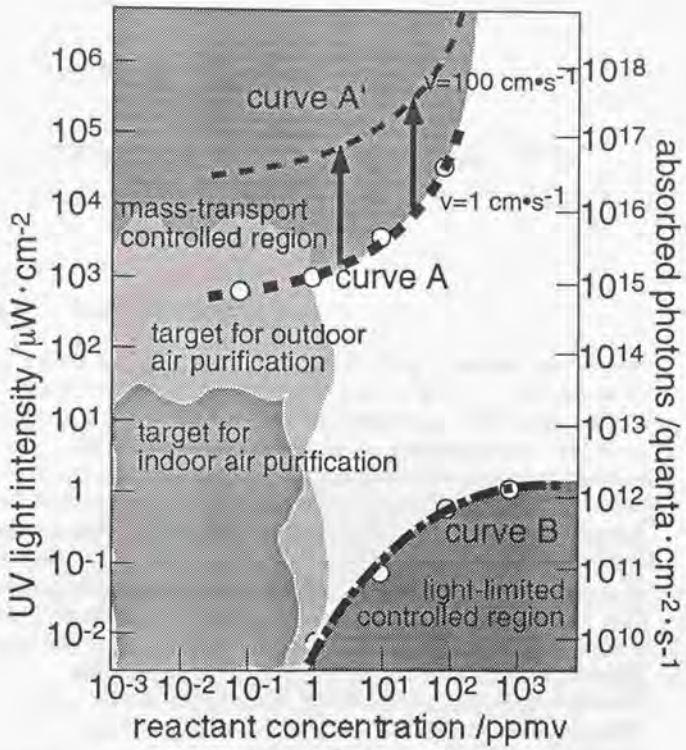

Figure 3.9: Illustration of regions of pure mass transport-limiting conditions and pure light intensity-limited conditions in the photocatalytic degradation of gas-phase organics on a plot of light intensity vs. initial reactant concentration: curve A: boundary of the mass transport-limiting region with natural convection; curve A': boundary of the mass transport-limiting region with forced convection (100 cm s^{-1}); curve B: boundary of the pure light intensity-limiting region).

Chapter 4

Autoxidation of acetaldehyde on TiO_2 photocatalyst under weak UV illumination

4.1 Introduction

Destruction of organic compounds by TiO_2 photocatalysis has been studied extensively for the purpose of water [6, 64, 74, 141, 142] and air [1, 38, 39, 41, 44, 45, 47, 69, 133, 143–147] purification. The photogenerated holes in TiO_2 photocatalysis have strong oxidizing power (3.0 V vs. SHE), at which potential nearly all types of toxic organic compounds, as well as other harmful agents such as pathogenic bacteria, can be oxidized and removed. In both liquid-solid and gas-solid photocatalytic systems, oxygen molecules play important roles in photocatalysis, i.e., one being to prevent carrier recombination by trapping photogenerated electrons, [8, 107, 148] and a second being to participate in the radical chain reactions that are known to be involved in the photocatalytic degradation of organic compounds. [48, 59] However, due to the higher mass-transport rates for oxygen in the gas-phase, the gas-solid-type photocatalytic reactions proceed in general more efficiently. For example, Anderson et al. reported apparent quantum yields (QY) ranging from 0.4 to 0.9 for the photocatalytic degradation of trichloroethylene. [132] Raupp et al. reported QY values ranging from 1 to 3 for the photocatalytic degradation of acetone and methyl-t-butyl ether. [119] However, the factors that determine photocatalytic efficiency have not yet been definitely established in conventional photocatalytic studies using strong UV light sources, such as mercury lamps and blacklight bulbs.

In contrast, I have been focusing attention on effective TiO_2 photocatalytic reactions under very weak UV illumination, e.g., at levels such as that of ordinary indoor room light (on the $\mu W\ cm^{-2}$ order). [32–35, 53, 108–110, 136] These types of reactions hold great promise in the realization of unique practical applications of photocatalysis for deodorizing, antibacterial and self-cleaning systems by using various TiO_2 coated or coating materials, such as paper, [109] tiles, [108] glass [32,34,35,110] and paints. [33] I have already reported that those materials serve as very effective photocatalysts for the decomposition of gas-phase acetaldehyde. [32–35, 109, 110] However, I have also reported that QY values are determined by the ratio of the number of absorbed photons to the number of adsorbed reactant molecules, based on a kinetic study of the photocatalytic degradation efficiency of gas-phase 2-propanol using a TiO_2 film photocatalyst under 36 nW - 45 $\mu W\ cm^{-2}$ intensity UV illumination. [137] This work indicated that ·OH radicals can diffuse and react with relatively low coverages of adsorbed 2-propanol on the TiO_2 surface.

In this chapter, I have carried out a similar analysis using acetaldehyde instead of 2-propanol. This is because acetaldehyde may be decomposed with a radical-chain mechanism (autoxidation mechanism [48, 59, 62, 149–151] in air in contrast to 2-propanol. Moreover, the decomposition of acetaldehyde is important from the viewpoint of practical applications, because it is known to be one of the principal odor causing gases in indoor air, particularly in cigarette smoke. [152–154] I have utilized the initial concentrations of acetaldehyde from 1 to 1000 ppmv and incident UV intensities from 1 $\mu W\ cm^{-2}$ to 1 $mW\ cm^{-2}$. I monitored the reaction products (CO_2, formaldehyde, acetic acid) both in the gas phase and on the TiO_2 surface. Based on these results, I will discuss the chain length of the radical reaction for acetaldehyde degradation on the TiO_2 surface.

4.2 Experimental section

TiO_2 anatase thin films were prepared on soda lime glass. The thickness of the semitransparent film was about 1.7 mm. The roughness factor of the film was about 150 $cm^2\ cm^{-2}$. [137] The sample size used for experiments was 7 7 cm. All of the experimental data were collected using the same TiO_2 thin film in order to avoid variations in activity caused by

the difference of thickness and surface area. Details of the preparation and regeneration of the film have been described previously. [137]

All of the photocatalytic degradation of gas-phase acetaldehyde was carried out at room temperature. An O_2 (20%) - N2 gas mixture adjusted to a relative humidity of 50% was used to fill the 1-liter Pyrex glass photocatalytic reaction vessel. For purposes of preparing the gas mixtures containing various concentrations of acetaldehyde, measured quantities of acetaldehyde (Takachiho, 5 vol.% in N_2) were injected into the 1-liter reactor using a syringe. The TiO_2 thin film was illuminated with a Hg-Xe lamp (Hayashi Tokei, Luminar Ace 210). To obtain monochromatic UV light, a 365 nm band-pass filter (FWHM = 2 nm, Kenko, BP-W1-365) was used. In order to control the intensity, polyethylene terephthalate sheets were used as neutral density filters. The UV intensity was measured using a UV intensity meter (TOPCON UVR-1) that had previously been calibrated using a thermopile meter (No. 30198E6, The Eppley Laboratory, Inc.). The incident light, which was transferred from the light source using a 1-m liquid fiber light pipe (Hayashi Tokei, RLGB1-5L1000), uniformly irradiated the whole area of the film. The fraction of the incident photon flux (365 nm) absorbed by the sample TiO_2 film was determined to be 0.65. Details concerning the determination of this factor have been described previously. [137] The acetaldehyde and CO_2 concentrations were measured using a gas chromatograph (Shimadzu Model GC-8A) equipped with a 2 m Porapak-Q column, a methanizer and a flame ionization detector, using N_2 as the carrier gas. The reaction products existing on the TiO_2 film were extracted into 0.01 M NaOH solution and were measured using a liquid chromatograph (TOYOSODA HPLC system, with a UV-8010 optical detector and a Shodex (Ionpak KC - 811) column).

The amount of adsorbed acetaldehyde on the TiO_2 sample was estimated by measuring the gas phase acetaldehyde concentration and subtracting the total amount in the gas phase from the total initial amount injected into the chamber. This was also corrected by the amount adsorbed on the chamber walls by carrying out similar measurements on a chamber with no film. The concentrations were measured 1 h after a given concentration gas mixture was introduced into each glass vessel.(47)

4.3 Results

The acetaldehyde adsorption isotherm was measured at room temperature with 50% relative humidity. The amounts of adsorbed acetaldehyde were analyzed in terms of the Langmuir-type isotherm,

$$\frac{1}{M} = \frac{1}{\mu} + \frac{1}{\mu TC} \tag{4.1}$$

where M is the weight of adsorbed acetaldehyde on the TiO_2 thin film (mg), C is the gas-phase acetaldehyde concentration (mg m^{-3}), m is the maximum weight of molecules in an adsorbed monolayer for a given TiO_2 sample, and T is the adsorption equilibrium constant. Figure 4.1 shows the experimental data for the adsorption isotherm in the form of an inverse plot of M vs. C. The values of m and T were approximately 0.13 mg and 0.00078 m^3 mg^{-1}, respectively. These results will be used in the discussion of the QY values for acetaldehyde degradation in the next section.

Figure 4.2 shows typical experimental data for the changes of gas-phase acetaldehyde and generated CO_2 concentrations, and amounts of acetic acid on the sample film as a function of time in the degradation of gas-phase acetaldehyde (incident UV intensity, 100 μW cm^{-2}; initial acetaldehyde concentration, 100 ppmv). The vertical axis corresponds to the amounts of each compound expressed as mmol of carbon. At equilibrium, the amount of adsorbed acetaldehyde on the sample was only 6% of the gas-phase acetaldehyde in the 1-liter glass vessel. Illumination was conducted at room temperature after equilibrium between gas-phase and adsorbed acetaldehyde on the TiO_2 thin film was achieved, as evidenced by a constant acetaldehyde concentration. The amount of generated CO_2 was not equivalent to that of the decomposed acetaldehyde. The dashed line in the figure represents the calculated difference between the amounts of decomposed acetaldehyde and generated CO_2. The amounts of acetic acid extracted from the photocatalyst surface fell precisely on this curve, indicating that CO_2 and acetic acid were the only reaction products. In fact, no other stable intermediates were detected either in the gas phase or on the photocatalyst film under these experimental conditions.

As seen in Figure 4.2, the generation of CO_2 was preceded by the generation of relatively large amounts of acetic acid, and therefore I as-

sumed that acetaldehyde is first decomposed to acetic acid, followed by the generation of CO_2. The apparent QY values, without considering radical chain reactions, were calculated using the following equations:

$$QY_{CH_3COOH} = \frac{1}{2} \times \frac{\text{number of generated acetic acid molecules}}{\text{number of absorbed photons}} \quad (4.2)$$

$$QY_{CO_2} = (1 + \frac{1}{2}) \times \frac{\text{number of generated } CO_2 \text{ molecules}}{\text{number of absorbed photons}} \quad (4.3)$$

$$QY_{total} = QY_{CO_2} + QY_{CH_3COOH} \quad (4.4)$$

where QY_{CH_3COOH} and QY_{CO_2} are QY values corresponding to generated acetic acid and CO_2, respectively. The initial amounts of acetic acid and CO_2 generated, which were determined after 5 min. illumination, were used in order to discuss the QY dependence on the initial reactant concentration and the number of absorbed photons.[1] The factors of 1/2 and (1+1/2) in eqs. 4.2 and 4.3, respectively, will be explained by considering the reaction mechanisms in the next section. Figure 4.3 shows log-log plots of the apparent total QY value (QY_{total}) versus the number of absorbed photons (I). The QY values increased with decreasing I, reaching 180% for the highest initial acetaldehyde concentration (1000 ppmv) for an I value of 1×10^{12} quanta cm^{-2} s^{-1}. The QY values also increased with increasing initial concentration. The QY plots for the various initial concentrations were found to be approximately linear, with similar slopes.

[1]This time is required to ensure that the aliquot of relatively highly concentrated (5 vol.%) acetaldehyde has time to mix thoroughly with the air in the 1-L reaction chamber and to reach equilibrium with the TiO_2 film. After the illumination is initiated, however, particularly during the first five minutes, at which point the initial rates were measured, the relatively small changes in the gas-solid equilibrium conditions were achieved quickly. It was also confirmed that there was no mass transport effect at light intensities below 1 mW cm^{-2} under the present experimental conditions by observing that there was no measurable effect of forced convection, which was induced by a miniature electric fan (IC-type fan, 3 cm diameter, Shicoh).(37) The sampling time of 5 minutes after the start of illumination was a compromise value that was selected in order to accommodate results from the wide range of light intensities and initial acetaldehyde concentrations.

4.4 Discussion

The initial steps in the photocatalytic process, prior to the initiation of acetaldehyde degradation, are well-known:

$$h\nu \longrightarrow h^+ + e^- \tag{4.5}$$

$$h^+ + OH^-(s) \longrightarrow \cdot OH, \text{or } h^+ + H_2O \longrightarrow \cdot OH + H^+ \tag{4.6}$$

$$e^- + O_2(s) \longrightarrow \cdot O_2^- \tag{4.7}$$

$$\cdot O_2^- + H^+ \longrightarrow HO_2\cdot \tag{4.8}$$

where (s) denotes a surface species. The degradation of alcohols and aldehydes in the presence of O_2 is known to proceed via radical chain reactions on the TiO_2 surface. [48, 59] Either the photogenerated hole or the ·OH radical reacts with acetaldehyde [155] [2], abstracting a hydrogen atom to form a $CH_3C\cdot O$ radical:

$$CH_3CHO + \cdot OH \longrightarrow CH_3C\cdot O + H_2O \tag{4.9}$$

Next, O_2 attacks the radical under ambient conditions, producing an unstable peroxo radical:

$$CH_3C\cdot O + O_2 \longrightarrow CH_3(CO)OO\cdot \tag{4.10}$$

This $CH_3(CO)OO\cdot$ radical reacts with another acetaldehyde, subsequently generating acetic acid and the $CH_3C\cdot O$ radical, [156]

$$CH_3(CO)OO\cdot + CH_3CHO \longrightarrow CH_3(CO)OOH + CH_3C\cdot O \tag{4.11}$$

$$CH_3(CO)OOH + CH_3CHO \longrightarrow 2CH_3(CO)OH \tag{4.12}$$

[2] The question of whether photogenerated holes or ·OH radicals react with organic compounds has still not been completely settled (see, e.g., [119, 132]. However, in the present paper, I still assume that the reacting species is the ·OH radical.

Overall, only 0.5 photons participate in generating one molecule of acetic acid:

$$3CH_3CHO + O_2 + \cdot OH \longrightarrow 2CH_3(CO)OH + CH_3C\cdot O + H_2O \quad (4.13)$$

Therefore, the QY_{CH_3COOH} values were calculated using eq. 4.2. In addition, this set of reactions also constitutes a chain reaction mechanism, so that $CH_3C\cdot O$ is recycled back to eq. 4.10. Subsequently, CO_2 is generated from acetic acid as follows: [48]

$$CH_3(CO)OH + \cdot OH \longrightarrow CO_2 + H_2O + CH_3\cdot \quad (4.14)$$

In eqs. 4.9-4.12 , a total of 1.5 photons participate in reactions involving CO_2 generation. I therefore calculated the QY_{CO_2} values using eq. 4.3. It should be stressed that, if the radical chain process (eqs. 4.10-4.12) proceeds, the observed QY values, i.e., QY_{CH_3COOH} and QY_{total}, can exceed 100%. In fact, QY_{total} exceeded 100% for the 1000-ppmv initial concentration and the 1×10^{12} quanta cm^{-2} s^{-1} level of absorbed photon flux, indicating that chain reactions do in fact proceed. It is being assumed that the concentrations of organic intermediate species are relatively low, as is the ·OH (or hole) concentration, so that I can safely ignore the contribution of reactions involving the attack of intermediates by these species (·OH, h^+).

In order to better understand the relatively high (> 100%) observed QY values, it is useful to put them into the context of the QY values obtained under the same conditions with 2-propanol, for which the photocatalytic oxidation process is comparatively simple, i.e., involving only the equivalent of a single absorbed photon, producing acetone, with negligible contribution from chain reactions:

$$CH_3CH(OH)CH_3 + \cdot OH \xrightarrow{-H} CH_3C\cdot(OH)CH_3 \xrightarrow{-H^+} CH_3COCH_3 + e^- \quad (4.15)$$

where the $CH_3C\cdot(OH)CH_3$ radical is decomposed either via the so-called current-doubling reaction or via reaction with other oxygen species. For this simple system, it was found that a maximum, limiting value of the QY was obtained at low light intensities. [137] In the very low light

intensity region, the QY values were found to be essentially independent of the light intensity. Consequently, the reaction rate was dependent only upon the light intensity and not the reactant concentration, i.e., light-limited conditions. This is similar to the result of Egerton, et al., [87] who also studied the photocatalytic oxidation of 2-propanol at low light intensities. Although their experimental conditions were different from ours, i.e., pure 2-propanol suspension, they also found the reaction rate to depend linearly upon the light intensity, and they found a constant QY value of 0.67 over the range of 2×10^{13} to 2×10^{15} quanta s^{-1}, for a TiO_2 powder photocatalyst. This type of maximum QY value can vary somewhat depending upon various factors, such as the TiO_2 particle size [125] and the presence of bulk defects and bulk impurities. It was found to be 28% for the particular TiO_2 film used in this work. The behavior of the QY has been little studied at very low light intensities, and thus the concept of an intensity-independent QY is unfamiliar. However, the idea is that the number of photons being absorbed is so small that each absorption event is essentially independent. [137] An additional important point to be made with respect to the maximum QY values obtained for 2-propanol is that such values were obtained even for surface coverages of 2-propanol substantially less than unity. In our previous work, it was concluded that the active species, e.g., ·OH, has a long enough lifetime on the TiO_2 surface that it can diffuse a non-negligible distance (> 11 nm) before reacting with the organic molecule. [137]

At either higher relative light intensities or lower relative 2-propanol coverages, the QY values were found to decrease. This was explained on the basis of the competition between the reaction of the hydroxyl radical with the organic molecule and reactions of this radical with other species, leading to "non-productive" side reactions. The latter can include reactions of ·OH either with itself or with HO_2· (generated via eq.4.8). The surface coverages of both of these species are expected to be light intensity-dependent. Thus, as the ·OH radical diffuses along the surface, the probability that it will react with an organic molecule decreases as the distance between molecules increases and as the light intensity increases. Indeed, I concluded that the QY values were determined by the ratio of the number of absorbed photons to the number of adsorbed 2-propanol molecules. In fact, our experimental results were that, for a remarkably wide range of 2-propanol coverages and light intensities (although still in a

range that is generally considered to be relatively low intensity), a dependence of the QY on the ratio of absorbed photons to adsorbed molecules was observed. I have termed this ratio the "normalized light intensity" or I_{norm}. This dependence also indicated that there was negligible influence of the type of bulk recombination process normally associated with high light intensity, because otherwise the QY values would have then been dependent on the absolute rather than relative light intensities. [137] In the present work, I have also plotted QY values for acetaldehyde degradation (QY_{total}), as a function of I_{norm} (Figure 4.4) in the same fashion as done previously in the analysis of 2-propanol degradation. [137] I have also included the curves for 2-propanol degradation for comparison. Surprisingly, the curves for both acetaldehyde and 2-propanol coincided over a wide range of I_{norm} values. This coincidence is proposed to exist for two reasons: 1) the reactivity of the ·OH radical is so great that it can react rather unselectively with many different types of organic compounds; and 2) in both cases, the downward slope of the curve is related to the competition between reactions of ·OH with the organic molecule and reactions of ·OH with either itself or with HO_2· radical, i.e., "non-productive" reactions. Regarding the first point, the rate constants for proton abtraction by ·OH from 2-propanol (eq.4.15) and acetaldehyde (eq. 4.9) in bulk solution were 5.6×10^{-12} and 1.6×10^{-11} cm^3 $molecule^{-1}$ s^{-1}, respectively, which indeed are rather similar. [128] Moreover, when the QY_{CH_3COOH} values and QY_{CO_2} values were plotted separately in Figure 4.5, the plots also followed the same general path. These observations indicate that not only the reaction rate but also the reaction pathway of acetaldehyde degradation is dependent upon I_{norm}. The fact that there was no obvious break in the essentially linear curves for QY_{total} (Fig. 4) or QY_{CH_3COOH} (Fig. 5) at I_{norm} values of $\sim 10^{-4}$ s^{-1} due to a change in the contributions of the respective pathways is puzzling. However, the changes in the respective contributions are clearly shown in Figure 4.5 as being self-consistent.

In Figure 4.4, the limiting QY value of 28% for 2-propanol photodegradation to acetone can clearly be seen at low I_{norm} values. In contrast, however, in the region of I_{norm} below 10^{-4} s^{-1}, the QY values for acetaldehyde degradation continued to increase with decreasing I_{norm} and reached 180% for the value of I_{norm} of 3×10^{-5} s^{-1}. This value indicates the involvement of the radical chain pathway. The maximum QY value of

28% observed for 2-propanol, for which there is negligible involvement of chain-type reactions, is proposed to be due to intrinsic losses, e.g., trapping of holes by bulk defects and impurities. Thus, normalizing to this value more clearly indicates the involvement of the chain type pathway in acetaldehyde degradation. The idea that the major reaction pathway in the very low light intensity region is that producing acetic acid (eqs. 4.9-4.11) is evidenced by the fact that the QY_{CH_3COOH} value is approximately a factor of 5 greater than QY_{CO_2} at $I_{norm} = 3 \times 10^{-5}$ s^{-1}, as seen in Figure 4.5. Taking the QY_{CH_3COOH} value at this point (150%) indicates that there was significant involvement of the chain-type process. Taking into account the intrinsic loss factor (28%), the chain length could reasonably be considered to be as high as 5. Another recent example of a radical chain mechanism being involved with a photocatalytic process on TiO_2 was reported by Sauer et al. for the photodegradation of mixtures of toluene and perchloroethylene. [41] However, to our knowledge, the present work represents the first report of the estimation of a radical chain length in a TiO_2 photocatalytic process.

Returning to Figure 4.4, in the region of I_{norm} above 10^{-4} s^{-1}, the QY values for both acetaldehyde degradation and 2-propanol degradation decreased monotonically with increasing I_{norm}, taking on similar values. This result indicates that the expected radical chain reactions do not proceed to a significant extent on the TiO_2 surface in the acetaldehyde degradation process at moderate relative UV light intensities (I_{norm} $\sim 10^{-1}$). The chain reaction step (eq. 4.11) is favored by higher relative surface concentrations of acetaldehyde, which would be the case for lower I_{norm} values. For higher I_{norm} values, this relative surface concentration would be lower. The amount of adsorbed acetaldehyde is at most ca. 1 molecule nm-2 at the highest initial concentration (1000 ppmv) used in this study. Moreover, the contribution of termination reactions (see below) is favored by higher relative concentrations of radical species, which would be the case for higher I_{norm} values. For example, greater numbers of $CH_3COO\cdot$ radicals are produced at higher I_{norm} values. In this case, the radical chain reactions may be terminated by radical coupling reactions as shown below. Because $\cdot OH$ and $CH_3(CO)OO\cdot$ radicals are much more reactive than the $HO_2\cdot$ radicals generated via eq.4.8 , the steady-state concentrations of $\cdot OH$ and $CH_3(CO)OO\cdot$ are probably much lower than that of $HO_2\cdot$. Therefore, the $CH_3(CO)OO\cdot$ radical would be ex-

pected to react with the $HO_2\cdot$ radical, in the moderate I_{norm} range (I_{norm} < 10^{-3}): [157]

$$CH_3(CO)OO\cdot + HO_2\cdot \longrightarrow CH_3(CO)OOOOH \quad (4.16)$$

$$CH_3(CO)OOOOH \longrightarrow CH_3(CO)OOH + O_2 \quad (4.17)$$

Therefore, this may be the main termination pathway in this range. However, with much larger I_{norm} values (I_{norm} ~10^{-1}), other termination reactions (eqs. 4.18 and 4.21) begin to produce acetic acid, formaldehyde, and CO_2 as follows: [62,149,150]

$$2CH_3(CO)OO\cdot \longrightarrow CH_3(CO)OOOO(CO)CH_3 \quad (4.18)$$

$$CH_3(CO)OOOO(CO)CH_3 \longrightarrow 2CH_3\cdot + 2CO_2 + O_2 \quad (4.19)$$

$$CH_3\cdot + O_2 \longrightarrow CH_3OO\cdot \quad (4.20)$$

$$CH_3OO\cdot + CH_3(CO)OO\cdot \longrightarrow CH_3OOOO(CO)CH_3 \quad (4.21)$$

$$CH_3OOOO(CO)CH_3 \longrightarrow CH_2O + CH_3(CO)OH + O_2 \quad (4.22)$$

The homogeneous reaction rates for eqs.4.16,4.18, and 4.20 were estimated to be on the order of 1.4×10^{-11}, 1.6×10^{-11}, and 5.5×10^{-12} cm^3 $molecule^{-1}$ s^{-1}, respectively. [158,159] It should also be stressed that this pathway is particularly important for relatively high coverages of the organic compounds and high-intensity UV illumination. This well-known pathway also involves a chain-type mechanistic pathway, with the chain-propagating steps (eqs.4.19 and 4.20), leading to the complete mineralization of acetaldehyde.

In Figure 4.5, for the highest I_{norm} values, it can be seen that CO_2 is the major product. This results either from the pathway just discussed (eqs. 4.18-4.22) or that previously discussed (eq.4.15). I have argued that over most of the I_{norm} range discussed here, CO_2 generation occurs via the latter step. However, with increasing UV intensity, the contribution of the former becomes more important.

Table 4.1: Reaction rate coefficiency of ·OH radical with organics

Reaction	k/cm^3 molecule^{-1}s^{-1}
$\cdot OH + CH_3CHO \longrightarrow H_2O + CH_3CO$	1.6×10^{-11}
$\cdot OH + C_2H_5CHO \longrightarrow$ products	2.0×10^{-11}
$\cdot OH + (CHO)_2 \longrightarrow$ products	1.1×10^{-11}
$\cdot OH + i - C_3H_7OH \longrightarrow$ products	5.6×10^{-12}

4.5 Conclusions

Thus, the simple model of reaction dynamics on the TiO_2 surface, in which QY values are determined by the ratio of the number of absorbed photons to the number of adsorbed reactant molecules (normalized light intensity or I_{norm}) can be applied to the degradation of a compound such as acetaldehyde, for which there is the possible involvement of radical chain reactions. By comparing the QY values for acetone production from 2-propanol, a process in which no chain reactions exist, to those for acetic acid production from acetaldehyde at very low I_{norm}, I have estimated the chain length to be ca. 5 for acetic acid production. At higher I_{norm} values, the involvement of radical chain reactions vanishes due to the increasing importance of termination reactions. In this range, interestingly, the dependence of QY_{CH_3COOH} on I_{norm} was almost the same as that previously found for 2-propanol oxidation to acetone, indicating the similarity of the proposed competition of the organic compound with other species ($HO_2\cdot$ and ·OH itself) for ·OH radicals. I believe that the simple model presented provides a basic framework for the analysis of these complicated reaction factors.

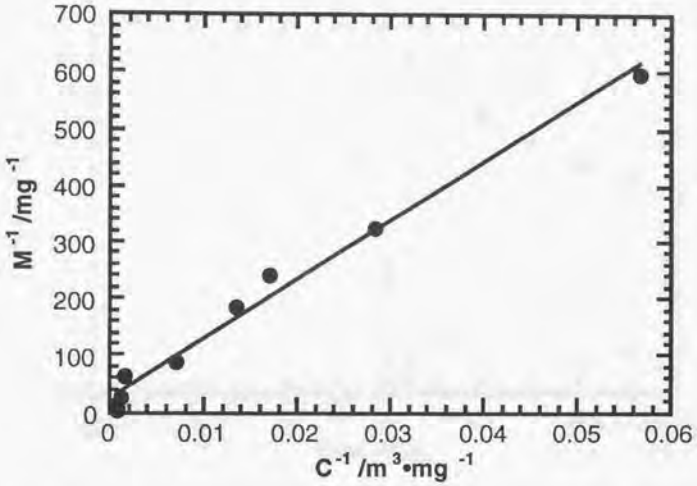

Figure 4.1: Inverse plots of the gas-phase acetaldehyde concentration (C /mg m^{-3}) and the weight of adsorbed acetaldehyde (M /mg) on the TiO_2 thin film used for analysis of the Langmuir-type isotherm.

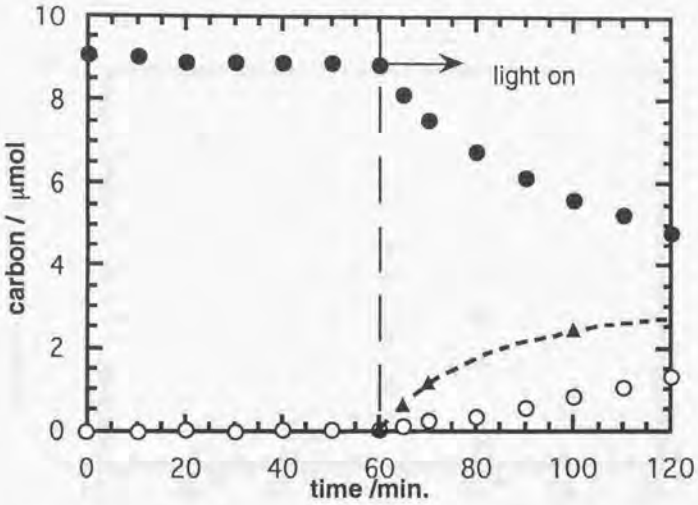

Figure 4.2: Experimental data for acetaldehyde photocatalytic degradation in the 1-L glass vessel, including intermediates and product evolution (incident UV intensity, 100 mW cm^{-2}; initial acetaldehyde concentration, 100 ppmv; ● acetaldehyde, ▲ acetic acid, ○ carbon dioxide; the dashed line indicates the carbon balance in the gas phase (see text)).

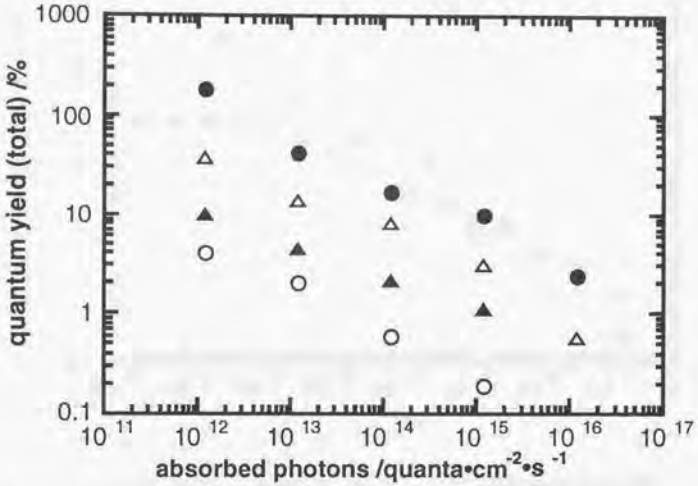

Figure 4.3: Dependence of QY_{total} on absorbed photons (initial acetaldehyde concentration, ● 1000 ppmv △ 100 ppmv, ▲ 10 ppmv, ○ 1 ppmv).

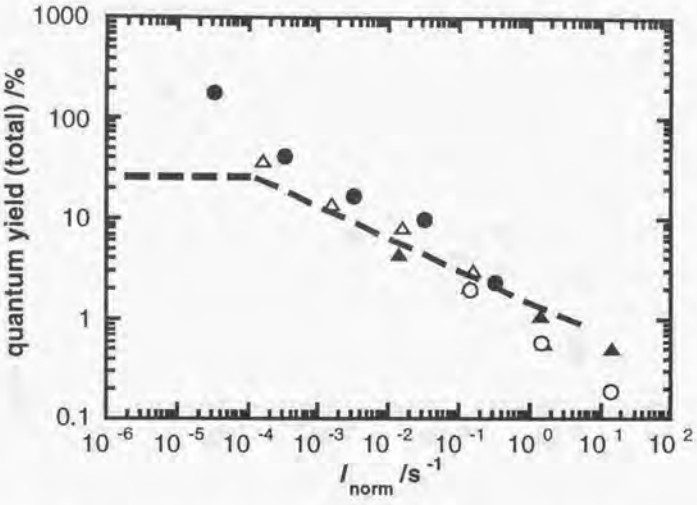

Figure 4.4: Plots of QY_{total} values vs. log I_{norm} (s^{-1}), defined as the ratio of the number of absorbed photons to the number of adsorbed acetaldehyde molecules (initial acetaldehyde concentration, ● 1000 ppmv △ 100 ppmv, ▲ 10 ppmv, ○ 1 ppmv; the dashed line indicates the QY-I_{norm} curve for 2-propanol degradation, as reported previously [136]).

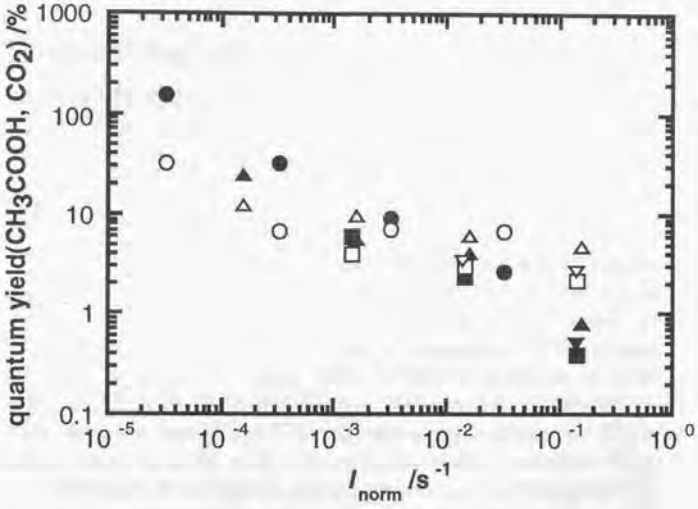

Figure 4.5: Log-log plots of QY_{CH_3COOH} values and QY_{CO_2} values vs. I_{norm} (s^{-1}) (initial acetaldehyde concentrations used for the determination of QY_{CH_3COOH}, ● 1000 ppmv, ▲ 100 ppmv, ■ 10 ppmv, ▼ 1 ppmv; those used for the QY_{CO_2} values, ○ 1000 ppmv, △ 100 ppmv, □ 10 ppmv, ▽ 1 ppmv).

Chapter 5

Photokilling effect of titanium dioxide containing papers

5.1 Introduction

Recently, the anti-bacterial effect has been paid much attention eigher in medical field and in our daily life, for example the food poisoning of O-157 bacteria and the infection of Staphylococcus in the hospitals. So far, some groups have reported that using suspension of TiO_2 powder bacteria was sterilized efficiently under UV light illumination for water treatment. [?, 52, 54–56, 58, 160] However, there are few quantitative reports using the immobilized TiO_2 not only in liquid phase but also in gaseous phase especially using TiO_2 containing building materials. Using our passive-type air purification system, not only the deodorizing function but also the antibacterial function is expected to be incorporated under lower level illumination from room light. More recently TOTO Co. Ltd. collaborating with this laboratory commercialized the tile coated with titanium dioxide (TiO_2) and a trace of Ag and Cu metals exibitng efficiently antibacterial function. In this Chapter, I examine anti-bacterial effects in order to determine whether they are also dependent on the concentration of *E. coli* cells and light intensity, using TiO_2 containing papers as a model of gaseous phase reaction. [109]

5.2 Experimental section

The TiO_2 containing paper was prepared by the following method. [109] A mixture of a softwood kraft pulp (NBKP) and TiO_2 aqueous sol (STS-01, 7 nm in diameter, Ishihara Sangyo Kaisha, Ltd.), coagulated on $Al(OH)_3$ in aqueous suspension, was flocculated with polycrylamide and polyamine binder. The amount of add TiO_2 was 10 wt% based on the weight of the pulp. The TiO_2-containing paper sheets were made using a Tappi standard sheet machine. The sheets were dried by press-drying at 115 $°C$ for 3 min. The basis weight of the pulp was 100 g cm^{-2}. TiO_2-containing papers were sterilized in an oven at 70 $°C$. *E. coli* cells (IFO 3301 strain) were grown aerobically in 2.5 mL of nutrient broth ("Daigo", Nippon Seiyaku) at 30 $°C$ for 16$\tilde{1}$8 h. The cells were centrifuged at 4000 rpm and suspended in sterilized water with appropriate dilution. *E. coli* cell suspension (150 mL,2×10^5 cells mL^{-1}, totally 3×10^4 cells) was pipetted onto the TiO_2-containing paper and sandwiched with two sterilized glasses. The pipetted suspension was sinked into the papers. The samples were illuminated with 15-W black fluorescent lamps (FL15 W, FL15 BL-B, National) and white fluorescent lamps; the light intensities were 1.0 mW cm^{-2} and 40 mW cm^{-2}, respectively, which was measured using a UV radiometer (UVR-36, TOPCON) at the sample position. After illumination, the sample paper was dipped into 0.15 mol L^{-1} aqueous sodium chloride solution and the cells were removed by shaking it hardly. However, the removing ratio is approximately 60 % either pulp sheets and TiO_2 containing papers. This solution was spread onto nutrient agar medium (Standard Method Agar "Nissui", Nissui Seiyaku) and incubated for 24 h in order to determine the number of viable cells in terms of colony-forming units.

5.3 Results and discussion

The time course change of the surviving ratio of *E. coli* cell is shown in Figure 5.1. The surviving ratio was initialized by the number of removed *E. coli* cells under no illumination. The E. coli cells on the TiO_2-papers were sterilized approximately 95% within 1.5 h under illumination with black fluorescent light (1.0 mW cm^{-2}), 60% with white fluorescent light

(0.3 mW cm^{-2}), and 40% even under dark conditions. The sterilizing ratio of *E. coli* cells using TiO_2-papers are summarized using different type of UV light source as comparing with that using the pulp sheets in Figure 5.2. Using pulp sheets, any E. coli cells were not sterilized under dark conditions, but sterilized approximately 25 % under UV light illumination. This is supposed to be due to drying and thermal effect. Therefore the net sterilization ratio was ca. 55 % and 20 % under black fluorescent light and white fluorescent light illumination respectively. The reason why the sterilization ratio of 40 % using TiO_2-paper under dark conditions are not well-known at this stage. It is noteworthy that the increasing quantum yield with decreasing light intensity seems to be higher than that of degradation reaction of gaseous organic molecules, that is the value of the slope, i.e., the exponent a in the $R = KI^a$ relation, is approximately ca. 0.3 from Figure 2. If the sterilization using TiO_2 containing materials is more effective under the low-intensity UV light illumination than the degradation reaction of gaseous organic molecules, a different reaction mechanism from the degradation reaction of gaseous organic molecules with ·OH radicals is considered for sterilization. Recently Kikuchi et al. proposed that the actual lethal agent for the photokilling effect using TiO_2 materials is H_2O_2, subsequently produced from ·OH and O_2^-. [53] Oxygen is reduced to superoxide anion (O_2^-), which is less reactive itself but produces more highly toxic species described as follows,

$$O_2 \xrightarrow{e^-} O_2^- \xrightarrow{-H} HOO\cdot \xrightarrow{H^+} H_2O_2 \qquad (5.1)$$

Under these ambient conditions, O2 molecules is to sufficient to supply on the TiO_2 surface that the photokilling effect by OH radical and H_2O_2 simultaneously also occur in this case. In the future, I try to examine photokilling effect dependence on the light intensity and cell concentration for their wide ranges more intensively.

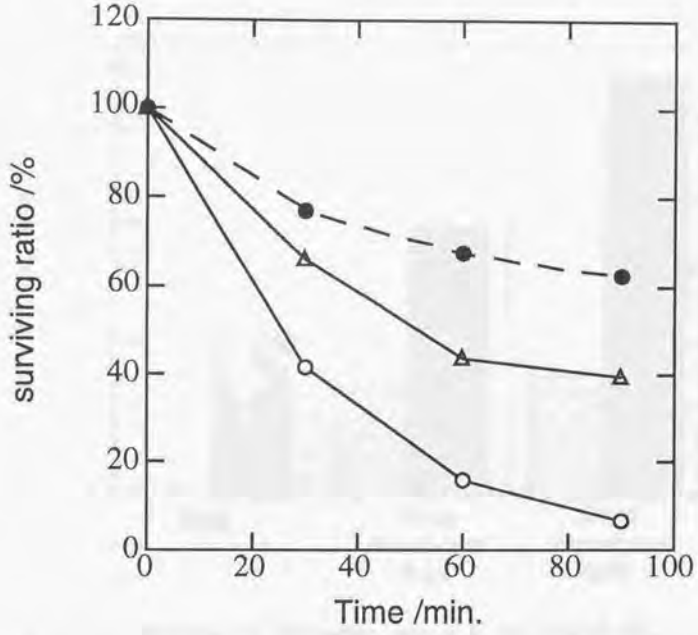

Figure 5.1: under ○,black fluorescent light (1.0 mW cm^{-2});△, white fluorescent light (0.3 mW cm^{-2}); and ●,dark conditions; initial concentration 1.2×10^3 cells cm^{-2}.

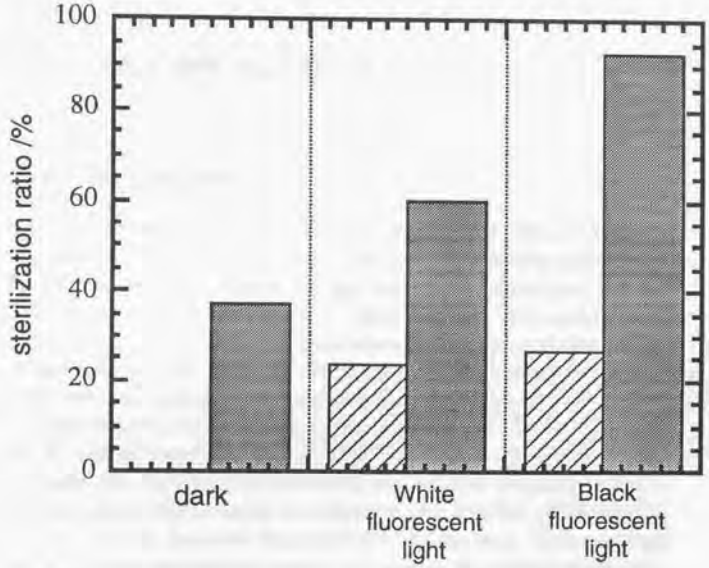

Figure 5.2: Dependence of sterilization ratio of *E. coli* cells of TiO_2 containing papers and pulp sheets on light intensity using different UV light sources; the light intensities were 1.0 mW cm $^{-2}$ for black fluorescent light and 0.3 mW cm^{-2} for white fluorescent light, respectively.

Chapter 6

Summary and further study

6.1 Summary

A new simple model of the reaction dynamics of the photocatalytic decomposition of gaseous organic molecules on the TiO_2 surface is concluded for the first time in the present study through the use of pure anatase TiO_2 sintered thin films under low-intensity UV light. This model considers the reaction rates and quantum efficiency as a function of the number of adsorbed reactant molecules and the number of absorbed photons. I summarize the findings below, distributing them roughly into two regions of light intensity: (1) extremely low-intensity UV light (down to 34 nW cm^{-2}), and (2) comparatively strong UV light (up to 60 mW cm^{-2}). As a results, the regions of light intensity and reactant concentration covered approximately 6 orders of magnitude and 5 orders of magnitude, respectively. As described in Section 2.2., all the data were supported by the reliable experimental procedures, such as the rigorous estimation of adsorbed light intensity of the sample film, the detection of reactants with so high sensitivity that the detection limits was achieved down to 1 ppbv using gas chromatography, and so forth.

It can be concluded that the quantum yield (QY) values for the photocatalytic decomposition of gaseous 2-propanol are determined by the ratio of the number of absorbed photons to the number of adsorbed 2-propanol molecules (i.e., a normalized light intensity, I_{norm}) under extremely low-intensity UV light illumination (36 nW - 45 μW cm^{-2}). Under such low-intensity UV illumination, the QY values increase gradually with decreasing numbers of absorbed photons and finally saturate (28%) for I_{norm}

less than 10^{-4} s^{-1}. These types of reaction dynamics are observed for a wide range of 2-propanol concentrations (1-1000 ppmv). On the basis of these results, it is estimated that either ·OH radicals or 2-propanol molecules can diffuse stably on the TiO_2 surface at least ca.. 11 nm in order to react with each other. The decrease in QY is attributed to increases in the rates of reaction for ·OH radicals with HO_2· radicals and ·OH with itself, relative to that with 2-propanol. The maximum QY value of 28% represents the intrinsic charge-separation efficiency of this particular TiO_2 thin film sample.

The photocatalytic decomposition efficiency of gas-phase acetaldehyde was studied using a titanium dioxide thin film under weak UV illumination. Acetic acid and carbon dioxide were detected as the main reaction products. It was found that the apparent quantum yields (QY) for acetaldehyde degradation are determined by the normalized absorbed photon number (I_{norm} /s^{-1}). This result is similar to that for 2-propanol degradation. However, although the QY values for 2-propanol degradation reached a constant value (ca. 28%) for very low relative light intensity (in the I_{norm} region less than 10^{-4} s^{-1}), those for acetaldehyde degradation continued to increase with decreasing I_{norm} and reached 180% for an initial concentration of 1000 ppmv, at an I_{norm} value of 3×10^{-5} s^{-1}. This discrepancy is due to the existence of radical chain reactions for the latter reaction. Compared to the maximum QY yield for 2-propanol decomposition (28%), which involves no chain-type reactions, the maximum QY for acetaldehyde conversion to acetic acid (150%) implies a radical chain-type process with a chain length of approximately five. This is because the frequency of radical chain-type decomposition reactions for acetaldehyde increases with decreasing numbers of absorbed photons, thus reducing the frequency of termination reactions. It was confirmed that the new simple model of the reaction dynamics is capable of being applied also to reactants such as acetaldehyde which are decomposed via complex radical chain reactions on the TiO_2 surface.

On the other hand, as a result of the degradation of gaseous 2-propanol under comparatively high-intensity UV light (35 μW cm^{-2} - 60 mW cm^{-2}), the degradation rates initially increased with increasing numbers of absorbed photons, then tending to saturate, and finally mass transport-limited conditions were reached. The values of the numbers of absorbed photons at which mass-transport-limited conditions began to be observed

varied for different initial concentrations, with the number of absorbed photons increasing drastically with increasing initial concentration. This can be explained by saying that, for the higher initial concentrations, larger numbers of absorbed photons are necessary for the photodegradation reaction proportional to the number of adsorbed reactant molecules, following the Langmuir-type isotherm on the TiO_2 surface, in order to overcome the increasing rates of reactant flux. The flux of gaseous reactant molecules for 1 ppmv under mass-transport limited conditions was shown to be 2.6×10^{12} molecules cm^{-2} s^{-1}. I was able to model the time course of changes of gaseous 2-propanol concentrations under mass-transport-limited conditions using the one-dimensional diffusion equation, assuming the thickness of the boundary layer to be 1.5 cm under a natural convective flow of 1 cm s^{-1}. In a similar fashion, an examination of the degradation reaction of acetaldehyde was carried out, and mass-transport-limited conditions appeared at almost the same value of light intensity as that for 2-propanol, and the degradation rate for acetaldehyde was also the same as that for 2-propanol under mass transport-limited conditions.

Based on these results, I succeeded in demonstrating a region of mass-transport-limited conditions and a region of purely light-limited conditions for the degradation reactions of gaseous organic compounds in terms of the reactant concentration and light intensity. From a plot of the latter two variables, one can estimate the maximum value of effective light intensity and the conversion time at the maximum removal rate for actual problematic reactants at ppbv levels. Assuming that the diffusion coefficient $D = 0.1$ cm^2 s^{-1} and that the degradation rate constant does not depend greatly on the type of gaseous organic reactant, the estimation of mass-transport-limited conditions can be applied to many kinds of organic reactants.

6.2 Further study

Many unknown factors to influence the quantum yield has been remaining to solve.

The first point is the maximum diffusion length of ·OH radical on TiO_2 surface. In this study as described in Chapter 2, the maximum QY

value under purely light-limited conditions was all the same for different initial concentrations between 1-1000 ppmv. However, according to the data obtained for 100 ppbv in Chapter 3, at the break points (I_b), at which mass transport control is reached, the QY values for 100 ppbv are different, less than that for 1 ppmv. The amount of adsorbed molecule was one tenth of 1 ppmv, then it should be the same as 1 ppmv because the R_A and R_B will be also ten times each. It means that $\tilde{3}0$ nm might be the limitation to diffuse on TiO_2 surface for ·OH radical.

The second point is that the type of adsorption, physisorbed or chemsorbed, hasn't been confirmed in this study. This term is a very fundamental one to solve which can diffuse longer, ·OH or reactant. There are many reports about the state of adsorption on TiO_2 surface. [161–165] Moreover the influence of adsorbed water to the photocatalysis like this study should be also solved in the future. [166, 167]

The third point is the influence of surface area (roughness) and porosity to Figure 3.9. In fact the photocatalysis is catalysis in one sense. It is influenced by both the surface area and the light intensity fundamentally. If the absorbed light intensity is the same, the higher the surface area is , the higher the reaction rate could be obtained. [74] Therefore the curves A and B in Figure 3.9 could be shifted dependent on the factor. There was supposed to be no influence of porosity in this study because of its meso-porosity. In general, there might be no influence in air-solid photocatalysis because the diffusion rate is high, but conversely, using an apparent flat type thin film including microporous leads to misestimating of reaction rate as higher light intensity. To regularize Figure 3.9, I have to use a different sample that is easy to modify the surface area.

To study further this reaction dynamics, I raise three options here: (1)using transparent thin film and measurement of photocatalysis by an optical method, (2)using the partial metal depositing film [57, 168] or adsorbent supported film, [120, 169–172] (3)detection of the amount of ·OH radical and HO_2· radical.

Regarding to (1), Mr. Kenzo Takahashi is efforting to investigate the *in-situ* observation of surface reaction using dye (malachite green) adsorbed on TiO_2 surface. [173] The same QY curve dependence on I_{norm} is confirmed. Moreover in the different humidity, the QY curve is drastically changed and shifted. The higher humidity condition, the maximum QY value raises, on the other hand, the lower the value of I_{norm} at which

QY value start to decrease. This phenomenon is apparently depending on the diffusion process of ·OH radical.

Regarding to (2), due to separation of the oxidation site and the reduction site, I could obtain more critical information about surface recombination step. In this study, bared TiO_2 film was used and I concluded that the reason why the QY value decrease is the surface recombination reaction of ·OH radical and HO_2· radical. In the case of (2), the point at the QY value decrease should indicate the surface recombination reaction of ·OH radical each other, not with HO_2· radical.

All of the advancement of this study are concerning (3). Recently, Mr. Ishibashi at KAST starts to study of detection of surface radical. [?] Using luminor,which is famous for the reaction with oxide radical, one can detect how much the surface radicals exist on TiO_2 surface. At this stage, there seems many problem, but in the future, it is definitely necessary to combine with this system to define the surface reaction dynamics quantitatively.

Reviewing the present work, I consider the possibility of a new environmental purification system employing many different types of TiO_2-containing building materials with high photocatalytic activities and large surface areas under low-intensity UV light and natural (i.e., not forced) convection. Even under extremely low-intensity UV illumination, ·OH radicals are generated on the TiO_2 photocatalyst surface, and some reactions always occur. However, practically speaking, the removal rate is too slow for indoor air purification under low-intensity UV light. In this case, it is suggested to use this system in conjunction with comparatively strong UV light sources, particularly for small closed spaces, while generating no additional noxious compounds as intermediates.

However, the reaction mechanisms for the self-cleaning effect and for the anti-bacterial effect are distinct from that for the degradation of gaseous reactants. At the present time, surface hydrophilicity is regarded as the most important factor in the self-cleaning effect, while the presence of H_2O_2 and HO_2· radicals is regarded as the most important factor in the anti-bacterial effect, based on research carried out in this laboratory. It seems that the charge separation efficiency and flux of reactant do not necessarily have an influence. Even though the mechanisms of photocatalytic reactions are quite complicated, it is expected that the relative importances of the various factors for these effects will be esti-

mated correctly by comparison with gaseous molecule degradation, as I have attempted to describe in this thesis.

It is the author's hope that the present study not only contributes to the progress of TiO_2 photocatalysis, both fundamentally and practically, but also helps researchers in other basic fields as an important foundation.

List of publications

1) Y. Ohko, K. Hashimoto, and A. Fujishima,
"Kinetics of photocatalytic reactions under extremely low-intensity UV illumination on titanium dioxide thin films,"
J. Phys. Chem. A **1997**, 101(43), 8053-8058. (Chapter 2)

2) Y. Ohko, K. Hashimoto, and A. Fujishima,
"Kinetic analysis of photocatalytic degradation of gaseous 2-propanol under mass-transfer-limited conditions with TiO_2 film photocatalyst,"
J. Phys. Chem., in press. (Chapter 3)

3) Y. Ohko, D. A. Tryk, K. Hashimoto, and A. Fujishima,
"Autoxidation of acetaldehyde initiated by TiO_2 photocatalysis under weak UV illumination,"
J. Phys. Chem., accepted. (Chapter 4)

(4) Y. Ohko, K. Matsubara, K. Hashimoto, and A. Fujishima,
"Photokilling effect of titanium dioxide containing papers,"
in preparation. (Chapter 5)

(5) Y. Ohko, M. Watanabe, K. Hashimoto, and A. Fujishima,
"Effects of cations coexisting in water on TiO_2 photocatalysis,"
in preparation.

Acknowledgments

I was able to finish writing this dissertation thanks to assistance of many people. First of all, I would like to thank Professor Akira Fujishima and Associate Professor Kazuhito Hashimoto (present belonging to Research Center for Advanced Science and Technology (RCAST), The University of Tokyo as a professor) for their helpful guidance, discussions, and continuous encouragement.

I would also like to thank the reviewers, Professor M. Misonō, Professor T. Kudo and Associate Professor M. Miyayama for their valuable comments and suggestions.

I express gratitude to the staffs in this laboratory, Dr. D. A. Tryk, Dr. R. Baba (present belonging to Tokyo University of Mercantile Marine), Dr. T. Miwa, and Dr. I. Yagi for their helpful advices, and Ms. Y. Takahashi for her constant help in official matters. In particular, I had Dr. D. A. Tryk spend much time to read and revise my three submitted manuscripts so carefully that they were all succeeded in being accepted to the Journal of Physical Chemistry.

I gratefully acknowledge the Ministry of Education, Science, and Culture of Japan for financial support for three years since July in 1995.

My elders, friends and juniors in this laboratory supported me so kindly and encouraged me so much that my curiosity has driven forward and I could have achieved my own work. In particular, I would like to thank Dr. O. Sato (present belonging to Hashimoto Project at Kanagawa Academy of Science and Technology (KAST) laboratory in University of Tokyo Institute of Polytechnics) Dr. T. Saeki (present belonging to Hitachi Ltd.), Dr. H. Sakai (present belonging to Science University of Tokyo), Dr. K. Ajito (present belonging to NTT Basic Research Lab.),

Dr. H. Yoshiki (present belonging to The Institute of Physical and Chemical Research), Mr. H. Hagiwara (present belonging to Toppan Printing Co., Ltd.), Mr. T. Tanabu (present belonging to Japanese Patent Office), Mr. K. Ikeda (present belonging to Fujikura Ltd.), Mr.Y. Morisaki, Mr. K. Nakayama, Mr. M. Yanagisawa, Ms. H. Fujii and Ms. F. Hosono.

It has been a great pleasure to spend my time with the 042 roommates, Dr. X. M. Yang, Dr. J. J. Kim (present belonging to LG Electronics Inc.), Mr. A. Muramatsu (present belonging to Sumitomo 3M Ltd.), Mr. Koichiro Takahashi (present belonging to Showa Denko K.K.), Mr. K. Hirota, Mr. Tetsuro Noguchi, Mr. Kenzo Takahashi, Mr. T. Yamamoto, Mr. Mitsutoshi Noguchi (present belonging to TOTO Ltd.), and Mr. K. Kunikane (I never forget his pleasant leading at the beginning of this research). It has also been a special pleasure to be collaborated eagerly with Mr. Y. Yoshida (present belonging to FUJITSU Ltd.), Mr. T. Noguchi, Mr. Kenzo Takahashi, Mr. Y. Wakatabi (present belonging to Dainichseika Color & Chemicals Mfg. Co., Ltd.), Mr. H. Matsubara (Gifu Prefectural Paper Research Institute), Mr. M. Watanabe (Ishihara Sangyo Kaisha), Mr. N. Nakada (YKK Co.), Mr. F. Sunada (Nisseki Co. Ltd.), and Mr. K. Takami (Ube Nitto-Kasei Co. Ltd.).

I received good and vigorous incentive from many researchers at KAST. In particular, Professor K. Iyoda (present belonging to Tokyo Metropolitan Univeristy), Dr. N. Neghishi (present belonging to National Institute for Resources and Environment), Dr. Y. Kikuchi (present belonging to CANON Inc.), Mr. Tagawa (Hokuto Denko Co.), Mr. S. Fukayama (Nippon Soda Co. Ltd.), Mr. T. Kawasaki (Tokyo Gas Co. Ltd.), Dr. S. Fujita, Ms. K. Sunada, Dr. S. Ohkoshi (present belonging to RCAST of Tokyo University), Dr. K. Nagai, Dr. L. Jiang, Dr. R. Wang, and Mr. Y. Einaga.

Every year, many great scientists visit to this laboratory. Among them, I would like to thank Professor Adam Heller (Texas University[1]) and Professor Marc A. Anderson (Wisconsin University) for their fruitful discussions.

Besides, I would like to thank Professor Y. Ujihira (retired last year), Dr. A. Uedono (present belonging to Tsukuba University), Dr. S. Watauchi

[1]I visited to his laboratory on the way to the 189th Meeting of the Electrochemical Society (Los Angeles) in May, 1996.

(present belonging to Yamanashi University) with whom I studied positron annihilation technique during 1991-1994, which was my precious experience.

I never forget the final interview I had last summer. It was memorable because almost all of above-mentioned people came to attend as audience and to watch me affectionately. However, unfortunately, I couldn't reply a few of the reviewer's comments promptly and accurately. I've thought it shameful to have fallen in such a situation in front of these guys. I repented this complete failure due to shortages of my preparation and capability. Even though, Professor Fujishima gave me a big chance to work in Osaka University as an assistant, which is, needless to say, one of best positions, scarcely in Japan. Therefore, I would like to swear my continuous efforts day by day ,that, I believe, make my dream of becoming a great professor come true.

Finally, I express my deep gratitude to my family and my best friends whose loves ask nothing in return. With listening to the cinema song, Hercules.

I have often dreamed
Of a far-off place
Where a great warm welcome
Will be waiting for me
Where the crowds will cheer
When they see my face
And a voice keeps saying
This is where I'm meant to be

I will find my way
I can go the distance
I'll be there someday
If I can be strong
I know every mile
Will be worth my while
I would go most anywhere to feel like I belong

February 1998
Tokyo, Japan

大古善久

Yoshihisa OHKO

Bibliography

[1] Sauer, M. L.; Ollis, D. F. *J. Catal.* **1996**, *158*, 570.

[2] Fujishima, A.; Honda, K. *Nature* **1972**, *238*, 37.

[3] Gratzel, M.; Wiley-Interscience: Amsterdam, 1989.

[4] Colombo, D. P.; Roussel, K. A.; Sae, J.; Skinner, D.; ; Cavaleri, J. J.; Bowman, R. M. *Chem.Phys. Lett.* **1995**, *232*, 207.

[5] Skinner, D. E.; Colombo, D. P.; Cavaleri, J. J.; Bowman, R. M. *J. Phys. Chem.* **1995**, *99*, 7853.

[6] Jackson, N. B.; Wang, C. M.; Luo, Z.; Schwitzgebel, J.; Ekerdt, J. G.; Brock, J. R.; Heller, A. *J. Electrochem. Soc.* **1991**, *138*, 3660–3664.

[7] Wang, C. M.; Heller, A.; Gerischer, H. *J. Am. Chem. Soc.* **1992**, *114*, 5230.

[8] Rosenberg, I.; Brock, J. R.; Heller, A. *J. Phys. Chem.* **1992**, *96*, 3423.

[9] Gao, Y. W.; Shen, H.; Dwight, K.; Wold, A. *Mater. Res. Bull.* **1992**, *27*, 1023.

[10] Albert, W.; Gao, Y. W.; Toft, D.; Dwight, K.; Wold, A. *Mater. Res. Bull.* **1992**, *27*, 961.

[11] Lee, W.; Do, Y.; Dwight, K.; Wold, A. *Mater. Res. Bull.* **1993**, *28*, 1127.

[12] Lee, W.; Shen, H.; Dwight, K.; Wold, A. *J. Solid State Chem.* **1993**, *106*, 288.

[13] Wold, A. *Chem. Mater.* **1993**, *5*, 280–283.

[14] Papp, J.; Shen, H.; Kershaw, R.; Dwight, K.; Wold, A. *Chem. Mater.* **1993**, *5*, 284.

[15] Cui, H.; Shen, H.; Dwight, K.; Wold, A. *Mater. Res. Bull.* **1993**, *28*, 195.

[16] Papp, J.; Soled, S.; Dwight, K.; Wold, A. *Chem. Mater.* **1994**, *6*, 496.

[17] Do, Y.; Lee, W.; Dwight, K.; Wold, A. *J. Solid. State. Chem.* **1994**, *108*, 198.

[18] Cui, H.; Dwight, K.; Soled, S.; Wold, A. *J. Solid. State. Chem.* **1995**, *115*, 187–191.

[19] Gerischer, H.; Heller, A. *J. Electrochem. Soc.* **1992**, *139*, 113.

[20] Gerischer, H.; Heller, A. *J. Phys. Chem.* **1991**, *95*, 5261.

[21] Gerischer, H. *J. Phys. Chem.* **1991**, *95*, 1356.

[22] Filimonov, V. N. *Dokl. Akad. Nauk SSSR* **1964**, *154*, 922.

[23] Bickley, R. I.; Stone, F. S. *J. Catal.* **1973**, *31*, 389.

[24] Goodeve, C. F.; Kithchener, J. A. *Trans. Faraday Soc.* **1938**, *34*, 570.

[25] Jacobsen, A. *Ind. Eng. Chem.* **1949**, *41*, 25.

[26] Gravelle, P.; Juillet, F.; Meriaudeau, P.; Teichner, S. J. *Discuss. Faraday Soc.* **1971**, *52*, 140.

[27] Munuera, G.; Stone, F. S. *Discuss. Faraday Soc.* **1971**, *52*, 205.

[28] Cunningham, J.; Meriaudeau, P. *Discuss. Faraday Chem. Soc.* **1975**, *58*, 1499.

[29] Cunningham, J.; Meriaudeau, P. *Discuss. Faraday Chem. Soc.* **1975**, *58*, 1495.

[30] Ohnishi, T.; Nakato, Y.; Tsubomura, H. *Ber. Bunsenges. Phys. Chem.* **1975**, *79*, 523.

[31] Okamoto, K.; Yamamoto, Y.; Taneka, H.; Itaya, A. *Bull. Chem. Soc. Jpn.* **1985**, *58*, 2023.

[32] Sopyan, I.; Watanabe, M.; Murasawa, S.; Hashimoto, K.; Fujishima, A. *Chem. Lett.* **1996**, 69.

[33] Sopyan, I.; Watanabe, M.; Murasawa, S.; Hashimoto, K.; Fujishima, A. *J. Electroanal. Chem* **1996**, *415*, 183.

[34] Sopyan, I.; Watanabe, M.; Murasawa, S.; Hashimoto, K.; Fujishima, A. *J. Photochem. Photobiol. A: Chem.* **1996**, *98*, 79.

[35] Sopyan, I.; Murasawa, S.; Hashimoto, K.; Fujishima, A. *Chem. Lett.* **1994**, 723.

[36] Yamashita, H.; Ichihashi, Y.; Harada, M.; Stewart, G.; Fox, M. A.; Anpo, M. *J. Catal.* **1996**, *158*, 97.

[37] Hidaka, H.; Zhao, J.; Satoh, Y.; Nohara, K.; Pelizzetti, E.; Serpone, N. *J. Mol. Catal.* **1994**, *88*, 239–248.

[38] Suzuki, K.; Satoh, S.; Yoshida, T. *Denki Kagaku* **1991**, *59(6)*, 521.

[39] Peral, J.; Ollis, D. *J. Catal.* **1992**, *136*, 554.

[40] Ollis, D. E.; Al-Ekabi, H., Eds. *Photocatalytic Purification and Treatment of Water and Air*; Elsevier: Amsterdam, 1993.

[41] Sauer, M.; Hale, M.; Ollis, D. *J. Photochem, Photobiol, A Chem.* **1995**, *88*, 169.

[42] Sauer, M.; Ollis, D. *J. Catal.* **1994**, *149*, 81.

[43] Upadhya, S.; Ollis, D. F. *J. Phys. Chem.* **1997**, *101*, 2625–2631.

[44] Peral, J.; Ollis, D. F. *J. Mol. Catal. A Chem.* **1997**, *115*, 347.

[45] Luo, Y.; Ollis, D. F. *J. Catal.* **1996**, *163*, 1–11.

[46] Heller, A. *Acc. Chem. Res.* **1995**, *28*, 503.

[47] Paz, Y.; Luo, Z.; Rabenberg, L.; Heller, A. *J. Mater. Res.* **1995**, *10*, 2842.

[48] Schwitzgebel, J.; Ekerdt, J. G.; Gerischer, H.; Heller, A. *J. Phys. Chem.* **1995**, *99*, 5633.

[49] Ibusuki, T.; Takeuchi, K. *J. Mol. Catal.* **1994**, *88*, 93.

[50] Zhang, S.; Kobayashi, T.; Nosaka, Y.; Fujii, N. *Denki Kagaku* **1995**, *63*, 927–931.

[51] Zafra, A.; Garcia, J.; Mill, A.; Domenech, X. *J. Mol. Catal.* **1991**, *70*, 343.

[52] Matsunaga, T.; Tomoda, R.; Nakajima, T.; Nakamura, N.; Komine, T. *Appl. Environ. Microbiol.* **1988**, *42*, 1330.

[53] Kikuchi, Y.; Sunada, K.; Iyoda, T.; Hashimoto, K.; Fujishima, A. *J. Photochem. Photobiol. A Chem.* **1997**, *106*, 51.

[54] Richardson, S. D.; Thruston, A. D.; Collette, T. W.; Patterson, K. S.; Lykins, B. W.; Ireland, J. C. *Environ. Sci. Technol.* **1996**, *30*, 3327–3334.

[55] Ireland, J. C.; Klostermann, P.; Rice, W.; Clark, R. M. *Appl. Environ. Microbiol.* **1993**, *59*, 1668.

[56] Wei, C.; Lin, W. Y.; Zaiinal, Z.; Williams, N. E.; Zhu, K.; Kruzic, A. P.; L., S. R.; Rajeshwar. *Environ. Sci. Technol.* **1994**, *28*, 934.

[57] Sakai, H.; Baba, R.; Hashimoto, K.; Fujishima, A. *J. Electroanal. Chem.* **1994**, *379*, 199–205.

[58] Cai, R.; Hashimoto, K.; Fujishima, A.; Kubota, Y. *J. Electroanal. Chem.* **1992**, *326*, 345.

[59] Ikeda, K.; Sakai, H.; Baba, R.; Hashimoto, K.; Fujishima, A. *J. Phys. Chem.* **1997**, *101*, 2617–2620.

[60] Russel, G. A. *J. Am. Chem. Soc.* **1957**, *79*, 3871.

[61] Bolland, J. L.; Cooper, H. R. *Proc. R. Soc.(London)* **1954**, *A255*, 405.

[62] Clinton, N. A.; Kenley, R. A.; Traylor, T. G. *J. Am. Chem. Soc.* **1975**, *97*, 3746.

[63] Yamagata, S. ——— **1989**, –, Ph.D. Thesis.

[64] Pruden, A. L.; Ollis, D. F. *J. Catal.* **1983**, *82*, 404.

[65] Bravo, A.; Garcia, J.; Domenech, X.; Peral, J. *J. Chem. Res.* **1993**, (9), 376–377.

[66] Brezova, V.; Stasko, A.; Biskupic, S.; Blazkova, A.; Halinova, B. *J. Phys. Chem.* **1994**, *98*, 8977.

[67] Blazkova, A.; Brezova, V.; Soldanova, Z.; Stasko, A.; Soldan, M.; Ceppan, M. *J. Mater. Sci.* **1995**, *30*, 729.

[68] Ohtani, B.; Kakimoto, M.; Nishimoto, S.; Kagiya, T. *J Photochem Photobiol A-Chem* **1993**, *70*, 265–272.

[69] Ohtani, B.; Nishimoto, S. *J. Phys. Chem.* **1993**, *97*, 920.

[70] Kominami, H.; Matsuura, T.; Iwai, K.; Ohtani, B.; Nishimoto, S.; Kera, Y. *Chem. Lett.* **1995**, (8), 693–694.

[71] Kominami, H.; Kato, J. I.; Kohno, M.; Kera, Y.; Ohtani, B. *Chem. Lett.* **1996**, (12), 1051–1052.

[72] Ohtani, B.; Goto, Y.; Nishimoto, S.; Inui, T. *J. Chem. Soc. Faraday Trans.* **1996**, *92*, 4291–4295.

[73] Cunningham, J.; Sedlak, P. *J. Photochem. Photobiol. A:Chem.* **1994**, *77*, 255–263.

[74] Aguado, M. A.; Anderson, M. A.; Hill, C. G. *J. Mol. Catal.* **1994**, *89*, 165.

[75] Kormann, C.; Bahnemann, D. W.; Hoffmann, M. R. *Environ. Sci. Technol.* **1991**, *25*, 494.

[76] Hoffman, A. J.; Yee, H.; Mills, G.; Hoffmann, M. R. *J. Phys. Chem.* **1992**, *96*, 5540.

[77] Hoffman, A. J.; Mills, G.; Yee, H.; Hoffmann, M. R. *J. Phys. Chem.* **1992**, *96*, 5546.

[78] Hoffmann, A. J.; Carraway, E. R.; Hoffmann, M. R. *Environ. Sci. Technol.* **1994**, *28*, 776.

[79] Trillas, M.; Peral, J.; Domenech, X. *Appl. Catal. B-Environ.* **1993**, *3*, 45–53.

[80] Lepore, G. P.; Langford, C. H.; Vichova, J.; Vlcek, A. J. *J. Photochem. Photobiol. A: Chem.* **1993**, *75*, 67.

[81] Lepore, G.; Pant, B.; Langford, C. *Can. J. Chem.* **1993**, *71*, 2051.

[82] Bideau, M.; Claudel, B.; faure, L.; Kazouan, H. *J. Photochem. Photobiol. A Chem.* **1991**, *61*, 269.

[83] Lai, C. W.; Kim, Y. I.; Wang, C. M.; Mallouk, T. E. *J. Org. Chem.* **1993**, *58*, 1393.

[84] Shiragami, T.; Ankyu, H.; Fukami, S.; Pac, C.; Yanagida, S.; Mori, H.; Fujita, H. *J. Chem. Soc. Faraday Trans.* **1995**, *88*, 1055.

[85] Shiragami, T.; Fukami, S.; Wada, Y. J.; Yanagida, S. *J. Phys. Chem.* **1993**, *97*, 12882.

[86] Harvey, P.; Rudham, R. *J. Chem. Soc., Faraday Trans. 1* **1988**, *84*, 4181.

[87] Egerton, T. A.; King, C. J. *J. OilCol. Chem. Assoc.* **1979**, *62*, 386.

[88] Nosaka, Y.; Nakaoka, Y. *Langmuir* **1995**, *11*, 1170.

[89] Nosaka, Y.; Fox, M. A. *J. Phys. Chem.* **1986**, *90*, 6521.

[90] Nosaka, Y.; Fox, M. A. *J. Phys. Chem.* **1988**, *92*, 1893.

[91] Nosaka, Y.; Ohta, N.; Miyama, H. *J. Phys. Chem.* **1990**, *94*, 3752.

[92] Nosaka, Y.; Fox, M. A. *Langmuir* **1987**, *3*, 1147.

[93] Arbery, W. J.; Bartlett, P. N.; Wilde, C. P.; Darwent, J. R. *J. Am. Chem. Soc.* **1985**, *107*, 1854.

[94] Brawn, G. T.; Darwent, J. R.; Fletcher, P. D. I. *J. Am. Chem. Soc.* **1985**, *107*, 6466.

[95] Mulvaney, P.; Swayambunathan, V.; Grieser, F.; Meisel, D. *J. Phys. Chem.* **1988**, *92*, 6732.

[96] Green, A.; Mills, A. *J. Photochem. Photobiol. A:Chem* **1992**, *64*, 211.

[97] Bedja, I.; Hotchandani, S.; Kamat, P. V. *J. Phys. Chem.* **1993**, *97*, 11064.

[98] Nosaka, Y.; Miyama, H.; Terauchi, M.; Kobayashi, T. *J. Phys. Chem.* **1988**, *92*, 255.

[99] Hasselbarth, A.; Eychmueller, A.; Weller, H. *Chem. Phys. Lett.* **1993**, *203*, 271.

[100] Renz, C. *Helv. Chim. Acta* **1921**, *4*, 961.

[101] Gerischer, H. *J. E.ectroanal. Chem.* **1975**, *58*, 263.

[102] Fujishima, A.; Kobayakawa, K.; Honda, K. *Bull. Chem. Soc. Jpn.* **1975**, *48*, 1041.

[103] Ellis, A. B.; Kaiser, S. W.; Wrington, M. S. *J. Am. Chem. Soc.* **1976**, *98*, 9418.

[104] Yoneyama, H.; Sakamoto, H.; Tamura, H. *Electrochim. Acta.* **1975**, *20*, 341.

[105] Laser, D.; Bard, A. J. *J. Electrochem.Soc.* **1976**, *123*, 1027.

[106] Riegal, G.; Bolton, J. R. *J. Phys. Chem.* **1995**, *99*, 4215.

[107] Sun, L. Z.; Bolton, J. R. *J. Phys. Chem.* **1996**, *100*, 4127.

[108] Watanabe, T.; Kitamura, A.; Kojima, E.; Nakayama, C.; Hashimoto, K.; Fujishima, A.; In *Photocatalytic Purification and Treatment of Water and Air*; Ollis, D. E.; Al-Ekabi, H., Eds.; Elsevier: Amsterdam, 1993; p 747.

[109] Matsubara, H.; Takada, M.; Koyama, S.; Hashimoto, K.; Fujishima, A. *Chem. Lett.* **1995**, *9*, 767.

[110] Negishi, N.; Iyoda, T.; Hashimoto, K.; Fujishima, A. *Chem. Lett.* **1995**, 841.

[111] Fujishima, A.; Sugiyama, E.; Honda, K. *Bull. Chem. Soc. Jpn.* **1971**, *44*, .

[112] Miller, B.; Heller, A. *Nature* **1976**, *262*, 680.

[113] Noufi, R.; J., F. A.; Nozik, A. J. *J. Am. Chem. Soc.* **1981**, *103*, 1849.

[114] Nakato, Y.; Ohnishi, T.; Tsubomura, H. *Chem. Lett.* **1974**, 883.

[115] Buhler, N.; Meier, K.; Reber, J. F. *J. Phys. Chem.* **1984**, *88*, 3261.

[116] Reber, J. F.; Rusek, M. *J. Phys. Chem.* **1986**, *90*, 824.

[117] Izumi, I.; Dunn, W. W.; Wilbourn, K. O.; Fan, F. F.; Bard, A. J. *J. Phys. Chem.* **1980**, *84*, 3207.

[118] Aguado, M. A.; Anderson, M. A. *Sol. Energy Mater. Sol. Cells* **1993**, *28*, 345.

[119] Raupp, G. R.; Junio, C. T. *Appl. Surf. Sci.* **1993**, *72*, 321.

[120] Takeda, N.; Torimoto, T.; Sampath, S.; fwabata, S.; Yoneyama, H. *J. Phys. Chem. B* **1995**, *99*, 9986–9991.

[121] Augugliaro, V.; Palmisano, L.; Schiavello, M. *AIChE. J.* **1991**, *37*, 1096.

[122] D?Oleivera, J.; Al-Sayyed, G.; Pichat, P. *Enviton. Sci. Technol.* **1990**, *24*, 990.

[123] Sitkiewitz, S.; Heller, A. *New J. Chem.* **1996**, *20*, 233.

[124] Harvey, P. R.; Rudham, R.; Ward, S. *J. Chem. Soc. Faraday Trans.* **1983**, *1*, 1381.

[125] Serpone, N.; Lawless, D.; Khairutdinov, R.; Pelizzetti, E. *J. Phys. Chem.* **1995**, *99*, 16655.

[126] Martin, S.; Herrmann, H.; Choi, W.; Hoffmann, M. *J. Chem. Soc. Faraday Trans.* **1994**, *90*, 3315.

[127] Martin, S.; Herrmann, H.; Hoffmann, M. *J. Chem. Soc. Faraday Trans.* **1994**, *90*, 3323.

[128] Atkinson, R.; Baulch, D. L.; Cox, R. A.; Hampson, R. F. J.; Kerr, J. A.; Tore, J. *J. Phys. Chem. Ref. Data* **1989**, *18*, p.932.

[129] Sclafani, A.; Palmisano, L.; Davi, E. *J. Photochem. Photobiol. A: Chem.* **1991**, *56*, 113.

[130] Palmisano, L.; Augugliaro, V.; Sclafani, A.; Schiavello, M. *J. Phys. Chem.* **1988**, *92*, 6710.

[131] *The International Conference on TiO_2 Photocatalytic Purification and Treatment of Air and Water.* London, Ontario, Canada, 1993-6.

[132] Yamazaki-Nishida, S.; Nagano, K. J.; Phillips, L. A.; Cerveramarch, S.; Anderson, M. A. *J. Photochem. Photobiol. A Chem.* **1993**, *70*, 95–99.

[133] Nimlos, M. R.; Wolfrum, E. J.; Brewer, M. L.; Fennell, J. A.; Bintner, G. *Environ. Sci. Technol.* **1996**, *30*, 3102.

[134] Raupp, G. R.; Dibble, L. A. *Environ. Sci. Technol.* **1992**, *26(3)*, 492.

[135] Fujishima, A.; In *The International Conference on TiO_2 Photocatalytic Purification and Treatment of Air and Water.* London, Ontario, Canada, 1993; p 98.

[136] Hashimoto, K.; Ohko, Y.; Watanabe, M.; Fujishima, A.; In *189th Meeting of the Electrochemical Society (Extended Abstracts):* Los Angeles, California, May 5-10 1996; p 697.

[137] Ohko, Y.; Hashimoto, K.; Fujishima, A. *J. Phys. Chem. A* **1997**, *101*, 8053.

[138] Sherwood, T. K.; Pigford, R. L.; Wilke, C. R. *Mass transfer*; McGraw-Hill: New york, 1975.

[139] Fuller, E. N.; Schettler, R. D.; Gidding, J. C. *Ind. Eng. Chem.* **1966**, *58(5)*, 19.

[140] Torii, K. *Proceedings of the 3rd Symposium on Flow Visualization*; Univ. of Tokyo, July 17-18 1975; p 5.

[141] Matthews, R. W. *J. Phys. Chem.* **1987**, *91*, 3328.

[142] Matthews, R.; Mcevoy, S. *J. Photochem. Photobiol. A Chem* **1992**, *64*, 231.

[143] Obee, T. N.; Brown, R. T. *Environ. Sci. Technol.* **1995**, *29*, 1223.

[144] Schwitzgebel, J.; Ekerdt, J. G.; Sunada, F.; Lindquist, S.; Heller, A. *J. Phys. Chem. B* **1997**, *101*, 2621.

[145] Vorontsov, A. V.; Barannik, G. B.; Snegurenko, O. I.; Savinov, E. N.; Parmon, V. N. *Kinet. Catal.* **1997**, *38*, 84.

[146] Pichat, P. *Catal. Today* **1994**, *19*, 313.

[147] Shin, E. M.; Senthurchelvan, R.; Munoz, J.; Basak, S.; Rajeshwar, K.; Benglassmith, G.; Howell, B. C. *J. Electrochem. Soc.* **1996**, *143*, 1562.

[148] Hoffmann, M. R.; Martin, S. T.; Choi, W. Y.; Bahnemann, D. W. *Chem. Rev.* **1995**, *95*, 69.

[149] Clinton, N. A.; Kenley, R. A.; Traylor, T. G. *J. Am. Chem. Soc.* **1975**, *97*, 3452.

[150] Clinton, N. A.; Kenley, R. A.; Traylor, T. G. *J. Am. Chem. Soc.* **1975**, *97*, 3757.

[151] Traylor, T. G.; Russel, C. A. *J. Am. Chem. Soc.* **1965**, *87*, 3698.

[152] Leonardos, G.; Kendall, D.; Barnard, N. *J. Air. Pollut. Control. Assoic.* **1969**, *19*, 91.

[153] Harke, H. P.; Baars, A.; Frahm, B.; Peters, H.; Schults, C. *Int. Arch. Arbeitsmed.* **1972**, *29*, 323–339.

[154] Wakeham, H. *Recent trends in tobacco smoke research*; Plenum Press: New York, 1972.

[155] Goldstein, S.; Czapski, G.; Rabani, J. *J. Phys. Chem.* **1994**, *98*, 6586.

[156] Phillips, B.; Frostick Jr., F. C.; Starcher, P. S. *J. Am. Chem. Soc.* **1957**, *79*, 5982.

[157] Schuchmann, M. N.; Sonntag, C. V. *J. Phys. Chem.* **1979**, *99*, 780.

[158] Moortgat, G.; Veyret, B.; Lesclaux, R. *J. Phys. Chem.* **1989**, *93*, 2362.

[159] Moortgat, G.; Veyret, B.; Lesclaux, R. *Chem. Phys. Lett.* **1989**, *160*, 443.

[160] Watts, R. J.; Kong, S.; Orr, M. P.; Miller, G. C.; Henry, B. E. *Water Res.* **1995**, *29*, 95.

[161] Carrizosa, I.; Munuera, G. *J. Catal.* **1977**, *49*, 174.

[162] Carrizosa, I.; Munuera, G. *J. Catal.* **1977**, *49*, 189.

[163] Walker, A.; Formenti, M.; Meriaudeau, P.; Teichner, S. J. *J. Catal.* **1977**, *50*, 237.

[164] Miyata, H.; Wakamiya, M.; Kubokawa, Y. *J. Catal.* **1974**, *34*, 117.

[165] Nakajima, T.; Miyata, H.; Kubokawa, Y. *Bull. Chem. Soc. Jpn.* **1982**, *55*, 609.

[166] Morimoto, T.; Nagao, M.; Tokuda, F. *Bull. Chem. Soc. Jpn.* **1968**, *41*, 1533.

[167] Omori, T.; Imai, J.; Nagao, M.; Morimoto, T. *Bull. Chem. Soc. Jpn.* **1969**, *42*, 2198.

[168] Sukharev, V.; Wold, A.; Gao, Y. M.; Dweight, K. *J. Solid State Chem.* **1995**, *119*, 339.

[169] Takeda, N.; Ohtani, M.; Torimoto, T.; Kuwabata, S.; Yoneyama, H. *J. Phys. Chem. B* **1997**, *101*, 2644.

[170] Torimoto, T.; Ito, S.; Kuwabata, S.; Yoneyama, H. *Environ. Sci. and Technol.* **1996**, *30*, 1275.

[171] Sampath, S.; Uchida, H.; Yoneyama, H. *J. Catal.* **1994**, *149*, 189.

[172] Uchida, H.; Itoh, S.; Yoneyama, H. *Chem. Lett.* **1995**, 1995.

[173] Takahashi, K.; Hashimoto, K.; Fujishima, A. *Proceedings of the 4th Symposium on Recent Development of Photocatalysis*: Univ. of Tokyo, Dec. 17 1997; p 80.

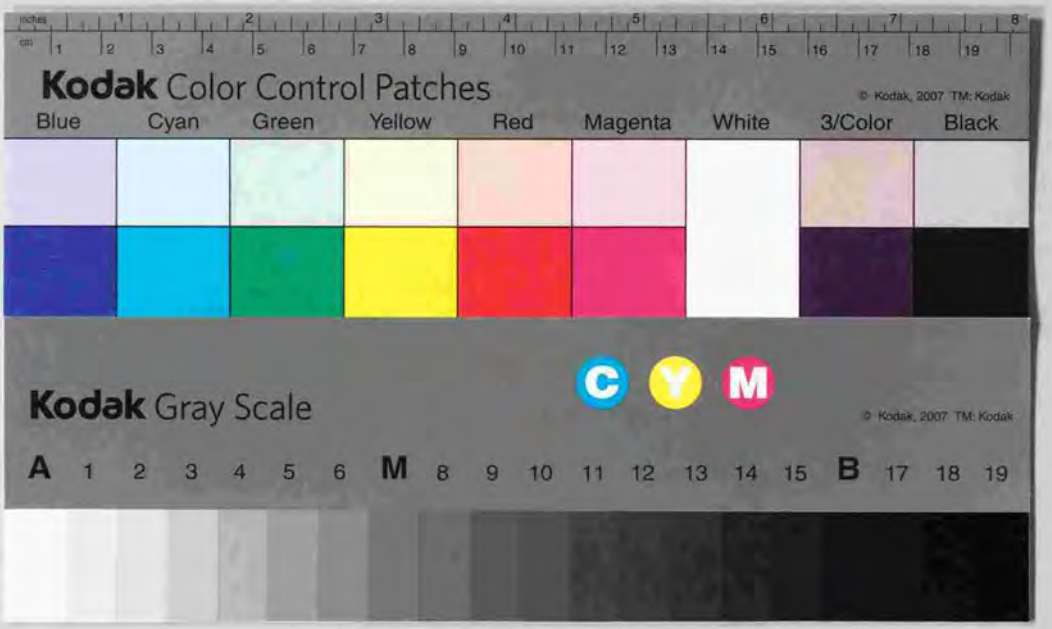
inches
cm
Kodak Color Control Patches
© Kodak, 2007 TM: Kodak
Blue
Cyan
Green
Yellow
Red
Magenta
White
3/Color
Black
Kodak Gray Scale
C
Y
M
© Kodak, 2007 TM: Kodak
A 1 2 3 4 5 6 M 8 9 10 11 12 13 14 15 B 17 18 19